



**Watershed Physical Processes Research Unit - National Sedimentation Laboratory  
Oxford, Mississippi**

## **Quantifying Sediment Loadings from Streambank Erosion in Selected Agricultural Watersheds Draining to Lake Champlain**



**By Eddy J. Langendoen, Andrew Simon, Lauren Klimetz, Natasha Bankhead,  
and Michael E. Ursic**

**Quantifying Sediment Loadings from Streambank Erosion in  
Selected Agricultural Watersheds Draining to Lake Champlain**

**Prepared by**

**U.S. Department of Agriculture – Agricultural Research Service  
National Sedimentation Laboratory**  
*Watershed Physical Processes Research Unit*

**For**

**The State of Vermont**

**December 2012**

# **Quantifying Sediment Loadings from Streambank Erosion in Selected Agricultural Watersheds Draining to Lake Champlain**

ARS Designated Representative and Project Manager:

**Eddy J. Langendoen, Andrew Simon**

Report Preparation:

**Eddy J. Langendoen, Andrew Simon, Lauren Klimetz, Natasha Bankhead, Michael E. Ursic**

Mapping, GIS:

**Danny Klimetz, Michael E. Ursic, Jiana ten Brinke**

Field Operations and Database Management:

**Brian Bell, Lauren Klimetz, Danny Klimetz**

Field Data Collection and Data Processing:

**Brian Bell, Andrew DelMastro, Danny Klimetz, Lee Patterson, Natasha Pollen-Bankhead, Ibrahim Tabanca, Robert Thomas**

## EXECUTIVE SUMMARY

Excessive erosion, transport, and deposition of sediment in surface waters are major water quality problems in the United States. Since 1992 the series of biennial National Water Quality Inventory Reports (Section 305(b) Report to Congress) have indicated that sediments and nutrients are ranked as leading causes of water-quality impairment of assessed rivers and lakes. At its mouth the Missisquoi River has a history of exceedance of phosphorus concentration target levels endorsed by the governments of Vermont, Québec, and New York. Observations along the study reach of the Missisquoi River and several of its tributaries, investigated in this report, have indicated that the river's streambanks could be a significant source of the suspended sediment and hence phosphorus to Missisquoi Bay. Indeed, significant portions of the study reach were estimated to have greater than 50% of their banks failing in the analysis carried out as part of this report. The main objective of this study, therefore, was to determine rates and loadings of sediment from streambank erosion along main stem reaches of the Missisquoi River located in the United States (US) and select Tributaries (Black Creek, Hungerford Brook, Jay Branch, Mud Creek, Trout River and Tyler Branch). Further, three mitigation scenarios were analyzed to determine the percent reduction in loadings that can be obtained by stabilizing streambanks: mitigation scenario 1) 25 year old mature trees on the bank top, mitigation scenario 2) banks graded to a 2H:1V slope, and mitigation scenario 3) banks graded to a 2H:1V slope in combination with 5-year old vegetative treatment on bank top and face.

Bank stability and toe erosion analyses were carried out using the model BSTEM at 27 study sites along the study reach using a 30-year, historic flow record. The flow record was constructed separately for each study site using the observed discharges at USGS gages 04293000 (MISSISQUOI RIVER NEAR NORTH TROY, VT) and 04293500 (MISSISQUOI RIVER NEAR EAST BERKSHIRE, VT) for the period 10/1/79 to 9/30/10. Predicted volumes of sediment eroded from the streambanks at each site ranged from 0.0559 to 1780 m<sup>3</sup> of sediment per one kilometer reach per year (m<sup>3</sup>/km/yr) under existing conditions with a median value of 69.3 m<sup>3</sup>/km/yr and an interquartile range (IQR) of 367 m<sup>3</sup>/km/yr. Contributions of sediment from streambank erosion along the US study reaches of the Missisquoi River were found to be about 36% (31,600 t/yr) of the total suspended-sediment load entering Missisquoi Bay. Maximum associated phosphorus loadings of up to 1,540 kg/km/yr were calculated in the lower portion of Tyler Branch and the confluence of the Missisquoi and Trout Rivers. The median calculated phosphorus loading was 41.7 kg/km/yr and the IQR was 312 kg/km/yr. The calculated streambank erosion volumes contributed about 36% (52.0 t/yr) to the total phosphorus load entering Missisquoi Bay.

Mitigation scenarios 1 and 2 provided similar percent reductions in sediment loadings. Median erosion volumes were reduced by 60% to 27.7 m<sup>3</sup>/km/yr for scenario 1 and 50% to 34.8 m<sup>3</sup>/km/yr for scenario 2. The IQR was reduced by 48% (190 m<sup>3</sup>/km/yr) for scenario 1 and 40% (221 m<sup>3</sup>/km/yr) for scenario 2. However, maximum eroded volumes of bank material increased to 2510 m<sup>3</sup>/km/yr (scenario 1) and 2360 m<sup>3</sup>/km/yr (scenario 2). The calculated reductions in eroded bank material volumes were greatest for scenario 3. The median value was reduced by 100% (0 m<sup>3</sup>/km/yr), the IQR was reduced by 99% (3.12 m<sup>3</sup>/km/yr), and the maximum value was reduced by 59% (740 m<sup>3</sup>/km/yr). Contributions of sediment from streambank erosion along the US study reaches of the Missisquoi River to the total suspended-sediment load entering

Missisquoi Bay were reduced by: scenario 1) 21% (25,000 t/yr), scenario 2) 12% (27,700 t/yr), and scenario 3) 85% (4,870 t/yr). The mitigation scenarios have a similar impact on phosphorus loadings as they have on sediment loadings, since phosphorus loadings are directly related to bank material loadings. Reductions in phosphorus loadings provided by mitigation scenarios 1 and 2 were moderate, whereas scenario 3 provided a significant reduction. The median value of calculated phosphorus loadings was reduced by 51% (20.3 kg/km/yr) for scenario 1, 34% (27.6 kg/km/yr) for scenario 2, and 97% (1.29 kg/km/yr) for scenario 3. The IQR of calculated phosphorus loadings was reduced by 55% (141 kg/km/yr) for scenario 1, 17% (260 kg/km/yr) for scenario 2, and 86% (44.2 kg/km/yr) for scenario 3. The maximum calculated phosphorus loading was reduced by 1% (1,520 kg/yr/km) for scenario 1, 7% (1,390 kg/yr/km) for scenario 2, and 80% (305 kg/yr/km) for scenario 3. The calculated contribution to the total phosphorus load into Missisquoi Bay is reduced by 29% (37.1 t/yr) for scenario 1, 14% (44.8 t/yr) for scenario 2, and 84% (8.43 t/yr) for scenario 3.

## TABLE OF CONTENTS

<b>EXECUTIVE SUMMARY .....</b>	<b>I</b>
<b>TABLE OF CONTENTS .....</b>	<b>III</b>
<b>LIST OF FIGURES .....</b>	<b>V</b>
<b>LIST OF TABLES .....</b>	<b>VII</b>
<b>LIST OF ABBREVIATIONS AND UNITS .....</b>	<b>VIII</b>
<b>CONVERSION FACTORS, TEMPERATURE, AND VERTICAL DATUM .....</b>	<b>X</b>
<b>INTRODUCTION AND PROBLEM.....</b>	<b>1</b>
<b>AIMS, OBJECTIVES AND SCOPE.....</b>	<b>1</b>
<b>TECHNICAL BACKGROUND .....</b>	<b>3</b>
<i>Channel Stability and Evolution .....</i>	<i>3</i>
<i>Quantification of Channel Processes.....</i>	<i>5</i>
Soil Geotechnical Resistance against Shearing .....	5
Modeling Streambank Stability: The Bank-Stability and Toe-Erosion Model (BSTEM) ...	10
<b>DATA COLLECTION AND METHODS .....</b>	<b>14</b>
<i>Introduction.....</i>	<i>14</i>
<i>Rapid Geomorphic Assessments: RGAs.....</i>	<i>14</i>
<i>Field Data Collection .....</i>	<i>15</i>
<i>Geotechnical Data Collection: Borehole Shear Tests .....</i>	<i>16</i>
<i>Erosion-Resistance Data Collection: Submerged Jet Test Device.....</i>	<i>18</i>
<i>Estimating Percent Reach Failing Using a Modified RGA .....</i>	<i>18</i>
<i>Soil Shear Strength Characterization: Measuring Root Reinforcement.....</i>	<i>19</i>
<i>Hydrologic Data .....</i>	<i>24</i>
<i>Bank-Stability Modeling using BSTEM-Dynamic .....</i>	<i>29</i>
<b>BSTEM MODELING RESULTS.....</b>	<b>33</b>
<i>Bank Material Loadings .....</i>	<i>33</i>
Existing Conditions.....	33
Mature Vegetation .....	35
Grading the Banks to 2:1 Slopes.....	37
Grading the Banks to 2:1 Slopes in Combination with Vegetative Treatment.....	37
Relation to Channel Stability Index.....	38
<i>Phosphorus Loadings Under Existing and Mitigating Conditions.....</i>	<i>38</i>
<i>Contribution of Bank Material to Suspended Sediment Load .....</i>	<i>40</i>
<i>Discussion .....</i>	<i>45</i>
Stage of Channel Evolution .....	45
Percent Reach Failing .....	47
Transport of Failed Material and Calculated Loads at the Watershed Outlet.....	47
Variability of Bank-Material Properties .....	48
Mitigation Scenarios .....	49
Closing .....	49

<b>CONCLUSIONS .....</b>	<b>50</b>
<b>REFERENCES.....</b>	<b>53</b>
<b>APPENDIX A. COMPARTMENTALIZATION OF MISSISQUOI RIVER AND ITS TRIBUTARIES FOR BANK LOADING CALCULATIONS.....</b>	<b>58</b>
<i>Two-mile reaches .....</i>	<i>58</i>
<b>APPENDIX B. CHANNEL STABILITY RANKING OF THE MISSISQUOI RIVER AND ITS TRIBUTARIES.....</b>	<b>60</b>
<b>APPENDIX C. BANK AND BED MATERIAL GRAIN SIZE DISTRIBUTIONS .....</b>	<b>61</b>
<b>APPENDIX D. BANK MATERIAL PROPERTIES.....</b>	<b>63</b>

## LIST OF FIGURES

Figure 1 – Modeling sites used to estimate streambank sediment input to Lake Champlain in the upper and lower portions of the Missisquoi River Basin.....	2
Figure 2 – Six stages of channel evolution from Simon and Hupp (1986) and Simon (1989) identifying Stages I and VI as dynamic equilibrium conditions (modified from Hupp and Simon, 1991).....	3
Figure 3 – Three modes of cohesive sediment erosion: a) surface erosion of bed aggregates; b) mass erosion of the bed; c) entrainment of fluid mud (from Mehta, 1991).....	9
Figure 4 – Schematic of jet-test device (from Hanson and Simon, 2001).....	10
Figure 5 – Example RGA form filled out for study site M2.....	16
Figure 6 – Schematic representation of borehole shear tester (BST) used to determine cohesive and frictional strengths of <i>in-situ</i> streambank materials. Modified from Thorne <i>et al.</i> , 1981. ....	17
Figure 7 – Photographs of the scaled-down mini-jet submerged jet test device, used <i>in situ</i> to measure soil erodibility.....	18
Figure 8 – Examples of different percent reach filing classes within the Missisquoi River Basin study area. ....	20
Figure 9 – Maximum percent of reach failing for the Missisquoi River and its tributaries. ....	21
Figure 10 – Percent of reach failing for the Missisquoi River main stem: (top) left and right bank, (bottom) reach average. ....	22
Figure 11 - Photos of the Root-Puller constructed at the USDA-ARS-NSL: (1) shows the most recent puller during construction phase before winch cable has been added; (2) shows original large puller built by USDA-ARS-NSL being used in the field to measure the strength of riparian tree roots; and (3) shows a close-up of the way that the load cell and roots are connected to the winching cable. ....	23
Figure 12 – Tensile strength curve for Silver Maple.....	24
Figure 13 – In order to develop regressions with which to extrapolate discharge data at USGS gauging stations where a short period of record existed, measured data at these stations were plotted against both long-term gages, 04293500 and 04293000. ....	27
Figure 14 – Visual comparison between discharges calculated based on upper and mid-mainstem USGS gages was part of the methodology used to determine which gage was used to extrapolate measured discharge values to the modeled time period.....	27
Figure 15 – Modeled time period discharge data for gage 04293795 as extrapolated from mainstem gage 04293500. ....	28
Figure 16 – Illustration of existing conditions and mitigation scenarios evaluated by BSTEM. .	31
Figure 17 – Average annual volume of eroded bank material estimated by BSTEM over the modeling period, under existing and mitigated conditions for the 27 study sites in the Missisquoi watershed.....	33
Figure 18 – Map of average annual sediment loadings from bank erosion under current conditions.....	35
Figure 19 – Map of average annual sediment loadings from bank erosion for the mature vegetation mitigation scenario.....	36
Figure 20 – Map of average annual sediment loadings from bank erosion for the mitigation scenario in which the bank profiles are graded at a 2:1 slope. ....	38

Figure 21 – Map of average annual sediment loadings from bank erosion for the mitigation scenario in which the bank profiles are graded at a 2:1 slope in combination with a vegetative treatment on bank face and bank top.....	39
Figure 22 – Plot of average annual sediment loadings from bank erosion for the various scenarios as a function of channel stability index obtained from the RGAs.....	40
Figure 23 – Map of phosphorus concentrations (in mg/kg of soil) used in the analysis to calculate phosphorus loadings from sediment loadings.....	42
Figure 24 – Maps of average annual total phosphorus loadings from bank erosion for: (a) current conditions scenario, (b) mature vegetation mitigation scenario, (c) mitigation in which the bank profiles are graded at a 2H:1V slope, and (d) mitigation in which the bank profiles are graded at a 2H:1V slope in combination with a vegetative treatment on bank face and bank top. (continued on next page).....	43
Figure 25 – Stage of channel evolution according to the conceptual channel evolution model of Simon and Hupp (1986) of the Missisquoi River and select tributaries.....	46
Figure 26 – Plot of erosion rate (kd) versus critical shear stress ( $\tau_c$ ) measured with the submerged jet test device.....	48
Figure A-1 – Map showing the locations of the 2-mile reaches and the intensive study sites.....	58

## LIST OF TABLES

Table 1 – Summary of conditions to be expected at each stage of channel evolution .....	4
Table 2 – Root tensile strength and root diameter distribution data used for input to the RipRoot model in BSTEM. ....	25
Table 3 – Nearest USGS gage to each site with discharge data and time period for which these discharge data were available. Table also provides USGS gage used to extrapolate discharge to modeled time period, where only a short time period was available from the nearest gage.....	26
Table 4 – Comparison of percentile values of measured and extrapolated discharges (at USGS gage 04293795) based on upper and mid main-stem USGS gages. ....	28
Table 5 – Root-reinforcement input values for existing and mitigated conditions.....	30
Table 6 – Average annual volume of eroded bank material estimated by BSTEM over the modeling period, under existing and mitigated conditions for selected sites in the Missisquoi watershed. ....	34
Table 7 – Average annual total phosphorus loading from streambank erosion (in kg/yr per unit length of streambank) simulated by BSTEM over the 30-year modeling period for existing and mitigation conditions.....	41
Table 8 – Metrics of average annual total phosphorus loadings (in kg/km/yr) from streambank erosion along two-mile reaches simulated by BSTEM over the 30-year modeling period for existing and mitigation conditions. ....	42
Table A-1 – List of the study site assigned to each 2-mile reach. ....	59
Table B-1 – Rapid Geomorphic Assessment conducted at the intensive study sites.....	60
Table C-1 – Grain size distribution of the dominant bank soil layer and that of the simulated eroded bank material for each study site.....	61
Table C-2 – Grain-size distribution of collected bed-material samples. ....	62
Table D-1 – Resistance to erosion of bank face and toe materials measured using a submerged jet-test device. ....	63
Table D-2 – Shear strength of bank materials measured using a borehole shear test device. ....	64

## LIST OF ABBREVIATIONS AND UNITS

<i>a</i>	exponent assumed to equal 1.0
<i>A</i>	shear surface or flow area; m <sup>2</sup>
<i>A<sub>r</sub></i>	root area in the plane of the shear surface; m <sup>2</sup>
AASL	Annual Average Sediment Loading; m <sup>3</sup> km <sup>-1</sup> yr <sup>-1</sup>
ARS	Agricultural Research Service
BST	Borehole Shear Test device
BSTEM	Bank Stability and Toe Erosion Model
<i>c'</i>	effective cohesion, in kilopascals; kPa
<i>c<sub>a</sub></i>	apparent cohesion, in kilopascals; kPa
<i>c<sub>f</sub></i>	non-dimensional bed roughness coefficient
<i>c<sub>r</sub></i>	cohesion due to roots, in kilopascals; kPa
<i>d</i>	root diameter, in meters; m
<i>D<sub>50</sub></i>	median diameter of grains in the bed, in meters; m
<i>e</i>	multiplier in the root tensile stress- root diameter function (MPa m <sup>-b</sup> )
<i>f</i>	exponent in the root tensile stress- root diameter function (dimensionless)
<i>F<sub>P</sub></i>	root pullout force, in Newtons; N
<i>F<sub>s</sub></i>	Factor of Safety
<i>g</i>	acceleration due to gravity, in meters per square second; 9.807 m s <sup>-2</sup>
<i>h</i>	groundwater elevation, in meters; m
<i>i</i>	layer, node, root, or flow segment index
<i>I</i>	total number of soil layers, or roots crossing the shear plane
<i>k</i>	erodibility coefficient, in cubic centimeters per Newton second; cm <sup>3</sup> N <sup>-1</sup> s <sup>-1</sup> or cubic meters per Newton second; m <sup>3</sup> N <sup>-1</sup> s <sup>-1</sup>
<i>k<sub>d</sub></i>	erosion rate coefficient, in meters per second; m s <sup>-1</sup>
<i>K<sub>r</sub></i>	relative permeability
<i>K<sub>sat</sub></i>	saturated hydraulic conductivity, in meters per second; m s <sup>-1</sup>
<i>l</i>	curve-fitting parameter in the van Genuchten (1980) equation, per meter; m <sup>-1</sup>
<i>L</i>	length of the failure plane, in meters; m
<i>L<sub>r</sub></i>	root length, in meters; m
<i>m</i>	curve-fitting parameter in the van Genuchten (1980) equation
<i>n</i>	Manning's roughness coefficient, in seconds per cubic root of a meter; s m <sup>-1/3</sup> . If present, the subscripts <i>g</i> , <i>f</i> and <i>v</i> signify the grain, form and vegetal components of the roughness
NSL	National Sedimentation Laboratory
<i>Q</i>	bankfull discharge, in cubic meters per second; m <sup>3</sup> s <sup>-1</sup>
<i>Q<sub>s</sub></i>	bed-material discharge per unit channel width, in cubic meters per meter per second; m <sup>3</sup> m <sup>-1</sup> s <sup>-1</sup>
<i>P</i>	hydrostatic-confining force due to external water level, in kilonewtons per meter; kN m <sup>-1</sup>
<i>R</i>	hydraulic radius (area/wetted perimeter), in meters; m
Re <sup>*</sup> <sub><i>c</i></sub>	critical roughness Reynolds number
RGA	Rapid Geomorphic Assessment
<i>S</i>	channel gradient, in meters per meter; m m <sup>-1</sup>
<i>t</i>	time, in seconds; s

$T_r$	root tensile strength per unit area of soil = ultimate root tensile stress, in kilopascals; kPa
$U$	mean flow velocity, in meters per second; $\text{m s}^{-1}$
USDA	U.S. Department of Agriculture
$W$	failure block weight, in kilonewtons; kN
$z$	water surface elevation, in meters; m
$\alpha$	local bank angle, in degrees from horizontal
$\beta$	failure-plane angle, in degrees from horizontal
$\varepsilon$	rate of erosion, in meters per second; $\text{m s}^{-1}$
$\zeta$	angle of a root at rupture relative to the failure plane, in degrees
$\theta$	angle of shear distortion, in degrees
$\mu_a$	pore-air pressure, in kilopascals; kPa
$\mu_w$	pore-water pressure, in kilopascals; kPa
$\nu$	kinematic viscosity of water, in square meters per second; $\text{m}^2 \text{s}^{-1}$
$\Theta$	soil saturation
$\Theta_r$	residual moisture content
$\Theta_s$	saturated moisture content
$\rho$	density of water, in kilograms per cubic meter; $1000 \text{ kg m}^{-3}$
$\rho_s$	density of the sediment, in kilograms per cubic meter; $2650 \text{ kg m}^{-3}$
$\sigma$	normal stress on the shear plane, in kilopascals; kPa
$\tau_c$	critical shear stress, in Pascals; Pa
$\tau^*_c$	dimensionless critical shear stress
$\tau_s$	soil shearing resistance, in kilopascals; kPa
$\tau_o$	bed shear stress, in Pascals; Pa. If present, the additional subscripts $g$ , $f$ and $v$ signify the grain, form and vegetal components of the bed shear stress.
$\phi'$	effective soil friction angle, in degrees
$\phi^b$	angle describing the increase in shear strength due to an increase in matric suction ( $\mu_a - \mu_w$ ), in degrees
$\chi$	initial root orientation relative to the failure plane, in degrees

## CONVERSION FACTORS, TEMPERATURE, AND VERTICAL DATUM

<i>Multiply</i>	<i>By</i>	<i>To obtain</i>
<b><i>Length</i></b>		
millimeter (mm)	0.03937	inch
meter (m)	3.281	foot
kilometer (km)	0.6214	mile
<b><i>Area</i></b>		
square meter (m <sup>2</sup> )	10.764	square foot
square kilometer (km <sup>2</sup> )	0.3861	square mile
<b><i>Volume</i></b>		
cubic meter (m <sup>3</sup> )	35.31	cubic foot
<b><i>Flow</i></b>		
meter per second (m s <sup>-1</sup> )	3.281	foot per second
cubic meter per second (m <sup>3</sup> s <sup>-1</sup> )	35.31	cubic foot per second
<b><i>Mass</i></b>		
kilogram (kg)	2.205	pound
tonne, metric	1.102	ton (short)
metric tonne per square kilometer per year (ton km <sup>-1</sup> yr <sup>-1</sup> )	2.855	ton (short) per square mile per year
<b><i>Force per unit length</i></b>		
kilonewton per meter (kN m <sup>-1</sup> )	5.710	pound-force per inch
kilonewton per meter (kN m <sup>-1</sup> )	68.52	pound-force per foot
<b><i>Stress</i></b>		
pascal (Pa) (= newton per square meter, N m <sup>-2</sup> )	0.02089	pound-force per square foot
kilopascal (kPa)	0.145	pound-force per square inch
kilopascal (kPa)	20.89	pound-force per square foot
<b><i>Unit weight</i></b>		
kilonewton per cubic meter (kN m <sup>-3</sup> )	6.366	pound-force per cubic foot

**Temperature:** Water temperature in degrees Celsius (°C) may be converted to degrees Fahrenheit (°F) as follows:

$$^{\circ}\text{F} = 1.8 \text{ }^{\circ}\text{C} + 32$$

**Sea level:** In this report *sea level* refers to the National Geodetic Vertical Datum of 1929 (NGVD of 1929) - a Geodetic datum derived from a general adjustment of the first order level nets of both the United States and Canada, formerly called “mean sea level of 1929”.

## **INTRODUCTION AND PROBLEM**

Spanning two countries, Lake Champlain is over 1200 km<sup>2</sup> in area, with the majority of this vast, naturally occurring lake lying in the United States. Within the U.S., Lake Champlain is located in both Vermont and New York. The lake is a primary source of drinking water for a large number of citizens in these states and provides important recreational opportunities for the region. As a result, the State of Vermont is concerned with the quality of water entering Lake Champlain and is investigating potential sources of sediment, and consequently phosphorus input.

Water from many different sources enter Lake Champlain, however this study is concerned primarily with portions of the Missisquoi River situated in the U.S. The Missisquoi River originates in Lowell, northern Vermont and passes into southern Quebec, Canada before re-entering the U.S. and eventually the Missisquoi Bay of Lake Champlain. The Missisquoi River runs a course of over 130 km, the bulk of which runs through Vermont. Major tributaries to the Missisquoi River include, but are not limited to, Black Creek, Mud Creek, Trout River, and Tyler Branch. For more than a century the Missisquoi River has undergone many anthropogenic alterations, which continue to this day, all of which can potentially affect sediment input to the lake. Not only is sediment an important pollutant, filling bed material interstitial space reducing macro-invertebrate habitat, but the resultant land loss can greatly affect regional farming and be expensive to prevent. It may not, however, be necessary to make large scale bank-stabilization efforts if target areas can be determined and vegetation effects be evaluated, major objectives of this study.

## **AIMS, OBJECTIVES AND SCOPE**

The aim of this study was to provide the State of Vermont with:

1. Sources of streambank sediment to Lake Champlain from the Missisquoi River and select Tributaries (Black Creek, Hungerford Brook, Jay Branch, Mud Creek, Trout River and Tyler Branch).
2. Estimated sediment loadings to Lake Champlain.
3. Associated phosphorus loadings.

There are six study sites on the upper main-stem Missisquoi River, before the river enters Canada, and two sites each on Mud Creek and Jay Branch in this upper part of the basin. Once the Missisquoi River flows back into the United States, there are nine main-stem sites, three sites each on Black Creek, Tyler Branch and Hungerford Brook, and two on the Trout River for a total of twenty sites in the lower portion of the basin (Figure 1).

Initial modeling efforts were to examine existing conditions at the 30 sites, forecasting streambank erosion from these sites and providing the State of Vermont with suspended-sediment loadings by grain size and associated phosphorus values. Scientifically defensible methodologies were to be used to determine streambank sediment loadings for a 30-year time frame. This was to be accomplished using the USDA-ARS-NSL model BSTEM (Bank-Stability and Toe-Erosion Model) in combination with its root-reinforcement sub-model RipRoot. These

models estimate streambank-erosion rates caused by hydraulic processes acting on the bank surface and geotechnical processes (mass failure) operating on the bank mass.

Following existing conditions runs, input values were altered to include vegetation growth and then a further set of mitigation runs investigated adjusting bank profiles to represent a 2H:1V bank slope with and without five year vegetation growth to examine load reductions from a constructed bank.

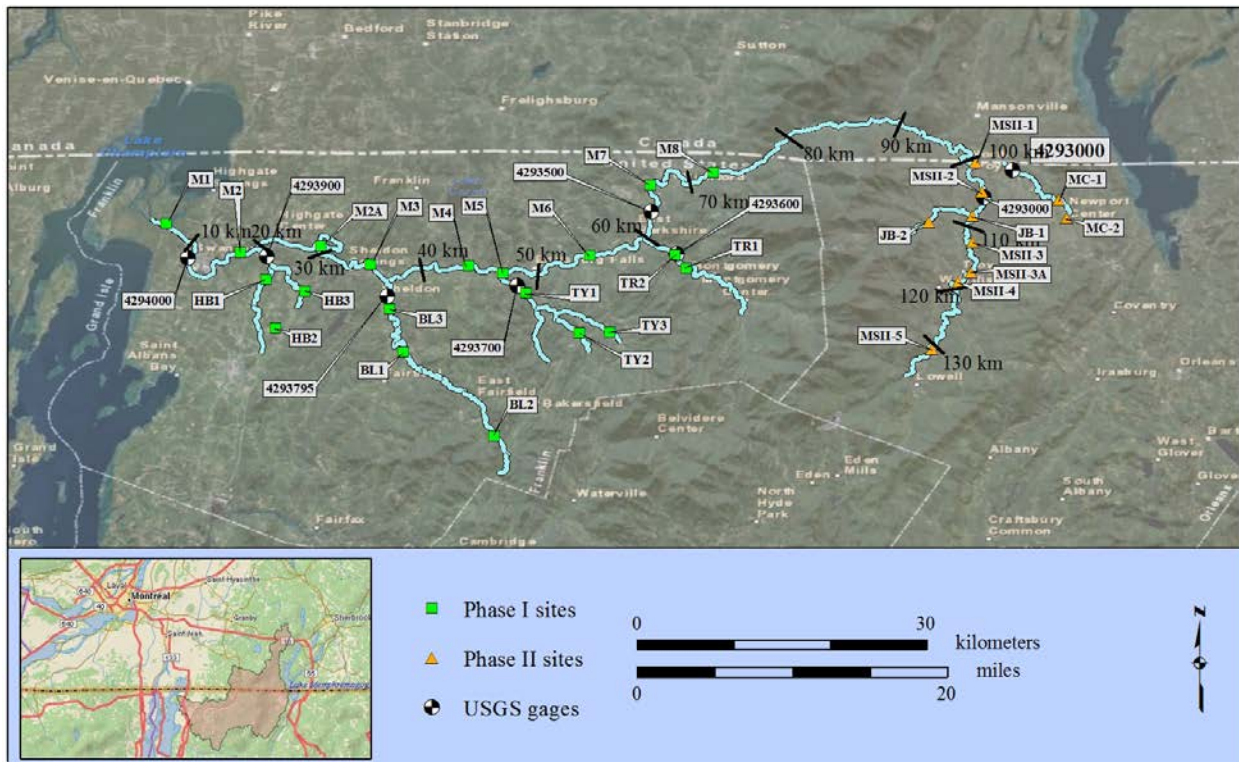


**Figure 1 – Modeling sites used to estimate streambank sediment input to Lake Champlain in the upper and lower portions of the Missisquoi River Basin.**

## TECHNICAL BACKGROUND

### Channel Stability and Evolution

Schumm *et al.* (1984) and Simon and Hupp (1986) note that following incision, a stream channel experiences a predictable, non-reversible series of adjustment processes (Figure 2). If the pre-disturbed channel is considered as the initial stage (I) of channel evolution and the disrupted channel as an instantaneous condition (stage II), rapid channel degradation can be considered stage III (Figure 2). Degradation flattens channel gradients and consequently reduces the available stream power for given discharges with time. Concurrently, bank heights are increased and bank angles are often steepened by fluvial undercutting and by pore-pressure induced bank failures near the base of the bank. Thus, the degradation stage (III) is directly related to destabilization of the channel banks and to channel widening by mass-wasting processes (stage IV) once bank heights and angles exceed the critical conditions of the bank material (as determined by its shear strength characteristics). If streambeds are composed of highly resistant materials, adjustment to heightened flow-energy conditions can only occur by lateral migration, bank erosion and channel widening (Simon and Darby, 1997).

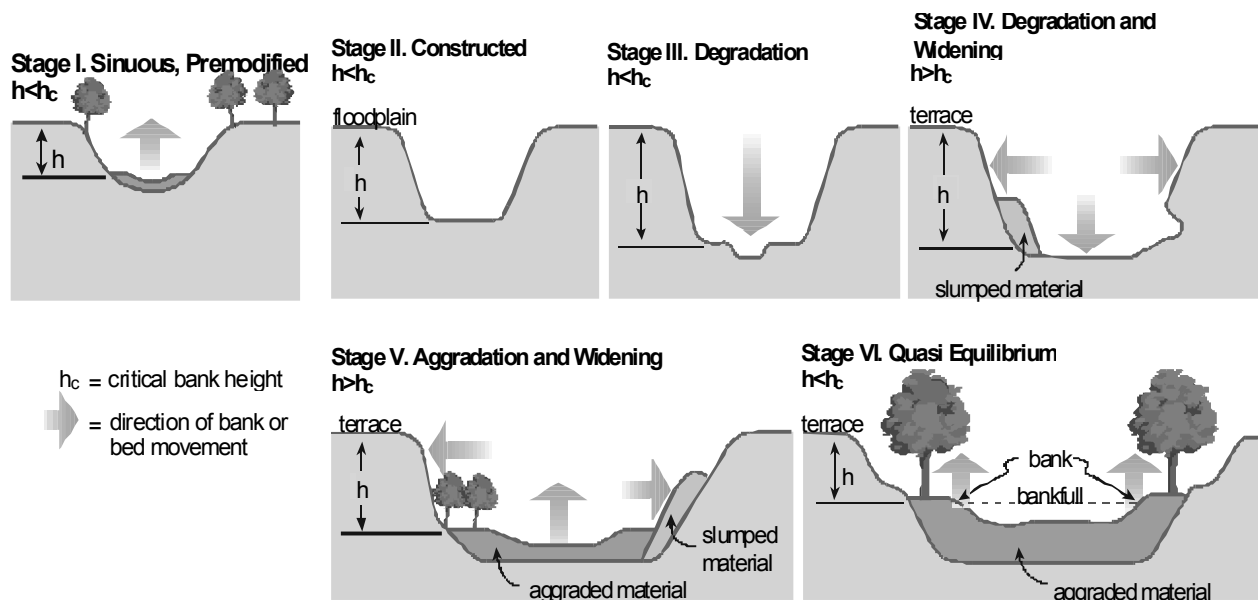


**Figure 2 – Six stages of channel evolution from Simon and Hupp (1986) and Simon (1989) identifying Stages I and VI as dynamic equilibrium conditions (modified from Hupp and Simon, 1991).**

As degradation migrates further upstream, aggradation (stage V) becomes the dominant trend in previously degraded downstream sites because the reduced gradient and hydraulic radius at the degraded site mean the stream cannot transport the heightened sediment loads originating from degrading reaches upstream. This secondary aggradation occurs at rates roughly 60% less than the associated degradation rate (Simon and Hupp, 1992). These reduced aggradation rates indicate that bed-level recovery will not be complete and that attainment of a new dynamic equilibrium will take place through: (1) further channel widening; (2) the establishment of

riparian vegetation that adds roughness elements and reduces the stream power for given discharges; and (3) further gradient reduction by meander extension and elongation. After sufficient bed-level rise and bank angle reduction, the frequency of mass-wasting events reduces and the channel reaches stage VI. Stage VI streams can be characterized as having a ‘channel-within-a-channel’, where the previous floodplain surface is less frequently inundated and can be described as a terrace. This morphology is typical of recovering and re-stabilized stream systems following incision. Flood flows are constrained below the terrace level and within this enlarged channel. Without proliferation of riparian vegetation within the channel, this results in a given flow having greater erosive power than an equivalent flow that could dissipate energy by spreading across the floodplain. Where vegetation does re-establish, the additional roughness limits the erosive power of flood events within the incised channel and constrains shear stress values to near bankfull levels (Simon *et al.*, 1999). It should be noted that stages I and VI represent dynamic (or quasi) equilibrium conditions, but that stage VI is the only attainable condition in previously disturbed systems (Table 1).

**Table 1 – Summary of conditions to be expected at each stage of channel evolution**

Stage	Descriptive Summary
I	<i>Pre-modified</i> – Stable bank conditions, no mass wasting, small, low angle bank slopes. Established woody vegetation, convex upper bank, concave lower bank.
II	<i>Constructed</i> – Artificial reshaping of existing banks. Vegetation often removed, banks steepened, heightened and made linear.
III	<i>Degradation</i> – Channel bed lowering and consequent increase of bank heights. Incision without widening. Bank toe material removed causing increased bank angles.
IV	<i>Threshold</i> – Degradation and basal erosion. Incision and active channel widening. Mass wasting from banks and excessive undercutting. Leaning and fallen vegetation. Vertical face may be present.
V	<i>Aggradation</i> – Deposition of material on bed, often sand. Widening of channel through bank retreat; no incision. Concave bank profile. Failed material re-worked and deposited. May see floodplain terraces. Channel follows a meandering course.
VI	<i>Restabilization</i> – Reduction in bank heights, aggradation of the channel bed. Deposition on the upper bank therefore visibly buried vegetation. Convex shape. May see floodplain terraces.

As stages of channel evolution are tied to discrete channel processes and not strictly to specific channel shapes, they have been successfully used to describe systematic channel-adjustment processes over time and space in diverse environments and subject to various disturbances, such as the following: channelization in the Southeast US Coastal Plain (Simon, 1994); volcanic eruptions in the Cascade Mountains (Simon, 1999); and dams in Tuscany, Italy (Rinaldi and Simon, 1998). Because the stages of channel evolution represent shifts in dominant channel processes, they are systematically related to suspended-sediment and bed-material discharge (Simon, 1989; Kuhnle and Simon, 2000), fish-community structure (Simon *et al.*, 2002), rates of channel widening (Simon and Hupp, 1992), and the density and distribution of woody-riparian vegetation (Hupp, 1992).

## **Quantification of Channel Processes**

Conceptual models of bank retreat and the delivery of bank sediments to the flow emphasize the importance of interactions between hydraulic forces acting at the bed and bank toe and gravitational forces acting on *in situ* bank materials (Carson and Kirkby, 1972; Thorne, 1982; Simon *et al.*, 1991; Langendoen, 2000). Failure occurs when erosion of the bank toe and the channel bed adjacent to the bank increase the height and angle of the bank to the point that gravitational forces exceed the shear strength of the bank material. After failure, failed bank materials may be delivered directly to the flow and deposited as bed material, dispersed as wash load, or deposited along the toe of the bank as intact blocks, or as smaller, dispersed aggregates (Simon *et al.*, 1991).

### ***Soil Geotechnical Resistance against Shearing***

Soil shear strength varies with the soil water content of the bank and the elevation of the saturated zone in the bank mass. In the part of the streambank above the “normal” level of the groundwater table, bank materials are unsaturated, pores are filled with both water and air, and pore-water pressure is negative. The difference ( $\mu_a - \mu_w$ ) between the air pressure,  $\mu_a$ , and the water pressure in the pores,  $\mu_w$ , represents matric suction. The increase in shear strength due to an increase in matric suction ( $\mu_a - \mu_w$ ) is described by the tangent of the angle  $\phi^b$ , where  $\phi^b$  varies for all soils and with water content for a given soil (Fredlund and Rahardjo, 1993), but generally takes a value between 10° and 20°, with a maximum of the effective soil friction angle,  $\phi'$ , under saturated conditions (Fredlund and Rahardjo, 1993). The effect of matric suction on shear strength is reflected in the apparent cohesion ( $c_a$ ) term (measured in kPa), which incorporates both electro-chemical bonding within the soil matrix (described by the effective cohesion,  $c'$ , in kPa) and cohesion due to surface tension on the air-water interface of the unsaturated soil:

$$c_a = c' + (\mu_a - \mu_w) \tan \phi^b \quad (2)$$

As can be seen from equation 2, negative pore-water pressures (positive matric suction) in the unsaturated zone provide for cohesion greater than the effective cohesion, and thus, greater shearing resistance. This is often manifest in steeper bank slopes than would be indicated by  $\phi'$ . Conversely, the wetter the bank and the higher the water table, the weaker the bank mass becomes and the more prone it is to failure. Accounting for the effects of friction, the shear strength of a soil,  $\tau_s$ , may thus be described by the Mohr-Coulomb shear strength criterion for unsaturated soils (Fredlund *et al.*, 1978):

$$\tau_s = c' + (\mu_a - \mu_w) \tan \phi^b + (\sigma - \mu_a) \tan \phi' \quad (3)$$

where  $\sigma$  = normal stress on the shear plane (kPa).

### ***Root Reinforcement by Riparian Vegetation***

Soil is generally strong in compression, but weak in tension. The fibrous roots of trees and herbaceous species are strong in tension but weak in compression. Root-permeated soil,

therefore, makes up a composite material that has enhanced strength (Thorne, 1990). Numerous authors have quantified this reinforcement using a mixture of field and laboratory experiments. Endo and Tsuruta (1969) used *in situ* shear boxes to measure the strength difference between soil and soil with roots. Gray and Leiser (1982) and Wu (1984) used laboratory-grown plants and quantified root strength in large shear boxes.

Many studies have found an inverse power relationship between ultimate tensile stress,  $T_r$  (in kPa), and root diameter,  $d$  (in mm), (examples include but are not limited to: Waldron and Dakessian, 1981; Riestenberg and Sovonick-Dunford, 1983; Coppin and Richards, 1990; Gray and Sotir, 1996; Abernethy and Rutherford, 2001; Simon and Collison, 2002; Pollen and Simon, 2005; Fan and Su, 2008):

$$T_r = e(1000d)^f \quad (4)$$

where  $e$  = multiplier ( $\text{MPa m}^{-f}$ ), and  $f$  = exponent (dimensionless) in the root tensile stress-diameter function, respectively. Note that  $f$  is always negative. Root tensile strength (in kN) can therefore be evaluated as the product of the root area,  $A_r$  ( $\pi d^2/4$ ), and the ultimate tensile stress,  $T_r$ :

$$T_r A_r = \frac{e\pi(1000^{1+f})d^{2+f}}{4} \quad (5)$$

Smaller roots are stronger per unit area (higher ultimate tensile stress), but the larger cross-sectional area of larger diameter roots means that the peak load they can withstand before breaking is higher than that of small roots.

Wu *et al.* (1979, after Waldron, 1977) developed a widely-used equation that estimates the increase in soil strength ( $c_r$ ) as a function of root tensile strength, areal density and root distortion during shear:

$$c_r = \frac{1}{A} \sum_{i=1}^{I} (A_r T_r)_i [\sin(90 - \xi) + \cos(90 - \xi) \tan \phi'] \quad (6)$$

where  $c_r$  = cohesion due to roots (kPa),  $T_r$  = tensile strength of roots (kPa),  $A_r$  = area of roots in the plane of the shear surface ( $\text{m}^2$ ),  $A$  = area of the shear surface ( $\text{m}^2$ ),  $I$  = total number of roots crossing the shear plane, the subscript  $i = i^{\text{th}}$  root, and

$$\xi = \tan^{-1} \left( \frac{1}{\tan \theta + \cot \chi} \right) \quad (7)$$

where  $\theta$  = angle of shear distortion (degrees), and  $\chi$  = initial orientation angle of fiber relative to the failure plane (degrees).

Pollen *et al.* (2004) and Pollen and Simon (2005) found that models based on equation 6 tend to overestimate root reinforcement because it is assumed that the full tensile strength of each root is mobilized during soil shearing and that the roots all break simultaneously. This overestimation was largely corrected by Pollen and Simon (2005) by developing a fiber-bundle model (RipRoot) to account for progressive breaking during mass failure. RipRoot was validated by comparing results of root-permeated and non-root-permeated direct-shear tests. These tests revealed that, relative to results obtained with the perpendicular model of Wu *et al.* (1979), accuracy was improved by an order of magnitude, but some error still existed (Pollen and Simon, 2005). One explanation for the remaining error in root-reinforcement estimates lies in the fact that observations of incised streambanks suggest that when a root-reinforced soil shears, two mechanisms of root failure occur: root breaking and root pullout. The anchorage of individual leek roots was studied by Ennos (1990), who developed a function for pullout forces based on the strength of the bonds between the roots and soil:

$$F_p = \pi d \tau_s L_r \quad (8)$$

where  $F_p$  = pullout force for an individual root (N), and  $L_r$  = root length (m), which can be estimated in the absence of field data using  $L_r = 123.1 d^{0.7}$  (Pollen, 2007).

The pullout force was not accounted for in the original version of RipRoot (Pollen and Simon, 2005) and so the role played by spatio-temporal variations in soil shear strength was neglected. Pollen (2007) tested the appropriateness of equation 8 through field measurements of the forces required to pull out roots. Pullout forces were then compared with breaking forces obtained from tensile strength testing and the RipRoot model was modified to account for both breaking and pullout. Thomas and Pollen-Bankhead (2010) improved equation 8 by employing Rankine's active earth pressure theory to compute  $\tau_s$ .

A second explanation is that, following the work of Wu *et al.* (1979), it has commonly been assumed that the  $\sin(90-\zeta) + \cos(90-\zeta)\tan\phi'$  term in equation 6 takes an approximately constant value of 1.2. Sensitivity analysis indicates that this assumption is flawed as this term varies from -1 when  $\zeta = 180^\circ$  to a maximum as  $\zeta \rightarrow \phi'$  (Thomas and Pollen-Bankhead, 2010). A series of Monte Carlo simulations was undertaken, assuming that  $\theta$  was uniformly distributed between  $0^\circ$  and  $90^\circ$  and assuming that  $\chi$  was uniformly distributed between  $\pm 90^\circ$  from the vertical, approximating a heartroot network. Friction angle was varied from  $0^\circ$  to  $44^\circ$  and failure plane angle was varied from  $10^\circ$  to  $90^\circ$ . For this assumed distribution, the  $\sin(90-\zeta) + \cos(90-\zeta)\tan\phi'$  term was found to be independent of failure plane angle. In addition, for a given friction angle, the distribution of values was highly skewed, with the median and 84<sup>th</sup> percentile being approximately equal but the 16<sup>th</sup> percentile being much smaller. It was found that it was possible to predict the median value of the  $\sin(90-\zeta) + \cos(90-\zeta)\tan\phi'$  term using a cubic polynomial involving only the friction angle.

The combination of the fiber bundle approach, in which roots break progressively during failure, the incorporation of pullout forces that vary as a function of the shear strength of the soil surrounding each root, and the variability in root orientation caused by local factors (e.g., water and nutrient availability, substrate and topographic variability) ensure that predictions of  $c_r$  cannot be readily extrapolated from one areal density to another nor from site to site.

### *Mechanisms of Cohesive Sediment Erosion*

Mechanistically, the detachment and erosion of cohesive (silt- and clay-sized) material by gravity and/or flowing water is controlled by a variety of physical, electrical, and chemical forces. Identification of all of these forces and the role they play in determining detachment, incipient motion, and erodibility, of cohesive materials is incomplete and still relatively poorly understood (Winterwerp and van Kesteren, 2004). Assessing the erosion resistance of cohesive materials by flowing water is complex due to difficulties in characterizing the strength of the electro-chemical bonds that define the resistance of cohesive materials. The many studies that have been conducted on cohesive materials have observed that numerous soil properties influence erosion resistance including antecedent moisture, clay mineralogy and proportion, density, soil structure, organic content, as well as pore and water chemistry (Grissinger, 1982). For example, Arulanandan (1975) described how the erodibility of a soil decreases with increasing salt concentration of the eroding fluid, inducing weakening of inter-particle bonds. Kelly and Gularte (1981) showed that for cohesive sediments, increasing temperature increases erosion rates, particularly at low salinity, while at high salinity, there is less of an effect on erosion. Furthermore, studies of streambank stability in cohesive materials (Casagli *et al.*, 1997; Rinaldi and Casagli, 1999; Simon *et al.*, 1999) led to the idea that positive and negative pore-water pressures may play an important role in the entrainment and erosion of cohesive streambed particles or aggregates (Simon and Collison, 2001). Negative pore-water pressures increase the shear strength of unsaturated, cohesive materials by providing tension between particles.

Cohesive materials can be eroded in three contrasting ways (Mehta 1991; Figure 3): (1) surface erosion of bed aggregates; (2) mass erosion of the bed; and (3) entrainment of fluid mud. Partheniades (1965) showed that clay resistance to erosion seemed to be independent of the macroscopic shear strength of the bed, provided that the bed shear stresses did not exceed the macroscopic shear strength of the material. Once the bed shear stress exceeds some critical value, then following Ariathurai and Arulanandan (1978) the rate of erosion,  $\varepsilon$ , of cohesive materials can be predicted by:

$$\varepsilon = \begin{cases} k_d \left( \frac{\tau_0}{\tau_c} - 1 \right)^a & \text{for } \tau_0 > \tau_c \\ 0 & \text{for } \tau_0 \leq \tau_c \end{cases} \quad (11)$$

where  $\varepsilon$  = erosion rate ( $\text{m s}^{-1}$ ),  $k_d$  = erosion rate coefficient ( $\text{m s}^{-1}$ ),  $\tau_0$  = bed shear stress (Pa),  $\tau_c$  = critical shear stress (Pa), and  $a$  = exponent assumed to equal 1.0. Equation 11 may also be written as (Partheniades, 1965):

$$\varepsilon = \begin{cases} \frac{k_d}{\tau_c} (\tau_0 - \tau_c) = k (\tau_0 - \tau_c) & \text{for } \tau_0 > \tau_c \\ 0 & \text{for } \tau_0 \leq \tau_c \end{cases} \quad (12)$$

where  $k$  = erodibility coefficient ( $\text{m}^3\text{N}^{-1}\text{s}^{-1}$ ), representing the volume of material eroded per unit force and per unit time.

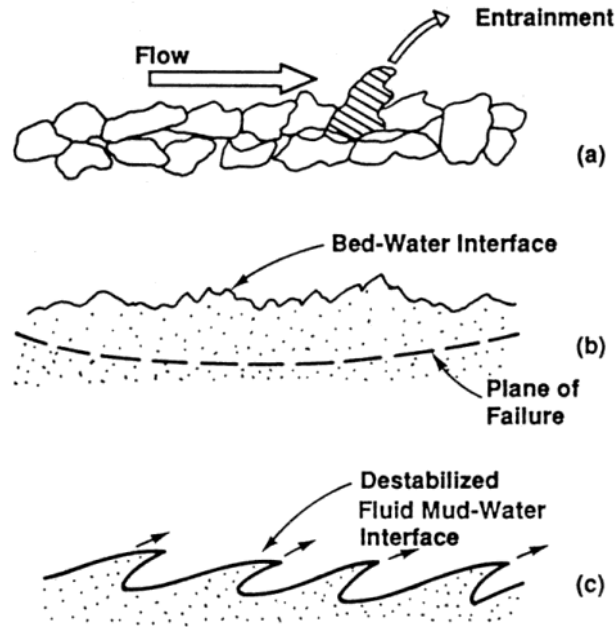


**Figure 3 – Three modes of cohesive sediment erosion: a) surface erosion of bed aggregates; b) mass erosion of the bed; c) entrainment of fluid mud (from Mehta, 1991).**

Both  $\tau_c$  and  $k$  are important parameters describing the resistance and erodibility of the materials and can be obtained indirectly from field measurements. A submerged jet-test has been developed by the Agricultural Research Service (Hanson, 1990; Figure 4) for testing the *in situ* erodibility of surface materials in the laboratory and in the field (ASTM, 1995). This device has been developed based on knowledge of the hydraulic characteristics of a submerged jet and the characteristics of soil-material erodibility. In an attempt to remove empiricism and to obtain direct measurements of  $\tau_c$  and  $k$ , Hanson and Cook (1997) developed analytical procedures for determining soil  $k$  based on the diffusion principles of a submerged circular jet and the corresponding scour produced by the jet. These procedures are based on analytical techniques developed by Stein *et al.* (1993) for a planar jet at an overfall and extended by Stein and Nett (1997). Stein and Nett (1997) validated this approach in the laboratory using six different soil types. As the scour depth increases with time, the applied shear stress decreases due to increasing dissipation of jet energy within the plunge pool. Detachment rate is initially high and asymptotically approaches zero as applied shear stress approaches the critical shear stress of the bed material. The difficulty in determining equilibrium scour depth is that the length of time required to reach equilibrium can be large. Blaisdell *et al.* (1981) observed during studies on pipe outlets that scour in cohesionless sands continued to progress even after 14 months. They developed a function to compute the equilibrium scour depth that assumes that the relation between scour and time follows a logarithmic-hyperbolic function. Fitting the jet-test data to the logarithmic-hyperbolic method described in Hanson and Cook (1997) can predetermine  $\tau_c$ .  $k$  is then determined by curve fitting measured values of scour depth versus time and minimizing the

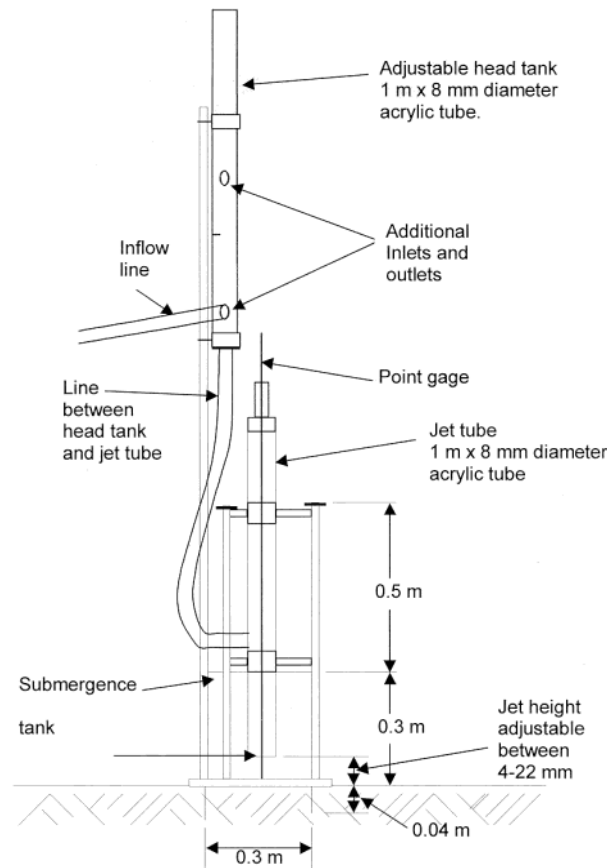


**Figure 4 – Schematic of jet-test device (from Hanson and Simon, 2001).**

error of the measured time versus the predicted time. Both  $k$  and  $\tau_c$  are treated as soil properties and the former does not generally correlate well with standard soil mechanical indices such as Atterberg limits. Instead,  $k$  is dependent on the physio-chemical parameters that determine the inter-particle forces characteristic of cohesive sediment (Parchure and Mehta, 1985; Mehta, 1991).

### ***Modeling Streambank Stability: The Bank-Stability and Toe-Erosion Model (BSTEM)***

The Bank Stability and Toe-Erosion Model (BSTEM; Simon *et al.* 1999) combines three limit-equilibrium methods that calculate the Factor of Safety ( $F_s$ ) of multi-layer streambanks.  $F_s$  is the ratio between the resisting and driving forces acting on a potential failure block. A value of unity indicates that the driving forces are equal to the resisting forces and that failure is imminent ( $F_s = 1.0$ ). Instability exists under any condition where the driving forces exceed the resisting forces ( $F_s < 1.0$ ), conditional stability is indicated by  $F_s$  values between 1.0 and 1.3, with stable bank conditions having a  $F_s$  value of  $>1.3$ . The methods employed within BSTEM are horizontal layers (Simon *et al.*, 1999), vertical slices with tension crack (Morgenstern and Price, 1965) and cantilever failures (Thorne and Tovey, 1981). All three methods account for the strength of up to five soil layers, the effect of pore-water pressure (both positive and negative), confining pressure due to streamflow and soil reinforcement due to vegetation. This description will focus upon the

first and third methods as the second method has not been used herein due to the absence of observed tension cracks in the field.

#### *Assessing Geotechnical Failure*

The bank-stability sub-model in the current version of BSTEM (dynamic version 5.4) incorporates a random walk search algorithm for the minimum  $F_s$ .  $F_s$  is given by:

$$F_s = \frac{\sum_{i=1}^I \left( [c'_i + c_r] L_i + (\mu_a - \mu_w)_i L_i \tan \phi_i^b + [W_i \cos \beta - \mu_{ai} L_i + P_i \cos(\alpha - \beta)] \tan \phi_i' \right)}{\sum_{i=1}^I (W_i \sin \beta - P_i \sin[\alpha - \beta])} \quad (13)$$

where  $c'_i$  = effective cohesion of  $i^{\text{th}}$  layer (kPa),  $L_i$  = length of the failure plane incorporated within the  $i^{\text{th}}$  layer (m),  $W_i$  = weight of the  $i^{\text{th}}$  layer ( $\text{kN m}^{-1}$ ),  $P_i$  = hydrostatic-confining force due to external water level ( $\text{kN m}^{-1}$ ) acting on the  $i^{\text{th}}$  layer,  $\beta$  = failure-plane angle (degrees from horizontal),  $\alpha$  = local bank angle (degrees from horizontal), and  $I$  = number of layers.

The cantilever shear failure algorithm results from inserting  $\beta = 90^\circ$  into equation 13.  $F_s$  is given by:

$$F_s = \frac{\sum_{i=1}^I \left( [c'_i + c_r] L_i + (\mu_a - \mu_w)_i L_i \tan \phi_i^b + [P_i \sin \alpha - \mu_{ai} L_i] \tan \phi_i' \right)}{\sum_{i=1}^I (W_i + P_i \cos \alpha)} \quad (14)$$

The  $F_s$  is therefore the ratio of the shear strength of the soil to the weight of the cantilever. The inclusion of  $\alpha$ -terms in equation 14 ensures that if the bank is partially or totally submerged, the weights of the layers affected by water are correctly reduced irrespective of the geometry of the basal surface of the overhang.

#### *Modeling Movement of the Groundwater Table*

It is apparent from equations 2, 3, 13 and 14 that the elevation of the groundwater table is an important parameter controlling soil shear strength. For the purposes of this study, a simplified one-dimensional (1-D) groundwater model, based on the 1-D Richards Equation, was developed to simulate the motion of the groundwater table. This model assumes that the dominant pressure gradient within a streambank is the difference between the groundwater table elevation and the in-channel water surface elevation (i.e., it neglects the influence of infiltrating precipitation) (e.g. Langendoen, 2010). Assuming that water infiltrates either into or out of the bank along a horizontal plane of unit length and computing distance-weighted mean soil properties between these two elevations, the simplified equation can be written as:

$$\frac{\partial h}{\partial t} - K_r K_{sat} |h - z|^2 = 0 \quad (15)$$

where  $h$  = groundwater elevation (m),  $z$  is the water surface elevation (m),  $t$  = time (s), and  $K_r K_{sat}$  = relative permeability  $\times$  saturated hydraulic conductivity.  $K_r$  is evaluated as  $K_r = \Theta^{1/2} \left[ 1 - (1 - \Theta^{1/b})^b \right]^2$ , where  $\Theta$  = soil saturation and, following van Genuchten (1980),  $\Theta$  is evaluated as:

$$\Theta = \Theta_r + \frac{\Theta_s - \Theta_r}{\left[ 1 + \left( \frac{[z - h]}{l} \right)^{1/m} \right]^m} \quad (16)$$

where the subscripts  $r$  and  $s$  denote the residual moisture content and saturated moisture content, and  $l$  and  $m$  are curve-fitting parameters. Note that if  $h \geq z$ ,  $K_r = 1$ .

### *Assessing Hydraulic Erosion*

The magnitude of bank-face, bank-toe and bed erosion and the extent of bank steepening by hydraulic forces are calculated using an algorithm that computes the hydraulic forces acting on either the left or right near-bank zone during a particular flow event. The boundary shear stress exerted by the flow on each node is estimated by dividing the flow area at a cross-section into segments that are affected only by the roughness of the bank or the bed and then further subdividing to determine the flow area affected by the roughness on each node (e.g., Einstein, 1942). The hydraulic radius of a segment,  $R_i$ , is the area of the segment,  $A_i$ , divided by the wetted perimeter of the segment. The boundary shear stress active at the node  $i$ ,  $\tau_{oi}$ , may then be estimated as:

$$\tau_{oi} = \rho g R_i S \quad (17)$$

Flow resistance in an open channel is a result of viscous and pressure drag over its wetted perimeter. For a vegetated channel, this drag may be conceptually divided into three components: (1) the sum of viscous drag on the ground surface and pressure drag on particles or aggregates small enough to be individually moved by the flow (grain roughness); (2) pressure drag associated with large non-vegetal boundary roughness (form roughness); and (3) drag on vegetal elements (vegetal roughness) (Temple *et al.*, 1987). As energy lost to the flow represents work done by a force acting on the moving water, the total boundary shear stress may also be divided into three components:

$$\tau_o = \tau_{og} + \tau_{of} + \tau_{ov} \quad (18)$$

where the subscripts  $g$ ,  $f$  and  $v$  signify the grain, form and vegetal components of the boundary shear stress, respectively.

If it is assumed that these components may be expressed in terms of a Manning's coefficient for each, and Manning's equation is assumed to apply for each component, equation 18 can be rewritten as (Temple, 1980):

$$n^2 = n_g^2 + n_f^2 + n_v^2 \quad (19)$$

where  $n$  = Manning's roughness coefficient ( $s\ m^{-1/3}$ ). Grain roughness is estimated for each node on the bank profile using the equation of Strickler (Chow, 1959):

$$n_g = 0.0417 (D_{50})^{1/6} \quad (20)$$

Combining equations 18 and 19, the effective boundary shear stress, the component of the boundary shear stress acting on the boundary in the absence of form and vegetal roughness, may be computed as:

$$\tau_g = \tau_o (n_g^2 / n^2) \quad (21)$$

The rate of erosion of bank-face, bank-toe and bed materials can then be calculated using equations 12 and 21 (Hanson, 1990). During the dynamic simulations described herein, the erosion distance during a time step is computed by multiplying the erosion rate within the time step by the time step size. It must be stressed that the model is incapable of routing flow and sediment, so that estimates of erosion are only valid for "clear-water" conditions where the amount of sediment being transported by the flow is lower than sediment transport capacity. That is no deposition on the bank toe of transported bed-material occurs. Field observations suggest that this is likely to be a reasonably safe assumption for the study reaches.

## DATA COLLECTION AND METHODS

### Introduction

Several different approaches were used during the course of this study. Aerial reconnaissance was initially carried out within the study area. With this comprehensive look at the study area, intensive sites were chosen to represent actively eroding sites, though landowner permission was a major consideration. An attempt was also made to equally distribute sites throughout the study area, both on the Missisquoi River main-stem and the seven tributaries being studied. Geotechnical data were collected at these intensive sites *in situ* and used as input parameters for streambank modeling with BSTEM-Dynamic, which was run for 30 years of flow data (1979-2009) to produce a sediment loading at each intensive modeling site. Total and daily suspended-sediment loadings from the streambanks at each site were broken down by particle size, and used to calculate loadings over 2-mile (3.2 km) reaches. In each case, the at-a-site BSTEM-Dynamic loading values obtained over the modeling period were then multiplied by the percent of each 2-mile reach that was observed to be actively failing, through aerial reconnaissance. In this way sediment loadings to Lake Champlain from the Missisquoi River Basin were quantified. In other words, if  $A_b$  is the at-a-site eroded bank volume per unit length of channel ( $\text{m}^3/\text{m}$ ) calculated by BSTEM over a given simulation period ( $T$  in years) and  $\text{PRF}_L$  and  $\text{PRF}_R$  represent the percent of a 2-mile reach that is actively failing along the left and right channel banks, respectively, the resulting average annual sediment loading (AASL) from streambanks calculated for each 2-mile reach is:

$$\text{AASL} = 1,000 A_b (\text{PRF}_L + \text{PRF}_R) / T \quad (22)$$

The unit of AASL is  $\text{m}^3/\text{km}/\text{yr}$ . As the grain-size distribution of the calculated eroded bank-material is known, the AASL for each particle size class (clay, silt, sand, etc.) can be calculated separately. The latter information is used to determine suspended sediment and phosphorus loadings at the downstream end of the studied reach.

Appendix A presents the 2-mile reaches and the study site used for each reach. This section concentrates on fieldwork used to establish geotechnical streambank conditions supporting numerical modeling. Brief descriptions of computational techniques and other input data to support BSTEM modeling that have not already been outlined are also included in this section.

### Rapid Geomorphic Assessments: RGAs

Current stability conditions within the Missisquoi River basin were examined using diagnostic criteria of contemporary geomorphic processes. These are called rapid geomorphic assessments (RGAs). RGAs use diagnostic criteria of channel form to infer dominant channel processes and the magnitude of channel instabilities through a series of questions. RGAs provide an efficient method of assessing in-stream geomorphic conditions, enabling the rapid characterization of the stability of long reaches of channel systems. Evaluations of this sort do not include an evaluation of watershed or upland conditions but because stream channels act as conduits for energy, flow and materials for the entire watershed, they reflect the balance or imbalance in the delivery of

sediment. Through observations of erosion, deposition and the condition of riparian vegetation, RGAs can therefore provide indications of channel stability.

An RGA was carried out at each site using the channel-stability ranking scheme to evaluate channel-stability conditions and stage of channel evolution. Figure 5 shows an example of an RGA form filled out for study site M2. Each criterion was ranked from zero to four and all values summed to provide an objective index of relative channel stability. The higher the number, the greater the instability. Based on vast experience conducting these assessments, sites with values greater than 20 exhibit significant instability with unstable banks and generally high erosion rates. Stable sites generally have an index of 10 or less. Intermediate values denote reaches of moderate instability. However, rankings are not weighted, thus a site ranked 20 is not twice as unstable as a site ranked 10. In practice, therefore, an RGA score of greater than 20 indicates that the channel is unstable, exhibiting widespread occurrence of the features and processes that would be associated with this condition (i.e., incision of the bed and mass wasting of the streambanks). Conversely, RGA scores of less than 10 indicate that a reach is predominantly stable and that the system is close to equilibrium in terms of energy and sediment supply, with limited incision or bank widening. For sites with an RGA score between 10 and 20, some instability was found within the reach, but areas of mass wasting, for example, were more isolated than in a reach with an RGA score of greater than 20. Appendix B summarizes the channel stability ranking for each intensive study site.

The RGA procedure consists of four steps to be completed on site:

1. Determine the extent of the 'reach'. The 'reach' is described as the length of channel covering 6-20 channel widths, thus is scale dependent and should cover at least two pool-riffle sequences.
2. Take photographs looking upstream, downstream and across the reach for quality assurance and quality control purposes. Photographs are used with RGA forms to review the field evaluation.
3. Make observations of channel conditions and diagnostic criteria listed on the channel-stability ranking scheme.
4. Sample bed material for later characterization of the grain size distribution.

### **Field Data Collection**

As bank stability is a function of the strength of the bank material to resist collapse under gravity, measurements of the components of shearing resistance (or shear strength) were required. *In-situ* tests of the shear strength of bank materials at intensive sites were conducted using a borehole shear-test device (BST; Lohnes and Handy, 1968). In addition, tests of the resistance of cohesive bank-toe materials to erosion by flowing water were carried out using a jet-test device, or particle size determined in the case of non-cohesive materials. Bank surveys were conducted at each site. Data obtained in the field were used as inputs to BSTEM-Dynamic to determine critical conditions for bank stability.

**CHANNEL-STABILITY RANKING SCHEME**

Station Name <i>Miss - Montane</i>	Station Description <i>On Montane farm R. Bank</i> <i>N. 44.9231</i> <i>W. 73.06344</i>
---------------------------------------	--

Date <i>10/26/09</i>	Time (24 hour) <i>10:05</i>	Crew <i>BB</i>	Samples	% PC	% PS	<i>No Bed samples</i>
Pictures (circle) <i>U/S</i> <i>D/S</i> <i>cross section</i> <i>bankfull</i>						
Survey (circle) <i>Thalweg</i> <i>Bankfull</i> <i>Survey ref. point</i> <i>TBM</i>						

*W. surface ~ 16 channel widths in boat + Bank profile*

*Lots of 'natural mining' from previous grass-covered failures*

1. Primary bed material
 

Bedrock	Boulder/Cobble	Gravel	Sand	Silt Clay	Sub-total
0	1	<i>2</i>	<i>3</i>	4	<i>2.5</i>

*Wakaputa From staci*
2. Bed/bank protection
 

Yes	No	(with)	1 bank	2 banks	
0	<i>1</i>		2	3	<i>1</i>
3. Degree of incision (Relative elevation of "normal" low water; floodplain / terrace @ 100%)
 

0-10%	11-25%	26-50%	51-75%	76-100%	
4	3	2	<i>1</i>	0	<i>1</i>

*depth? ~ 3m deep from staci*
4. Degree of constriction (Relative decrease in top-bank width from up to downstream)
 

0-10%	11-25%	26-50%	51-75%	76-100%	
<i>0</i>	1	2	3	4	<i>0</i>
5. Stream bank erosion (Each bank)
 

	None	Fluvial	Mass wasting (failures)	
Left	0	<i>1</i>	<i>2</i>	<i>1.5</i>
Right	0	<i>1</i>	<i>2</i>	<i>1.5</i>

*Equal amounts on both No real dominant process*
6. Stream bank instability (Percent of each bank failing)
 

	0-10%	11-25%	26-50%	51-75%	76-100%	
Left	0	<i>0.5</i>	1	1.5	2	<i>0.5</i>
Right	0	<i>0.5</i>	1	1.5	2	<i>0.5</i>
7. Established riparian woody-vegetative cover (Each bank)
 

	0-10%	11-25%	26-50%	51-75%	76-100%	
Left	2	1.5	1	0.5	<i>0</i>	<i>0</i>
Right	2	1.5	1	<i>0.5</i>	0	<i>0.5</i>
8. Occurrence of bank accretion (Percent of each bank with fluvial deposition)
 

	0-10%	11-25%	26-50%	51-75%	76-100%	
Left	<i>2</i>	1.5	1	0.5	0	<i>2</i>
Right	<i>2</i>	1.5	1	0.5	0	<i>2</i>
9. Stage of channel evolution
 

I	II	III	IV	V	VI	
0	1	2	4	<i>3</i>	1.5	<i>3</i>

*almost a V trough - not a box going on*

Total Rank	<i>16</i>
------------	-----------

10. Condition of adjacent side slope (circle)    N/A    Bedrock    Boulders    *Gravel SP*    *Fines*
11. Percent of slope (length) contributing sediment    *Left 20%*    *Right 25%*
12. Severity of side-slope erosion    None    *Low*    Moderate    High

**Figure 5 – Example RGA form filled out for study site M2.**

**Geotechnical Data Collection: Borehole Shear Tests**

To gather data on the internal shear strength properties of the banks, *in-situ* Borehole Shear Test (BSTs) devices were used. To properly determine the resistance of cohesive materials to erosion

by mass movement, data must be acquired on those characteristics that control shear strength; that is cohesion, angle of internal friction, pore-water pressure, and bulk unit weight. Cohesion and friction angle data can be obtained from standard laboratory testing (triaxial shear or unconfined compression tests), or by *in-situ* testing with a borehole shear-test (BST) device (Lohnes and Handy 1968; Thorne *et al.* 1981; Little *et al.* 1982; Lutenegger and Hallberg 1981). The BST provides direct, drained shear-strength tests on the walls of a borehole (Figure 6). Advantages of the instrument include:

1. The test is performed *in situ* and testing is, therefore, performed on undisturbed material.
2. Cohesion and friction angle are evaluated separately with the cohesion value representing apparent cohesion ( $c_a$ ). Effective cohesion ( $c'$ ) is then obtained by adjusting  $c_a$  according to measured pore-water pressure and  $\phi^b$ .
3. A number of separate trials are run at the same sample depth to produce single values of cohesion and friction angle based on a standard Mohr-Coulomb failure envelope.
4. Data and results obtained from the instrument are plotted and calculated on site, allowing for repetition if results are unreasonable; and
5. Tests can be carried out at various depths in the bank to locate weak strata (Thorne *et al.* 1981).

At each testing depth, a small core of known volume was removed and sealed to be returned to the laboratory. The samples were weighed, dried and weighed again to obtain values of moisture content and bulk unit weight, both required for analysis of streambank stability. Bulk particle size samples were also taken at each depth and tested in order to classify materials.

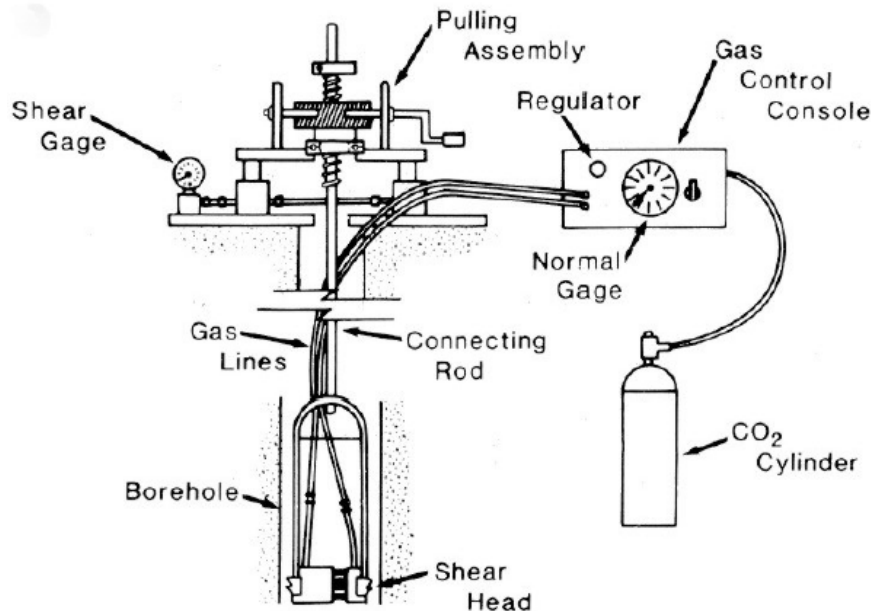


**Figure 6 – Schematic representation of borehole shear tester (BST) used to determine cohesive and frictional strengths of *in-situ* streambank materials. Modified from Thorne *et al.*, 1981.**

### Erosion-Resistance Data Collection: Submerged Jet Test Device

Resistance properties of the bank-toe and face are input properties of the bank stability model. Where materials are non-cohesive, a bulk particle size or particle count are sufficient to describe resistance properties. However, cohesive materials are not entrained into the water column predictably due to particle size, as a result of electro-chemical bonds between particles. In order to test *in-situ* erodibility of cohesive materials, a submerged jet-test has been developed by the Agricultural Research Service (Figure 7) and is described in the “*Mechanisms of Cohesive Sediment Erosion*” Section. The mini-jet apparatus consists of an electric submersible 950 GPH pump powered by a portable A/C generator, a scaled-down 0.15 m-diameter submergence tank with an integrated, rotatable 3.18 mm-diameter nozzle and depth gauge, and delivery hoses. The nozzle is submerged within a cylindrical tank that is driven into the *in situ* material. The initial height of the nozzle above the streambed is noted and can be easily adjusted prior to initiating a test. Changes in maximum scour are measured using a point gauge at specific time increments and an asymptotic regression fitted to the erosion curve to calculate an initial point of entrainment, or material critical shear stress.

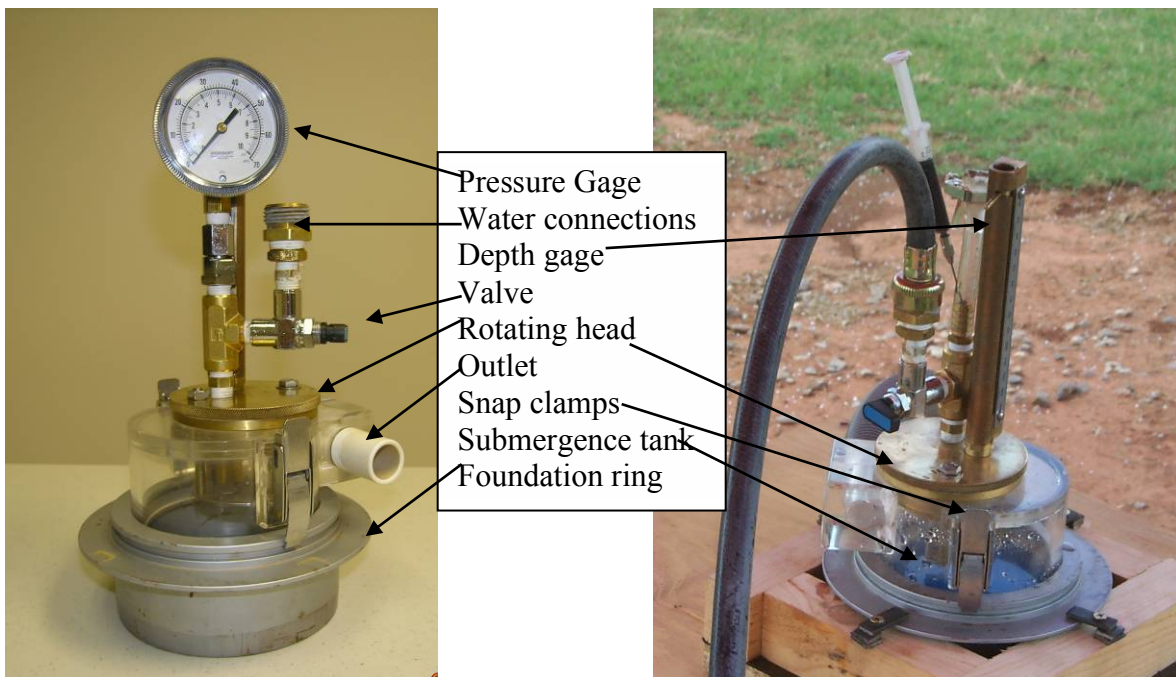


**Figure 7 – Photographs of the scaled-down mini-jet submerged jet test device, used *in situ* to measure soil erodibility.**

### Estimating Percent Reach Failing Using a Modified RGA

The length of the Missisquoi River and main tributaries that fell within the study reach were videoed from a low-flying helicopter. Video recorders were geo-referenced with an attached GPS. From these videos it was possible to characterize active geomorphic processes and relative

stability along different sections of the study reach, for example, by observing bank failures, and areas of significant aggradation. Modified Rapid Geomorphic Assessments (MRGAs; Bankhead and Simon, 2009) were conducted on 2-mile reaches, establishing the longitudinal extent of recent streambank failures. This was quantified as the percent of the reach failing as estimated from the video taken during air reconnaissance. These percentages were broken into classes (0-10, 11-25, 25-50, 51-75 and 76-100) and used as a measure of the severity of bank instability and when mapped, the extent of that instability. Photographs showing example reaches in these percent reach failing classes are shown in Figure 8.

Figure 9 maps the maximum percent of reach failing for the 2-mile reaches. Most banks are failing in the headwaters above river kilometer 100 and along the main stem between river kilometer 50 and river kilometer 60. Figure 10 plots left bank ( $PRF_L$ ), right bank ( $PRF_R$ ), and average percent reach failing for 2-mile reaches along the main stem of the Missisquoi River. The average percent of reach failing increases nearly linearly with river kilometer from about 15% (class 2) to about 70% (class 4) at river kilometer 140. Only a few reaches have values exceeding 75% (class 5): (a) left banks between river kilometer 121-127 and 131-134; and (b) right banks between river kilometer 111-114, 131-134, and 140-143.

Percent reach failing could not be determined for the small tributaries on which study sites HB2 and TY3 were located. Because these study sites only showed minor to no erosion locally, their respective tributaries were omitted from the BSTEM analysis.

### **Soil Shear Strength Characterization: Measuring Root Reinforcement**

Roots of Silver maple and Reed canarygrass were measured using a device called the Root-Puller (Figure 11), based on a design by Abernethy and Rutherford (2001). This is comprised of a metal frame with a winch attached to a load cell and displacement transducer and an in-field data logger. The Root-Puller is attached to the bank face and different-sized roots. Cranking the winch applies a tensile strength to the root (measured as a load, in Newtons) that increases until tensile failure of the root occurs. The diameter of each root is recorded along with the logged history of tensile strength and shear displacement. The maximum load applied to each root before breaking and root diameter were used to calculate the strength of each root. Root diameter-strength relations were established for the two species to use as input to the fiber-bundle root-reinforcement model, RipRoot (Pollen and Simon, 2005; Pollen, 2007; Thomas and Pollen-Bankhead, 2010).

0 to 10 % reach failing – riprap protects toe and bank face from hydraulic scour and steepening of bank. Little to no erosion.



11 to 25 % reach failing – localized failures occurring in this reach.



51 to 75 % reach failing – parts of this outer bendway are eroding, where not protected by banktop and/or bankface vegetation.



76 to 100 % reach failing – in this photo the entire outer bank of the bendway is eroding.



**Figure 8 – Examples of different percent reach filing classes within the Missisquoi River Basin study area.**

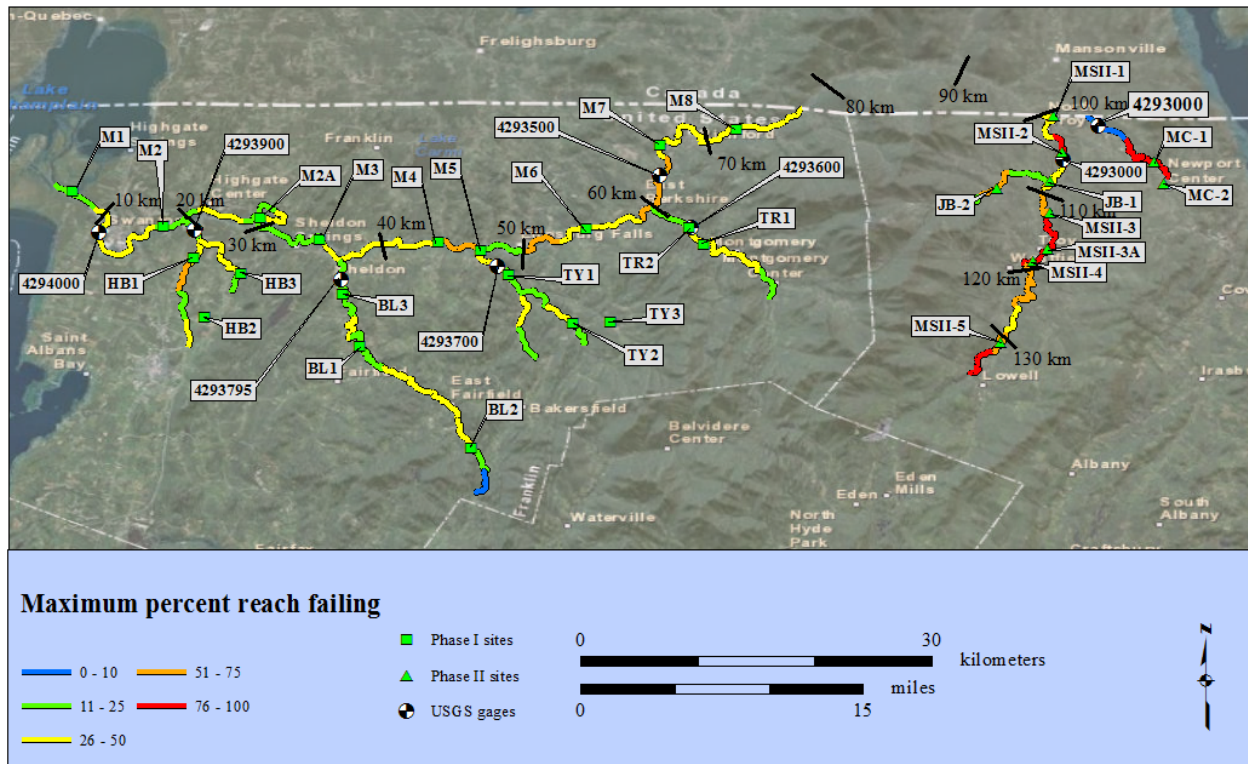


**Figure 9 – Maximum percent of reach failing for the Missisquoi River and its tributaries.**

Root tensile strength data collected for Reed canarygrass was compared to data collected for the same species at other riparian locations throughout the USA. The data were shown to be within the same population and so were added to the overall dataset for this species. Tensile strength measurements were not taken for Speckled alder because the root architecture of the plants at bankfaces made them hard to study. Most of the roots were found to be growing directly back into the bank, with only dead, and therefore, brittle roots being exposed at the bank face. Brittle roots are not suitable for tensile strength testing, as the cell walls and cellulose within the roots have broken down, and results from this sub-set of roots would not be representative of live roots growing within the streambank. A tensile strength curve for Speckled alder was therefore taken from the RipRoot database which contained data from another genus of Alder sampled in western USA. Enough silver maple roots were sampled to be able to add this species to the database of root diameter-tensile strength curves within RipRoot (Figure 12).

Root systems of all three riparian species were also examined and recorded using the wall-profile method (Bohm, 1979). Root diameters were measured and recorded according to depth in the bank profile. The root density associated with a range of ages of each tree species were also recorded, so that changes in rooting density and root diameter distributions over time could be modeled within RipRoot and BSTEM.

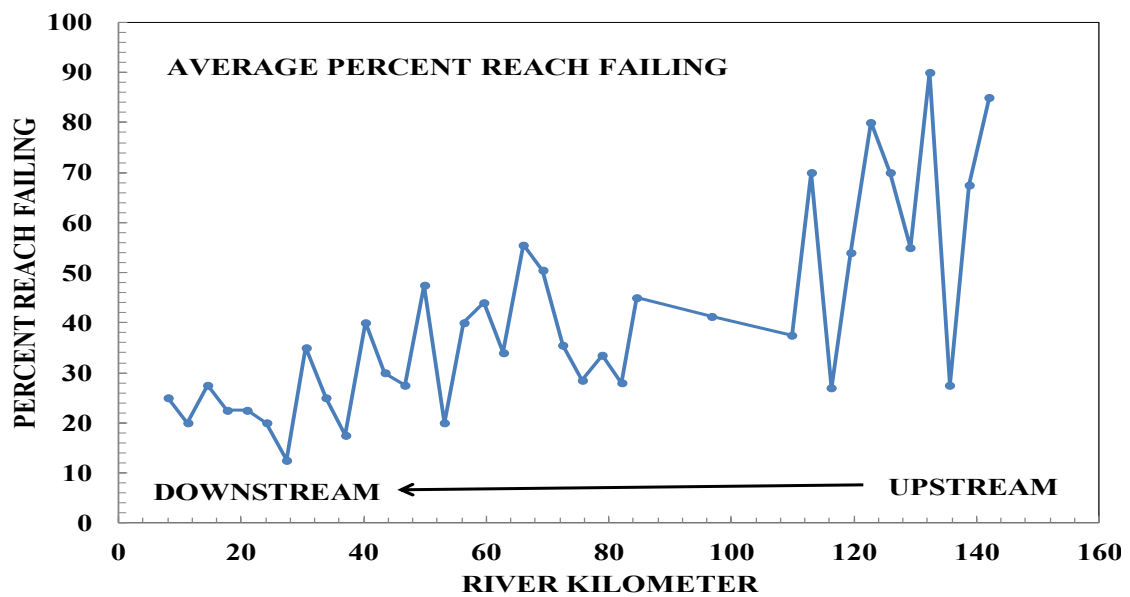
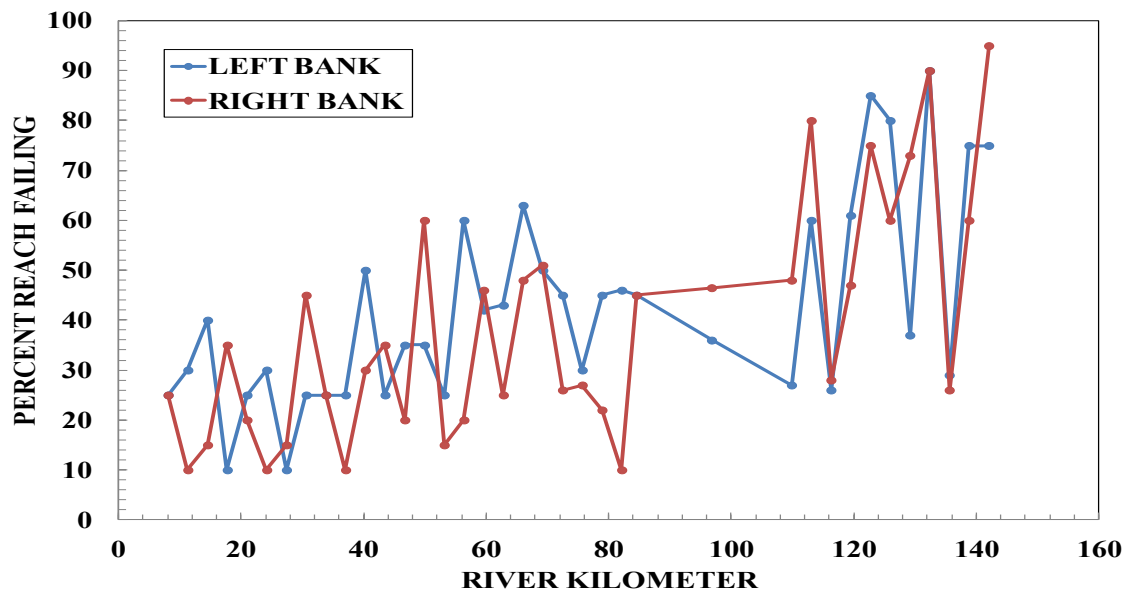
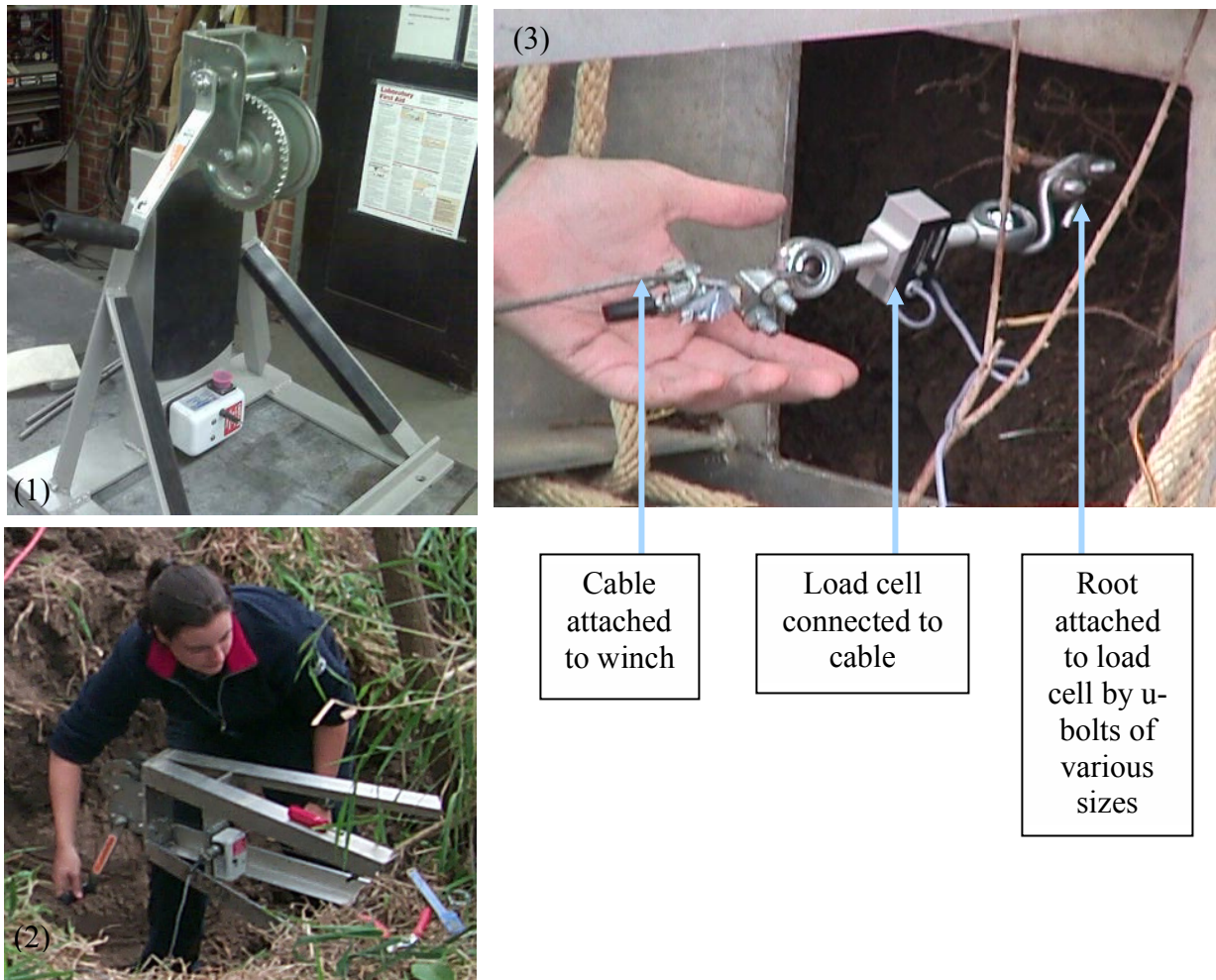


Figure 10 – Percent of reach failing for the Missisquoi River main stem: (top) left and right bank, (bottom) reach average.



**Figure 11 - Photos of the Root-Puller constructed at the USDA-ARS-NSL: (1) shows the most recent puller during construction phase before winch cable has been added; (2) shows original large puller built by USDA-ARS-NSL being used in the field to measure the strength of riparian tree roots; and (3) shows a close-up of the way that the load cell and roots are connected to the winching cable.**

To model existing bank conditions, at each intensive BSTEM modeling site the vegetation composition on the bank being studied was noted. In the model runs, where significant grasses or woody vegetation were present, root-reinforcement was estimated using site-specific species assemblages in RipRoot, and added to the effective cohesion value for relevant layers in the bank. To account for different vegetation scenarios in the BSTEM mitigation runs, the root density and root diameter distribution data collected in the field were used to calculate the average number of roots present in each diameter size class, at different stages of growth (Table 2). In one set of mitigation runs this involved calculating the root diameter distribution and density for a species assemblage composed of 25% each of 25-year-old Speckled alder, Silver maple, Sandbar willow, and 5-year old Reed canarygrass. This species assemblage was added to runs that tested existing bank geometries with a mature riparian corridor. A second set of

mitigation runs utilized a species assemblage composed 25% each of the same species, but for 5-year old plants, growing on the bank face and bank top of 2:1 graded banks.

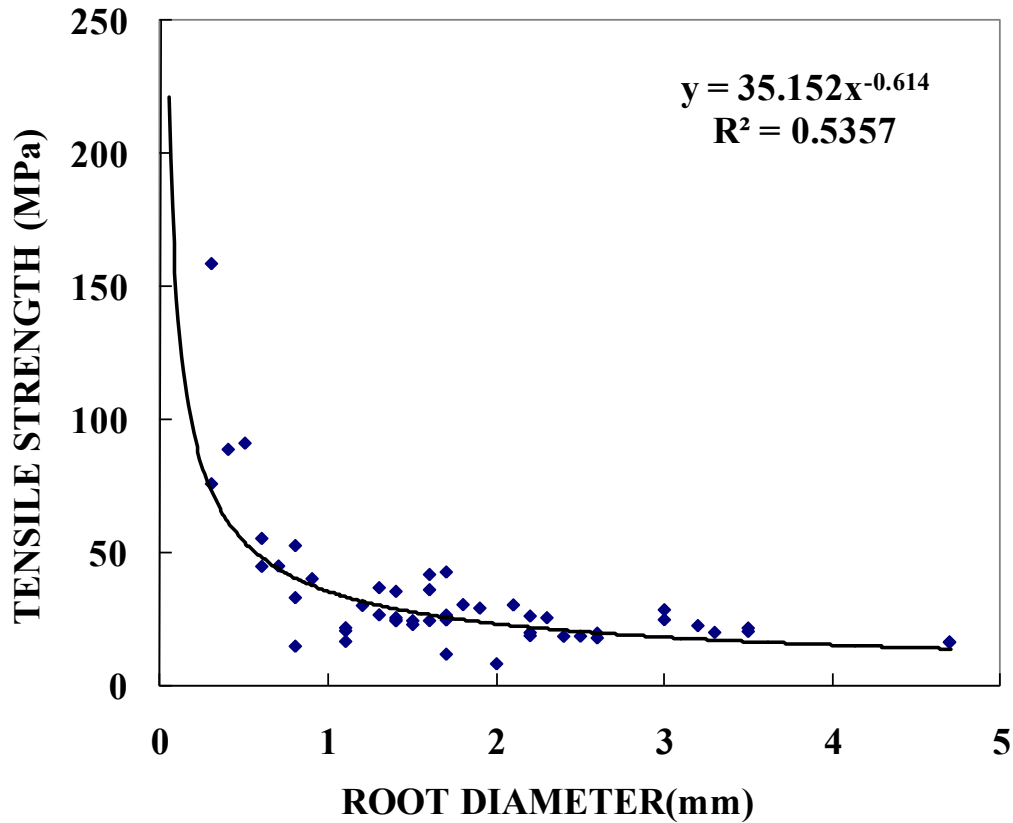


Figure 12 – Tensile strength curve for Silver Maple.

### Hydrologic Data

One of the key driving variables controlling the adjustment of a stream channel is the hydrologic regime. A number of instrumented US Geologic Survey (USGS) stream gages exist in the basin. Unfortunately only two gages on the main-stem Missisquoi River had a sufficiently long period of record to cover the entire modeling period, 10/1/79 to 9/30/10: 04293000 (MISSISQUOI RIVER NEAR NORTH TROY, VT) and 04293500 (MISSISQUOI RIVER NEAR EAST BERKSHIRE, VT). For sites near these two gages on the main-stem, a drainage basin area analysis was carried out and discharges scaled accordingly (Table 3). For sites on the lower main-stem and tributaries, flow data calculations were then twofold:

- 1) A regression was created between short- and long-term gages in order to ‘extend’ the flow series to the full 30-year modeling period.
- 2) Drainage basin area analysis enabled extrapolation of flow data from gages to intensive sites.

**Table 2 – Root tensile strength and root diameter distribution data used for input to the RipRoot model in BSTEM.**

Tree specie	Tensile strength curve parameters	
	<i>a</i>	<i>b</i>
SPECKLED ALDER	21.58	-0.8
SILVER MAPLE	35.2	-0.61

Tree specie	Root Diameter Size Classes						
	<1 mm	1 to 2 mm	2 to 3 mm	3 to 5 mm	5 to 10 mm	10 to 20 mm	>20 mm
5 year SPECKLED ALDER (25% of assemblage)	22	26	19	5	8	4	1
mature SPECKLED ALDER (25 % of assemblage)	67	46	22	24	12	7	2
5 year SILVER MAPLE (25% of assemblage)	27	15	6	3	2	2	1
mature SILVER MAPLE (25% of assemblage)	116	20	6	2	2	1	1

In most cases, both long-term gages were plotted against the measured gage discharge data and a regression determined (Figure 13). These regressions were then used to calculate discharges for the measured time period and the data compared both visually with time series graphs and by calculation of percentiles using the two regressions (Figure 14, Table 4). The regression which most closely ‘predicted’ the measured time period discharge data was then used (Figure 15). When comparing percentiles of measured and calculated discharges, an attempt was made to ensure that, in general, infrequent channel forming flows were matched more closely than low discharge frequent flows. This is because when modeling bank stability, although the largest events are not *always* correlated with mass failure events, the drawdown that occurs after peak flows do often correspond to critical conditions for bank instability. Correctly characterizing the peak flows and their drawdown rates is therefore an important component of the hydrologic regime to capture. In some cases, where calculated peak values were not well represented by regression calculations, an adjustment factor was established to better represent peak discharge events. The adjustment factor was determined by calculating the ratio between measured and predicted discharge values over an arbitrary peak value. Where appropriate, ratios were calculated for different categories of peak discharge. Averages were taken of the ratio factor and used to multiply calculated discharge values once the regression had been applied. In this way, greater peaks at tributary sites were accounted for, however it is noted that there may have been time lags between calculated and real-time site values as discharges for tributaries were calculated from main-stem gages.

**Table 3 – Nearest USGS gage to each site with discharge data and time period for which these discharge data were available. Table also provides USGS gage used to extrapolate discharge to modeled time period, where only a short time period was available from the nearest gage.**

Site	Drainage basin area in km <sup>2</sup>	Nearest USGS gage		USGS gage used to extrapolate discharge data
		Number	Time period	
M1	2230	04294000	1990-present	04293500
M2	2171	04294000	1990-present	04293500
M2a	2092	04294000	1990-present	04293500
M3	2076	04294000	1990-present	04293500
M4	1708	04293500	1928-present	04293500
M5	1539	04293500	1928-present	04293500
M6	1493	04293500	1928-present	04293500
M7	1218	04293500	1928-present	04293500
M8	1011	04293500	1928-present	04293500
MSII-1	357	04293000	1931-present	04293000
MSII-2	346	04293000	1931-present	04293000
MSII-3	264	04293000	1931-present	04293000
MSII-3a	256	04293000	1931-present	04293000
MSII-4	220	04293000	1931-present	04293000
MSII-5	121	04293000	1931-present	04293000
TR2	204	04293600	2009-2011	04293500
TR1	184	04293600	2009-2011	04293500
TY1	142	04293700	2009-2011	04293000
TY2	26	04293700	2009-2011	04293000
BL3	304	04293795	2009-2011	04293500
BL1	217	04293795	2009-2011	04293500
BL2	66.9	04293795	2009-2011	04293500
HB1	12.9	04293900	2009-2011	04293500
HB3	9.73	04293900	2009-2011	04293500
JB-1	62.1	-	-	04293000
JB-2	36.0	-	-	04293000
MC-1	71.5	04293200	2009-2011	04293000
MC-2	21.1	04293200	2009-2011	04293000

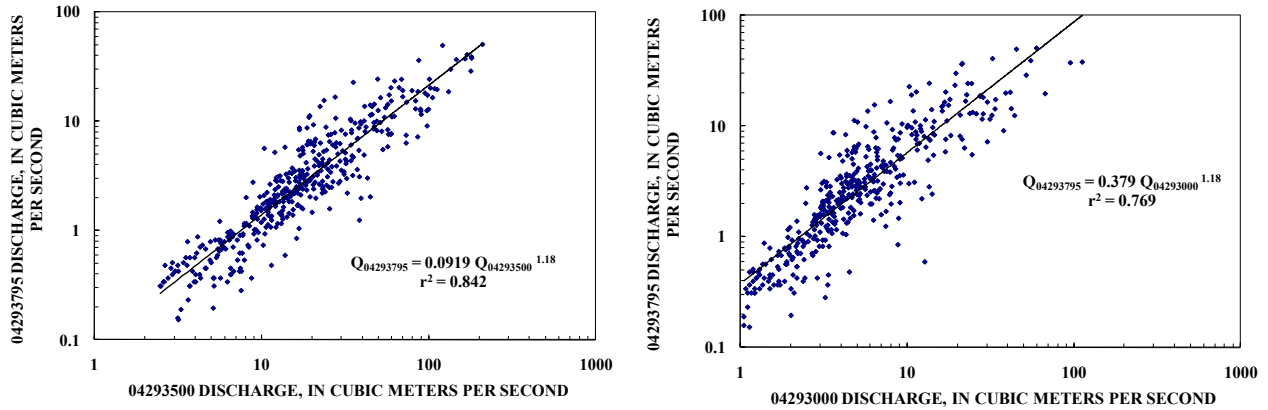


Figure 13 – In order to develop regressions with which to extrapolate discharge data at USGS gauging stations where a short period of record existed, measured data at these stations were plotted against both long-term gages, 04293500 and 04293000.

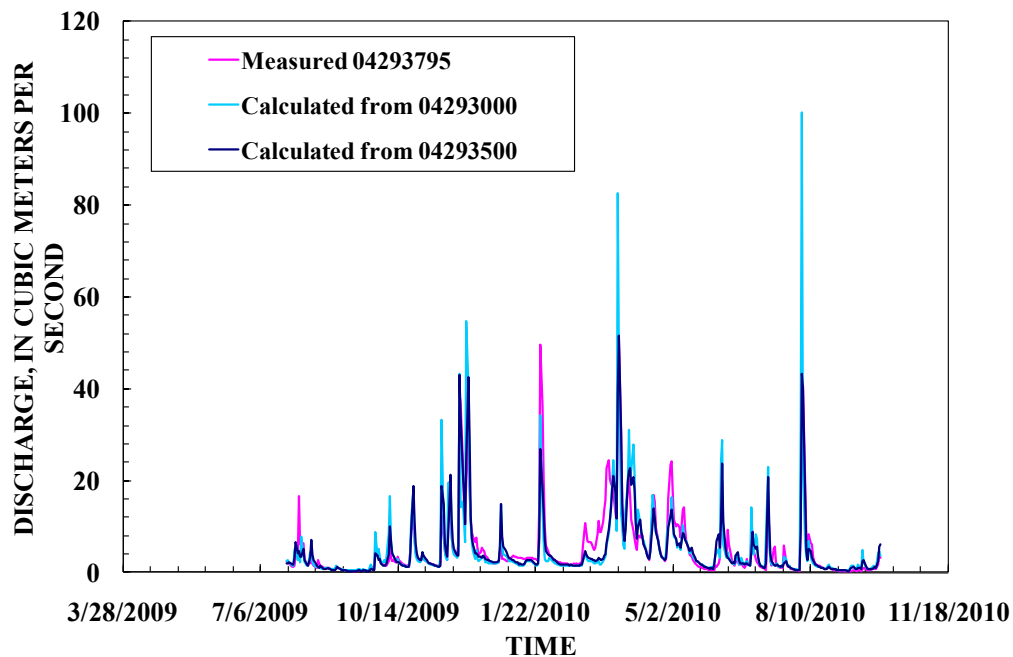
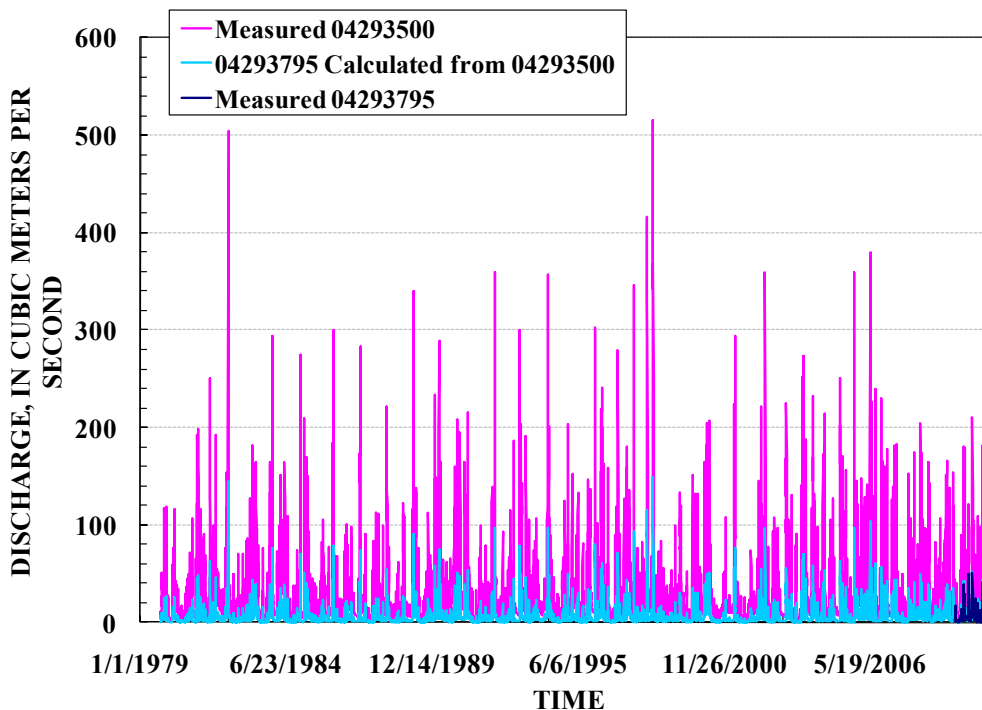


Figure 14 – Visual comparison between discharges calculated based on upper and mid-mainstem USGS gages was part of the methodology used to determine which gage was used to extrapolate measured discharge values to the modeled time period.

**Table 4 – Comparison of percentile values of measured and extrapolated discharges (at USGS gage 04293795) based on upper and mid main-stem USGS gages.**

Percentile	Measured discharge at 04293795 cms	Calculated discharge from 04293500 cms	Calculated discharge from 04293000 cms
10	0.510	0.644	0.782
25	1.22	1.36	1.40
50	2.49	2.52	2.27
75	6.03	5.03	4.54
90	12.9	11.2	11.0
95	18.9	18.8	19.2
98	29.3	27.8	31.2
99	37.8	39.6	42.3
99.9	50.2	47.9	92.6
100	50.7	51.5	100



**Figure 15 – Modeled time period discharge data for gage 04293795 as extrapolated from mainstem gage 04293500.**

### **Bank-Stability Modeling using BSTEM-Dynamic**

Twenty-seven of the original 30 intensive sites were modeled along the mainstem of the Missisquoi River and its tributaries. Study sites M5, HB2, and TY3 were not modeled. As mentioned in the section “Estimating Percent Reach Failing Using a Modified RGA” sites HB2 and TY3 were not modeled because percent reach failing could not be determined for their respective tributaries. As observed bank erosion near these study sites was minor, it was assumed that these small tributaries did not contribute significantly to suspended load and phosphorus concentrations in the stream. At study site M5 the Missisquoi runs against a ridge exposing toe material from a large rotational failure that is not representative for the longer section of river between sites M4 and M6. Sites M4 and M6 are therefore used to quantify streambank erosion loadings near study site M5 (see also Appendix A).

The first set of model runs was conducted to establish existing conditions of bank instability, sediment and phosphorus loadings. For the existing condition model runs, bank geometries recorded during cross sectional surveys taken at each site as part of this project were used as the initial bank geometry input. Discharge data for the period 10/1/79 to 9/30/10 were used in combination with the cross sectional channel geometry, and channel slope measured at each site, to calculate mean daily stage for each BSTEM timestep. The dominant vegetation recorded at each site was also accounted for in the RipRoot root-reinforcement algorithm in BSTEM (Table 5). In most cases existing vegetation consisted of Reed canarygrass, willow spp, Speckled Alder and Silver Maple.

The at-a-site sediment loadings output from the thirty-year simulations were then used to estimate phosphorus loadings emanating from streambanks. Phosphorus loadings were calculated from sediment loadings by applying the measured weighted mean-by-depth phosphorus concentrations in the soil to the portion of the bank sediment load fraction measuring 2 mm or less. At-a-site sediment and phosphorus loadings from the streambanks were then converted to annual loading rates before being extrapolated from site loadings to reach length loadings using Eq. (22). In this way we were able to produce average annual sediment and phosphorus loadings emanating from streambanks for the entire study reach. Depth-averaged Total Phosphorus (TP) concentrations (not Mehlich-3) were supplied by Stone Environmental Inc. as part of the report “Modeling Efforts and Identification of Critical Source Areas of Phosphorus Within the Vermont Sector of the Missisquoi Bay Basin” by Howe *et al.* (2011).

This modeling and extrapolation process was then repeated for three sets of alternative bank conditions (Figure 16):

- i) Grading the banks to 2:1 slopes;
- ii) Grading the banks to 2:1 slopes, and planting riparian vegetation;
- iii) Existing bank geometries with a mature (25-yr-old) riparian corridor.

**Table 5 – Root-reinforcement input values for existing and mitigated conditions.**

Creek	Site	RR cohesion added to top 1m (kPa)	RR cohesion added to top 1m (kPa)	RR cohesion added to all layers (kPa)
		EXISTING RIPARIAN VEGETATION	25-yr-old MATURE RIPARIAN CORRIDOR ON BANK TOP	5-yr-old RIPARIAN VEGETATION ON 2:1 SIDE- SLOPE
Black	BL1	2.60	6.99	3.08
Black	BL2	0.40	7.75	3.86
Black	BL3	2.40	7.35	3.54
Hungerford	HB1	0.50	8.32	4.37
Hungerford	HB3	2.60	7.50	3.98
Missisquoi	M1	1.60	6.99	3.10
Missisquoi	M2	0.30	1.98	0.53
Missisquoi	M2A	1.00	2.59	1.27
Missisquoi	M3	2.60	4.04	1.98
Missisquoi	M4	2.30	7.73	5.15
Missisquoi	M6	2.70	6.40	3.54
Missisquoi	M7	2.60	4.54	2.17
Missisquoi	M8	1.80	3.09	1.51
Trout	TR1	2.70	5.14	2.44
Trout	TR2	1.40	6.75	3.05
Tyler Branch	TY1	1.50	7.24	3.14
Bogue Branch	TY2	2.60	3.78	1.85
Jay Branch	JB-1	0.20	4.44	2.15
Jay Branch	JB-2	2.40	2.14	1.05
Missisquoi	MSII-1	0.30	6.43	2.96
Missisquoi	MSII-2	2.60	4.94	2.18
Missisquoi	MSII-3	2.50	4.24	2.07
Missisquoi	MSII-3a	0.70	8.06	4.32
Missisquoi	MSII-4	1.70	5.40	2.38
Missisquoi	MSII-5	0.40	6.24	2.78
Mud Creek	MC-1	2.60	7.44	3.17
Mud Creek	MC-2	2.60	8.08	4.25

In set i) the bank-top vegetation used in the existing runs was applied, with root-reinforcement therefore being added to just the top meter of the soil profile. The 2:1 bank side slopes were assumed to be bare of vegetation. In set ii) it was assumed that a 5-year-old vegetation

assemblage composed 25% each of Silver maple, Speckled alder, Reed canarygrass and willow spp., had been allowed to establish on the 2:1 bank slopes. Root-reinforcement was therefore added to the entire bank profile in this set of runs (Table 5). In addition, the roughness of the channel was modified to account for the increased bank roughness provided by the 5-year side-slope vegetation; at main stem sites Manning’s  $n$  was increased by 0.01 from the existing condition runs, and on the tributaries by 0.02. Roughness values were increased more at the tributary sites than on the main stem sites as at narrower cross-sections, the proportion of the channel wetted-perimeter affected by the side-slope vegetation is greater than for wide channel cross-sections. By increasing channel roughness the shear stresses exerted on the banks in the hydraulic erosion algorithm were reduced, in addition to the geotechnical reinforcing effect of the roots provided in the bank stability algorithm. In set iii) the existing bank geometries were used, but a 25-year-old species assemblage of Silver maple, Speckled alder, Reed canarygrass and willow spp., was applied to the top of the bank, with root-reinforcement being added to the top meter of each streambank. Roughness values in this set of runs were not modified from the existing conditions runs as the riparian corridor was considered to be growing on the bank top. Increases in root-reinforcement for 25-year-old species with respect to 5-year-old species are caused by increased root biomass (see Table 2 and Section “Soil Shear Strength Characterization: Measuring Root Reinforcement”).

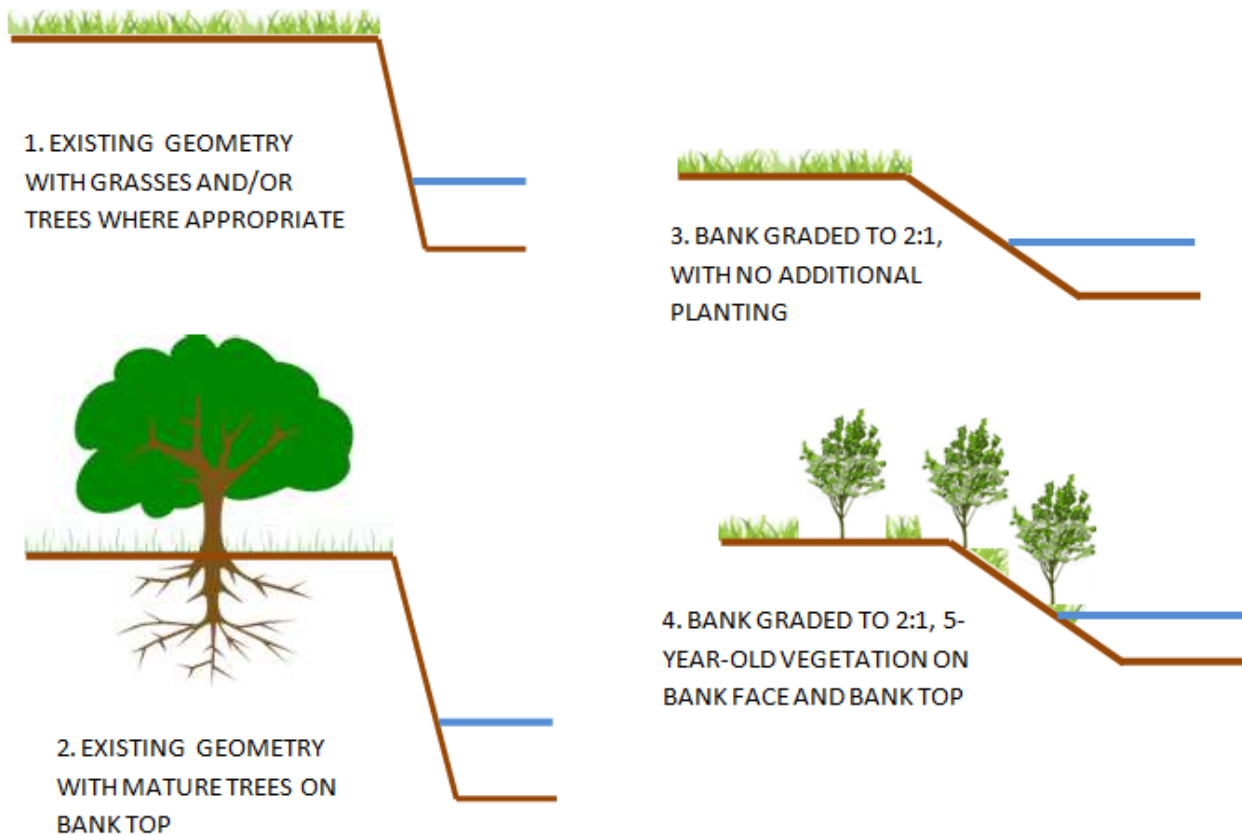


**Figure 16 – Illustration of existing conditions and mitigation scenarios evaluated by BSTEM.**

Note the following assumptions made in the BSTEM modeling methodology:

1. Channel slope is constant during the modeling period. This assumes that channel morphology is static, that is channel grade and width adjustment as a response to runoff and sediment supply is not accounted for. Typically in a disturbed stream system channel slope (representing stream power) will reduce over time and therefore shear stress and possibly bank erosion.
2. Percent reach failing is constant during the modeling period and is the same for each scenario. For the mitigation scenarios, one could reasonably expect percent reach failing to be reduced. Therefore, calculated bank material loadings for the mitigation scenarios can be seen as an upper bound of expected loadings.
3. As BSTEM is a single site model, no sediment routing is performed. The fate of eroded material is therefore not known. Assumptions have to be made regarding the portion of the eroded material transported to the watershed outlet. Further, the model does not account for possible armoring of the bank caused by failed bank-material blocks.
4. The bank profile and bank soil properties measured at a study site are assumed to be representative for both sides of the channel and constant over reach lengths exceeding 6 miles at times.

Further, no BSTEM model calibration or validation was conducted. Model calibration and validation using historical observations of channel evolution of the studied reaches of the Missisquoi River and its tributaries could have been used to reduce the uncertainty introduced by the assumption 4 above. It would not have helped to overcome the uncertainty introduced by assumptions 1 to 3.

## BSTEM MODELING RESULTS

### Bank Material Loadings

Table 6 summarizes the volume of eroded bank material calculated by BSTEM for the 27 study sites over a 30-year period for both existing and mitigated conditions, which is also shown in Figure 17. Three loading categories were established based on the percent of reach failing (PRF): 1) low,  $PRF < 20\%$ ; 2) moderate,  $20 \leq PRF < 40\%$ ; and 3) high,  $PRF \geq 40\%$ . The corresponding average annual sediment loading from streambank erosion (AASL, in  $m^3$  per km of channel per year) of each loading category was determined from the distribution of AASL at each study site calculated by BSTEM for the existing conditions scenario. For study sites with a low PRF,  $AASL < 15 m^3/km/yr$ ; for study sites with a moderate PRF,  $15 \leq AASL < 150 m^3/km/yr$ ; and for study sites with a high PRF,  $AASL \geq 150 m^3/km/yr$ .

### *Existing Conditions*

Study sites M7, TR1, TY1, and MSII-1 exhibit the most bank erosion under current conditions, exceeding about  $900 m^3/km/yr$  (or  $1,160 t/km/yr$ ). The calculated retreat of the top bank for these sites is approximately: 10 m (M7), 20 m (TR1), 35 m (TY1), and 9 m (MSII-1). Sites with moderate bank retreat are M2 (about 7 m of top bank retreat, however only for the top 2 m of the 6 m-high bank), M3 (2 m of top-bank retreat), M4 (3 m of top-bank retreat), M6 (about 5 m of bank retreat over the upper half of the 4 m high bank), TY2 (about 7 m of top-bank retreat), and MSII-3a (about 4.5 m of top-bank retreat).

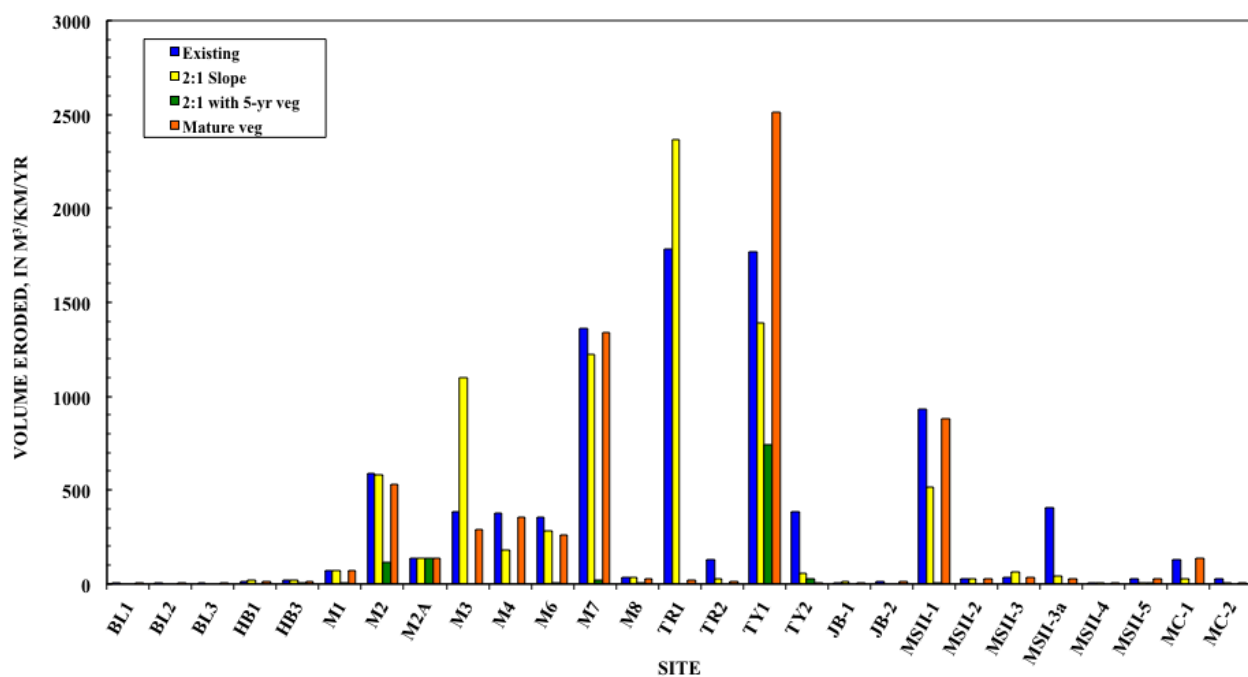


**Figure 17 – Average annual volume of eroded bank material estimated by BSTEM over the modeling period, under existing and mitigated conditions for the 27 study sites in the Missisquoi watershed.**

**Table 6 – Average annual volume of eroded bank material estimated by BSTEM over the modeling period, under existing and mitigated conditions for selected sites in the Missisquoi watershed.**

Site number	Volume of bank erosion in m <sup>3</sup> /km/yr				Percent reduction		
	Existing conditions	2-1 bank sloping	2-1 bank sloping & 5-yr vegetation	Mature vegetation	2-1 bank sloping	2-1 bank sloping & 5-yr vegetation	Mature vegetation
<b>Missisquoi River</b>							
M1	69.3	70.9	3.10	69.3	-2.27	95.5	0
M2	592	581	116	531	1.8	80.4	10.3
M2A	140	140	140	140	0	0	0
M3	383	1,100	0	289	100	100	24.7
M4	377	178	0	355	52.7	100	5.78
M6	357	280	1.33	258	21.5	99.6	27.9
M7	1,360	1,230	23.3	1,340	9.73	98.3	1.39
M8	32.1	34.8	0.367	28.9	-8.3	98.9	10.3
MSII-1	933	513	7.67	877	45.0	99.2	5.97
MSII-2	28.5	28.4	0	28.5	0.1	100	0
MSII-3	33.5	64.8	0	33.5	-93.8	100	0
MSII-3a	410	43.3	0	27.7	89.4	100	93.3
MSII-4	2.20	3.66	0	0.004	-66.3	100	99.8
MSII-5	27.2	1.87	3.13	25.3	93.1	88.5	6.9
<b>Black Creek</b>							
BL1	5.43	0	0	5.43	100	100	0
BL2	0.0559	0	0	0.056	100	100	0
BL3	1.82	0	0	1.82	100	100	0
<b>Hungerford Brook</b>							
HB1	15.8	18.5	0	15.8	-17.3	100	0
HB3	18.9	23.4	0.160	14.3	-24.2	99.2	24.0
<b>Trout River</b>							
TR1	1,780	2,360	0	18.6	-32.7	100	99.0
TR2	133	28.6	0	16.3	78.5	100	87.7
<b>Tyler Branch</b>							
TY1	1,770	1,390	740	2,510	21.3	58.2	-41.8
TY2	385	59.1	25.3	7.33	84.6	93.4	98.1
<b>Jay Branch</b>							
JB-1	8.11	13.8	0	6.21	-69.7	100	23.5
JB-2	10.5	0	0	10.5	100	100	0
<b>Mud Creek</b>							
MC-1	130	28.4	0	138	78.1	100	-6.59
MC-2	24.9	0.069	0	0.067	99.7	100	99.7

Figure 18 shows the spatial distribution of average annual sediment loadings from streambank erosion. The percentage of the assessed 2-mile reaches in each loading category is: 1) low, 37%; 2) moderate, 31%; and 3) high, 32%. The majority of the reaches classified as high-loading are on the Missisquoi River main stem. The highest loadings are found between river mile 36 (river kilometer 64.4) and 44 (river kilometer 77.3) on the Missisquoi, with average annual sediment loadings ranging from 774 to 1507 m<sup>3</sup>/km/yr. The distribution of calculated AASL is greatly skewed towards lower values. The 25<sup>th</sup>-, 50<sup>th</sup>-, and 75<sup>th</sup>-percentiles are 5.47 m<sup>3</sup>/km/yr, 34.9 m<sup>3</sup>/km/yr, and 232 m<sup>3</sup>/km/yr, respectively, whereas the mean AASL is 169 m<sup>3</sup>/km/yr. Intensive study sites exceeding the mean AASL are: TR1 (749 m<sup>3</sup>/km/yr), MSII-1 (681 m<sup>3</sup>/km/yr), M7 (611 m<sup>3</sup>/km/yr), TY1 (301 m<sup>3</sup>/km/yr), MSII-3a (250 m<sup>3</sup>/km/yr), M4 (226 m<sup>3</sup>/km/yr), and M3 (192 m<sup>3</sup>/km/yr). Note that these loadings are adjusted for local PRF and therefore do not equal those in Table 6.

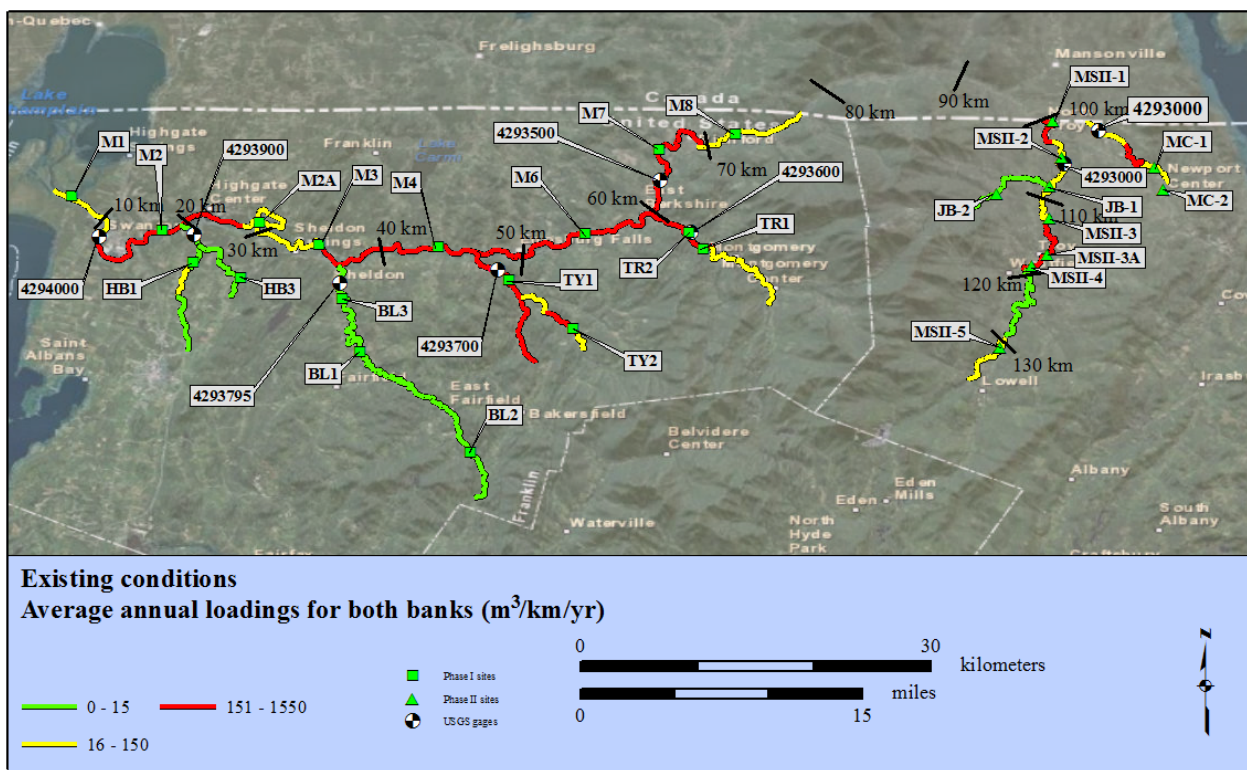


**Figure 18 – Map of average annual sediment loadings from bank erosion under current conditions.**

### *Mature Vegetation*

The effect on bank erosion of establishing a 25-year old, mature riparian buffer on the current bank profiles varies greatly (see Table 6 and Figure 17): from nearly 100% reduction in eroded volumes of bank material (sites MSII-3a, MSII-4, TR1, TY2, and MC-2) to enhanced erosion at sites MC-1 (increase of 7%) and TY1 (increase of 42%). The average percentage reduction

equals 24.8. Only site TR1 exhibited a significant reduction in bank erosion out of those sites with the highest bank erosion values under current conditions.

Figure 19 shows the spatial distribution of average annual sediment loadings from streambank erosion for the mature vegetation scenario. The percentage of the assessed 2-mile reaches in each loading category is: 1) low, 44%; 2) moderate, 27%; and 3) high, 29%. The percentage of reaches falling in the high-loading category is reduced by 3% and the percentage of reaches falling in the low-loading category has increased by 7%. The majority of the reaches classified as high-loading are on the Missisquoi River main stem and are roughly the same as those for current conditions. The highest loadings are again found between river mile 36 (river kilometer 64.4) and 44 (river kilometer 77.3) on the Missisquoi, with AASL ranging from 763 to 1486 m<sup>3</sup>/km/yr. However, large loadings are also found between river mile 0 and 8 (river kilometer 12.9) on Tyler Branch, with values ranging between 853 and 1531 m<sup>3</sup>/km/yr. The quartiles are reduced to 4.5 m<sup>3</sup>/km/yr, 19.4 m<sup>3</sup>/km/yr, and 198 m<sup>3</sup>/km/yr, respectively. However, the mean AASL has increased by 10% to 186 m<sup>3</sup>/km/yr. Intensive study sites exceeding the mean AASL under current conditions are: MSII-1 (640 m<sup>3</sup>/km/yr), M7 (603 m<sup>3</sup>/km/yr), TY1 (427 m<sup>3</sup>/km/yr), and M4 (213 m<sup>3</sup>/km/yr).

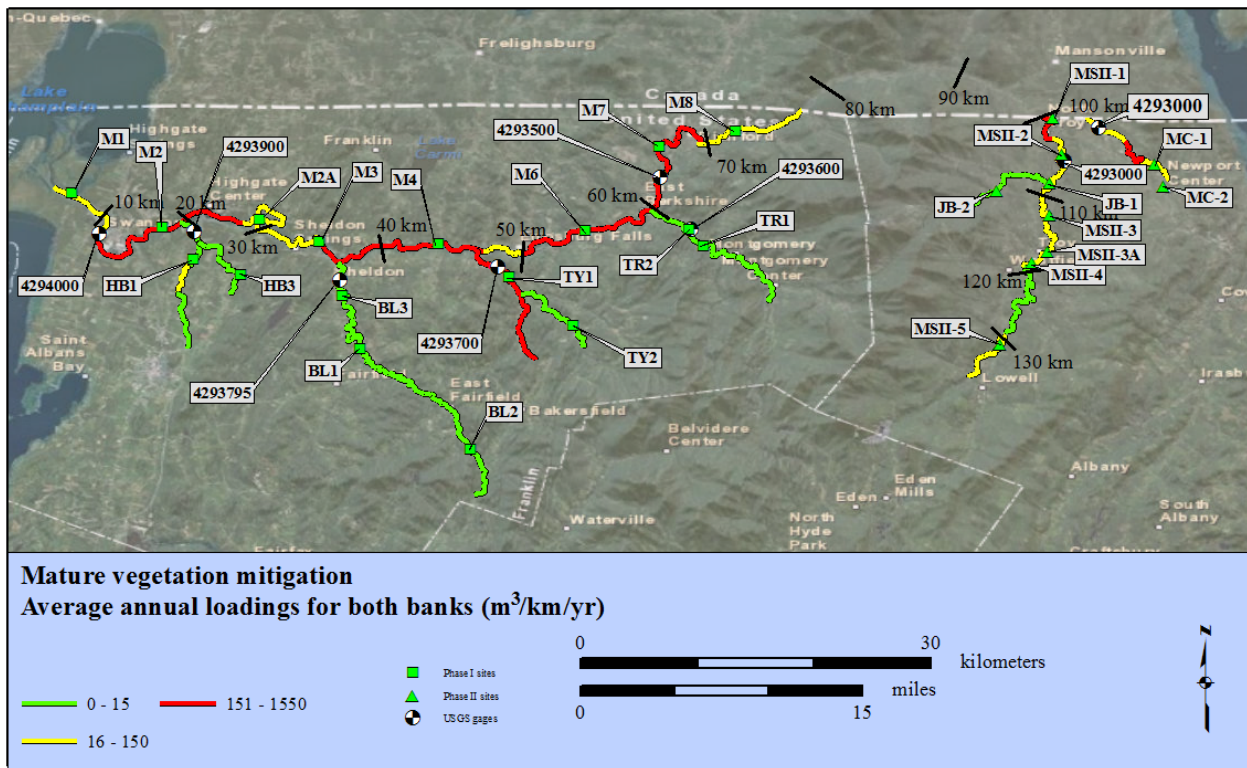


Figure 19 – Map of average annual sediment loadings from bank erosion for the mature vegetation mitigation scenario.

### ***Grading the Banks to 2:1 Slopes***

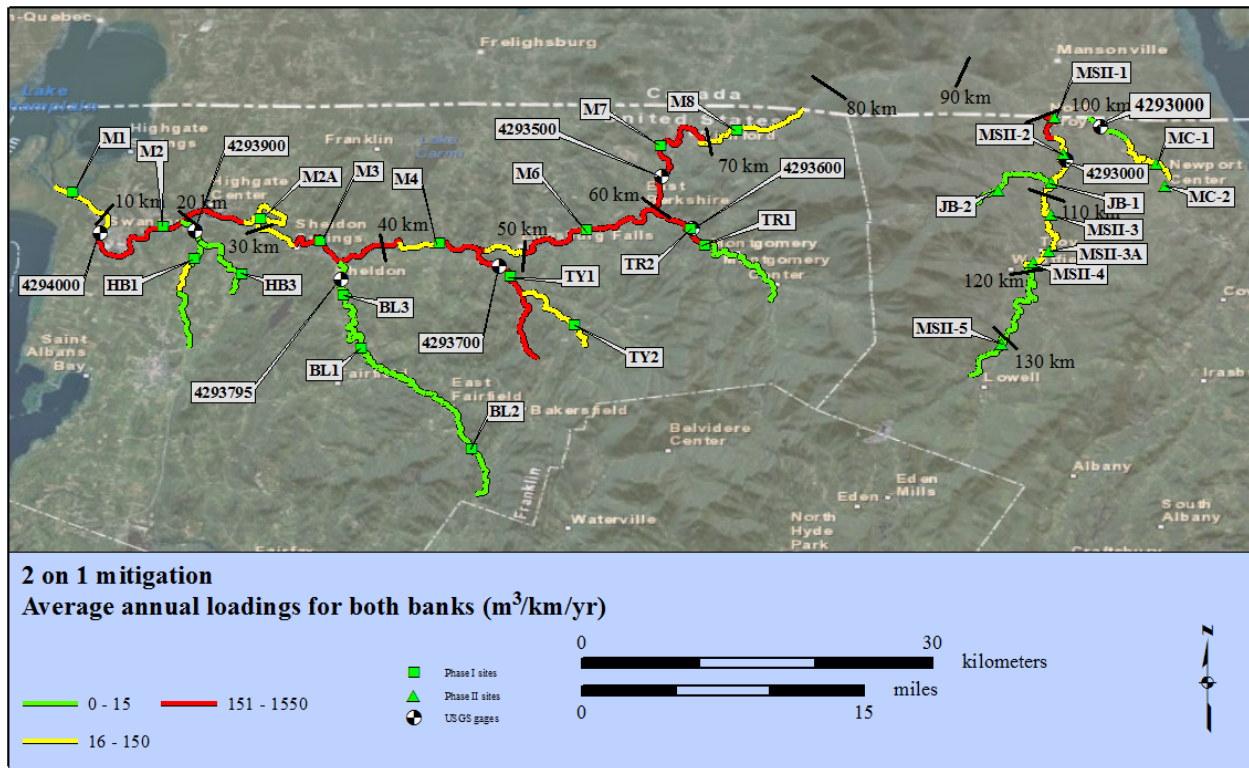
The effect of grading the banks to 2H:1V slopes on bank erosion also varies greatly (see Table 6 and Figure 17): from nearly 100% reduction in eroded volumes of bank material (sites BL1, BL3, TY1, JB-2, and MC-2) to moderately or significantly enhanced erosion at sites M3, MSII-3, MSII-4, the Hungerford Brook sites, TR1, and JB-1. It should be noted that bank erosion under current conditions at sites BL1, BL3, JB-2, and MC-2 is small. The average percentage reduction in eroded volumes equals 21.3%. Only site TY1 exhibited a significant reduction in bank erosion out of those sites with the highest bank erosion values under current conditions. Site TR1 showed a significant increase in streambank erosion.

Figure 20 shows the spatial distribution of average annual sediment loadings from streambank erosion for the 2:1 mitigation scenario. The percentage of the assessed 2-mile reaches in each loading category is: 1) low, 41%; 2) moderate, 29%; and 3) high, 30%. The percentage of reaches falling in the high- and moderate-loading categories is reduced by 2% for each category, and the percentage of reaches falling in the low-loading category has increased by 4%. However, the percentage of reaches falling in the high-loading category is still about the same as the current conditions and mature vegetation scenarios. Also, their spatial distribution has not changed much. The highest loadings are again found between river mile 36 (river kilometer 64.4) and 44 (river kilometer 77.3) on the Missisquoi, with AASL ranging from 699 to 1360 m<sup>3</sup>/km/yr. The 50<sup>th</sup>-percentile is reduced to 24.2 m<sup>3</sup>/km/yr, but the 25<sup>th</sup>- and 75<sup>th</sup>-percentiles have increased to 5.6 m<sup>3</sup>/km/yr and 236 m<sup>3</sup>/km/yr, respectively. Also, the mean AASL has increased by 9% to 188 m<sup>3</sup>/km/yr. Intensive study sites exceeding the mean AASL under current conditions are: TR1 (993 m<sup>3</sup>/km/yr), M7 (552 m<sup>3</sup>/km/yr), M3 (548 m<sup>3</sup>/km/yr), MSII-1 (374 m<sup>3</sup>/km/yr), and TY1 (237 m<sup>3</sup>/km/yr).

### ***Grading the Banks to 2:1 Slopes in Combination with Vegetative Treatment***

Grading the banks to 2H:1V slopes in combination with a vegetative treatment on both the bank face and bank top significantly reduced the estimated amount of bank erosion (see Table 6 and Figure 17). The percent reduction ranged in general from 58% to 100%, except for site M2A where there was no reduction in erosion. Site TY1 showed the largest amount of bank erosion, 740 m<sup>3</sup>/km/yr, which is about 58% smaller than under current conditions. The average percentage reduction equaled 93%.

Figure 21 shows the spatial distribution of average annual sediment loadings from streambank erosion for the 2:1 regrading with vegetation scenario. The percentage of the assessed 2-mile reaches in each loading category is: 1) low, 66%; 2) moderate, 27%; and 3) high, 7%. Only five reaches, between river mile 4 (river kilometer 12.9) and 6 (river kilometer 16.1) on the Missisquoi and between river mile 0 and 8 (river kilometer 12.9) on Tyler Branch, are classified as high-loading. The quartiles are reduced to 0.0 m<sup>3</sup>/km/yr, 0.0 m<sup>3</sup>/km/yr, and 35.6 m<sup>3</sup>/km/yr, respectively. Compared to current conditions the mean AASL is reduced by 77% to 39.2 m<sup>3</sup>/km/yr. Intensive study sites with moderate AASL are TY1 (126 m<sup>3</sup>/km/yr), M3 (34.9 m<sup>3</sup>/km/yr), and M2 (23.2 m<sup>3</sup>/km/yr).



**Figure 20 – Map of average annual sediment loadings from bank erosion for the mitigation scenario in which the bank profiles are graded at a 2:1 slope.**

### *Relation to Channel Stability Index*

Figure 22 plots the calculated average annual bank material loadings in  $m^3/km/yr$  at the intensive study sites against the channel stability index obtained from the RGAs (see also Appendix B). Bank material loadings for reaches with a channel stability index lower than 14 are negligible. For channel stability indices exceeding 14 there is not a general trend in calculated bank material loadings.

### **Phosphorus Loadings Under Existing and Mitigating Conditions**

Figure 23 shows a map with the phosphorus concentrations used to calculate the phosphorus loadings for the different scenarios. The calculated phosphorus loadings at the intensive study sites for each scenario are listed in Table 7. Maps of the phosphorus loadings emanating from the two-mile reaches are shown in Figure 24. As phosphorus loadings are directly related to bank-material loadings, they show a similar spatial distribution (cf. Figures 18 through 21). Greatest reductions in phosphorus loadings are mainly provided by the mitigation scenario in which the banks are graded at a 2H:1V slope in combination with a vegetative treatment on bank top and bank face.

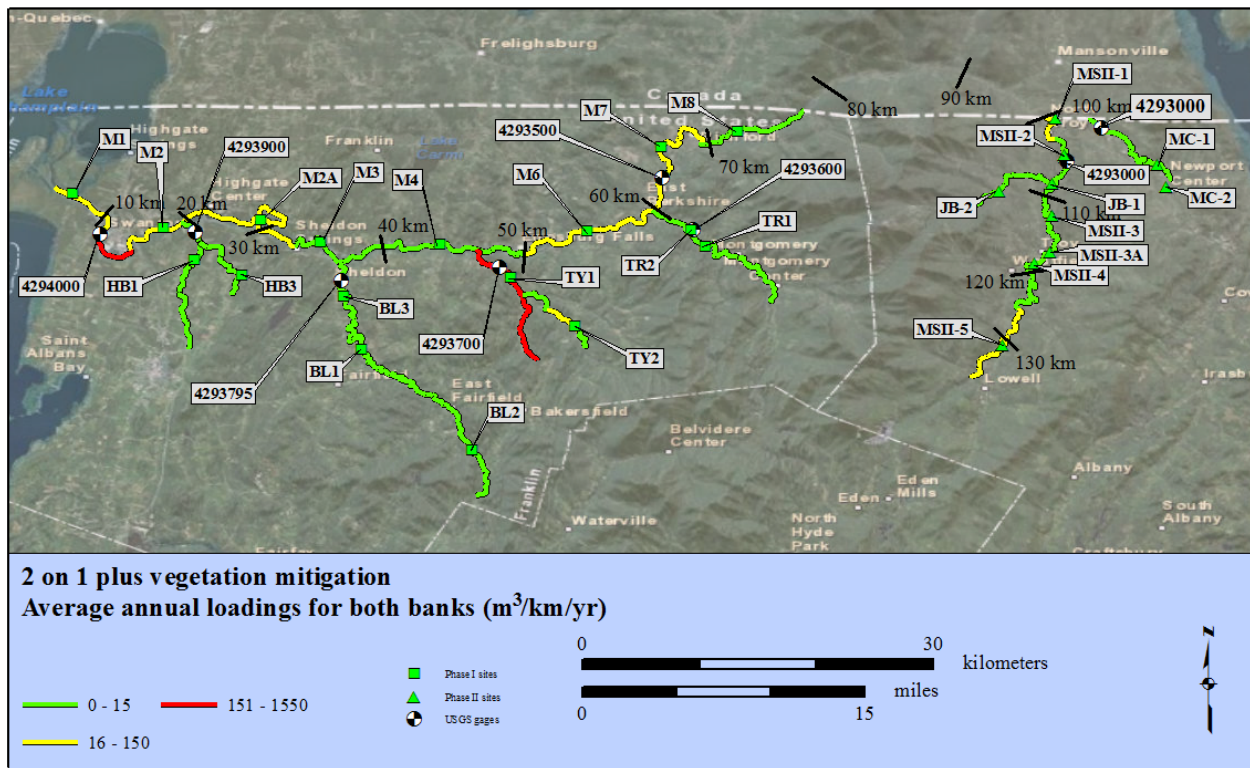


**Figure 21 – Map of average annual sediment loadings from bank erosion for the mitigation scenario in which the bank profiles are graded at a 2:1 slope in combination with a vegetative treatment on bank face and bank top.**

Largest phosphorus loadings are found along the middle reach of the Missisquoi (related to site M7) and the lower reaches of Trout River (related to site TR1) and Tyler Branch (related to site TY1) with maximum loadings up to 1,540 kg/km/yr (Figure 24 and Table 8). These loadings are much higher than are found elsewhere along the studied Missisquoi reaches, and result in large mean annual loading values that are similar to the 75<sup>th</sup> percentile of annual loading values (see Table 8). These high phosphorus loadings are all reduced for the scenario in which the banks are graded at a 2H:1V slope in combination with a vegetative treatment. Grading the banks at a 2H:1V slope only reduces loadings significantly along the lower reaches of Tyler Branch, while the mature vegetation treatment only reduces phosphorus loadings along the lower reaches of Trout River.

Table 8 shows that grading the banks at a 2H:1V slope only reduces mean phosphorus loadings by 14%. Planting mature vegetation reduces the mean phosphorus loadings by approximately 29%. Grading the banks in combination with a vegetative treatment reduces the mean phosphorus loadings by approximately 84%.

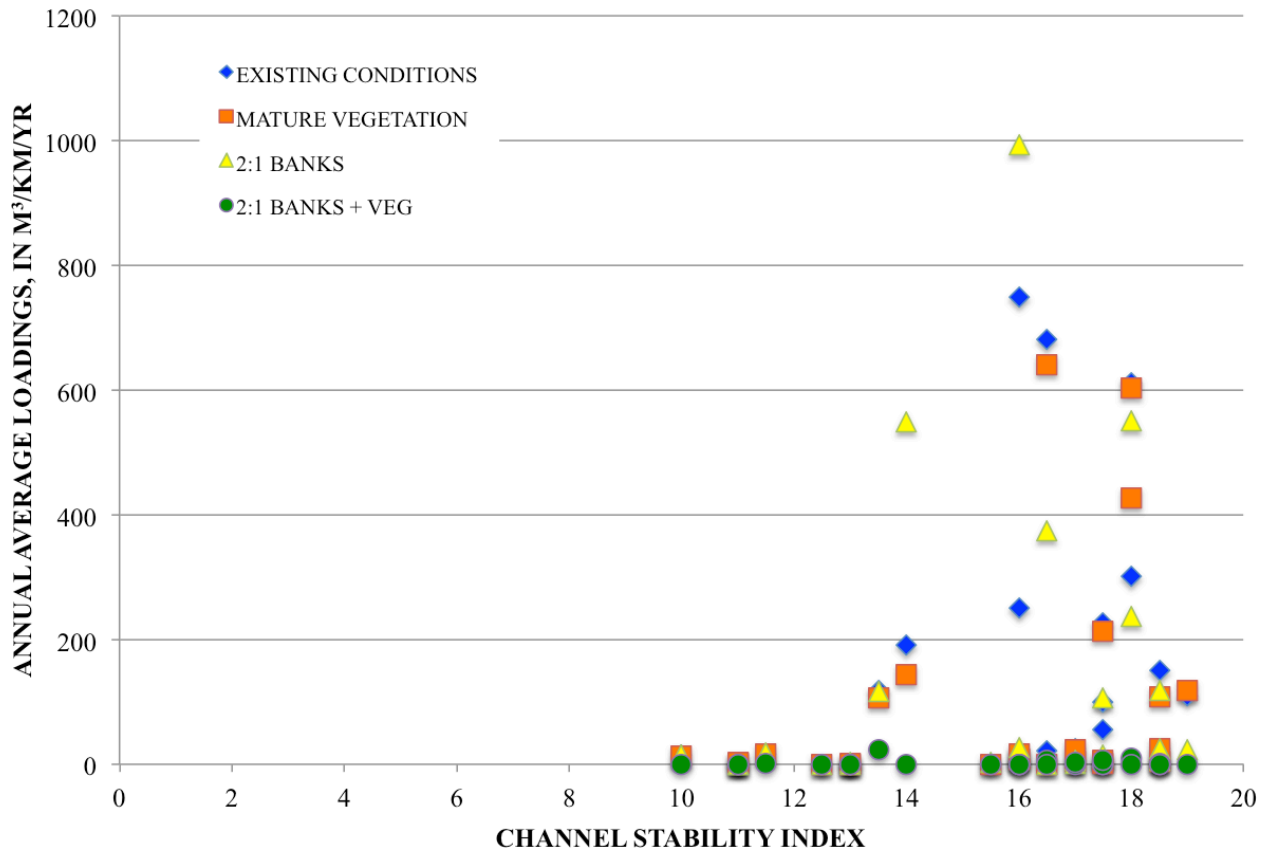


**Figure 22 – Plot of average annual sediment loadings from bank erosion for the various scenarios as a function of channel stability index obtained from the RGAs.**

**Contribution of Bank Material to Suspended Sediment Load**

Using the US Army Corps of Engineers FLUX computer program (Walker, 1996), the Vermont Department of Environmental Conservation has derived daily fluxes of Total Phosphorus (TP) and Total Suspended Solids (TSS) at the various gage locations throughout the Missisquoi River watershed. At USGS gage 04294000 (MISSISQUOI RIVER AT SWANTON, VT) the calculated annual average TSS and TP loadings between 1995 and 2009 are 88,700 t/yr and 145,000 kg/yr, respectively. Assuming that particles with a diameter less than 125  $\mu\text{m}$  (that is clay, silt, and very fine sand) make up the suspended load, the BSTEM bank-material loadings of such particles integrated (that is, summed) over the studied two-mile reaches are: 1) Existing Conditions scenario, 31,600 t/yr; 2) Mature vegetation scenario, 25,000 t/yr; 3) 2H:1V Bank Regrading scenario, 27,700 t/yr; and 4) 2H:1V Bank Regrading + Vegetation, 4,870 t/yr. The volumetric loadings were converted to mass loadings using a median dry density of the soil equal to 1,285  $\text{kg}/\text{m}^3$ .

**Table 7 – Average annual total phosphorus loading from streambank erosion (in kg/yr per unit length of streambank) simulated by BSTEM over the 30-year modeling period for existing and mitigation conditions.**

Site number	Existing conditions	Average Annual Total Phosphorus Load (kg/km/yr)		
		2-1 bank sloping	2-1 bank sloping with 5-yr vegetation	Mature vegetation
<b>Missisquoi River</b>				
M1	84.6	86.5	86.5	84.6
M2	60.5	586	351	533
M2A	144	144	144	144
M3	389	1,120	0	106
M4	463	202	6.04	227
M6	472	373	53.2	336
M7	1,390	1,260	113	1,370
M8	33.3	40.4	2.31	30.3
MSII-1	1,120	612	67.7	654
MSII-2	13.6	13.6	2.96	13.6
MSII-3	41.2	79.7	3.44	41.1
MSII-3a	45.4	44.6	1.72	30.5
MSII-4	0.328	0.544	0	0.00147
MSII-5	30.9	2.09	36.4	29.1
<b>Black Creek</b>				
BL1	8.48	0	0	8.49
BL2	0.105	0	0	0.105
BL3	2.53	0	0	1.92
<b>Hungerford Brook</b>				
HB1	17.2	19.7	0	17.2
HB3	20.9	25.2	1.30	0
<b>Trout River</b>				
TR1	2,970	3,250	0	3.38
TR2	64.6	8.10	0	2.46
<b>Tyler Branch</b>				
TY1	1,220	943	499	1,700
TY2	649	92.0	63.5	6.41
<b>Jay Branch</b>				
JB-1	8.80	15.0	0	6.73
JB-2	1.58	0	0	1.58
<b>Mud Creek</b>				
MC-1	119	26.0	0	124
MC-2	21.1	0	0	0

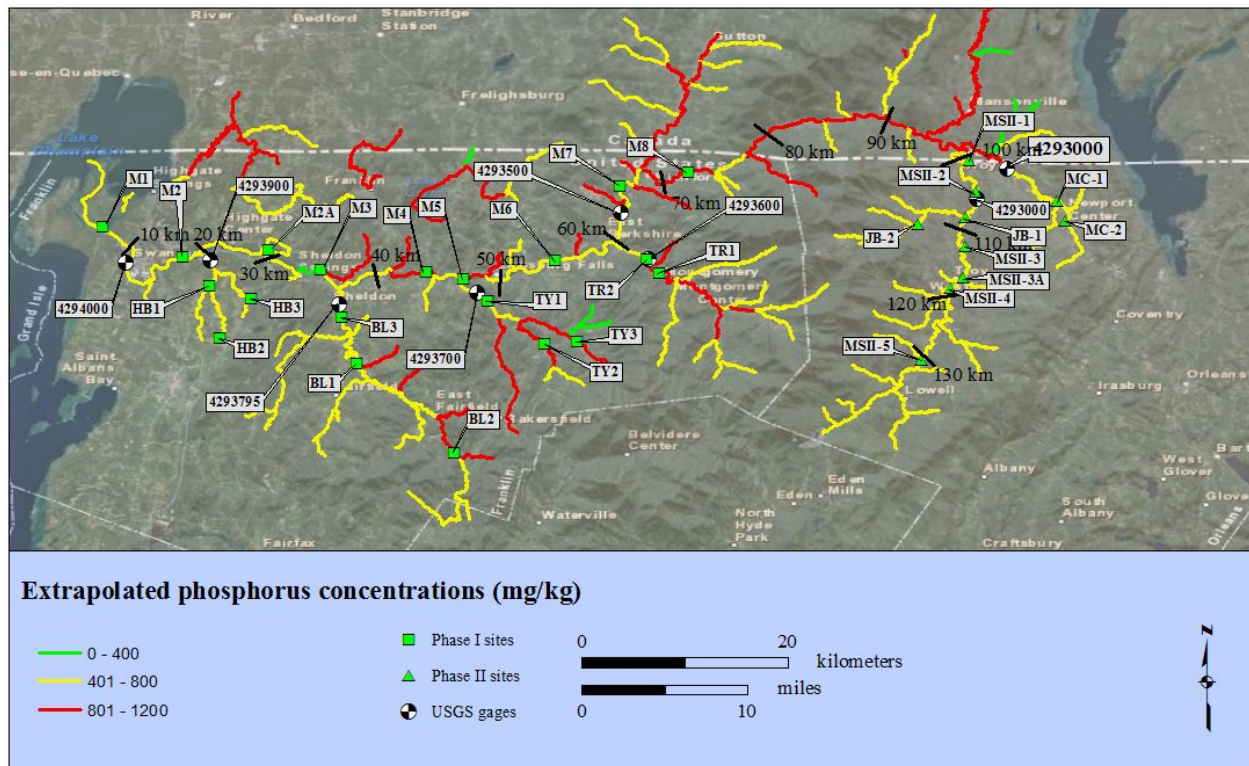


**Figure 23 – Map of phosphorus concentrations (in mg/kg of soil) used in the analysis to calculate phosphorus loadings from sediment loadings.**

**Table 8 – Metrics of average annual total phosphorus loadings (in kg/km/yr) from streambank erosion along two-mile reaches simulated by BSTEM over the 30-year modeling period for existing and mitigation conditions.**

Phosphorus loadings metric	Existing conditions	Phosphorus loadings in kg/km/yr		
		2-1 bank sloping	2-1 bank sloping with 5-yr vegetation	Mature vegetation
mean	222	191	36.0	158
25 <sup>th</sup> percentile	6.67	3.32	0	2.08
50 <sup>th</sup> percentile	41.7	27.6	1.29	20.3
75 <sup>th</sup> percentile	319	263.8	44.2	143
max	1,540	1,390	305	1,520

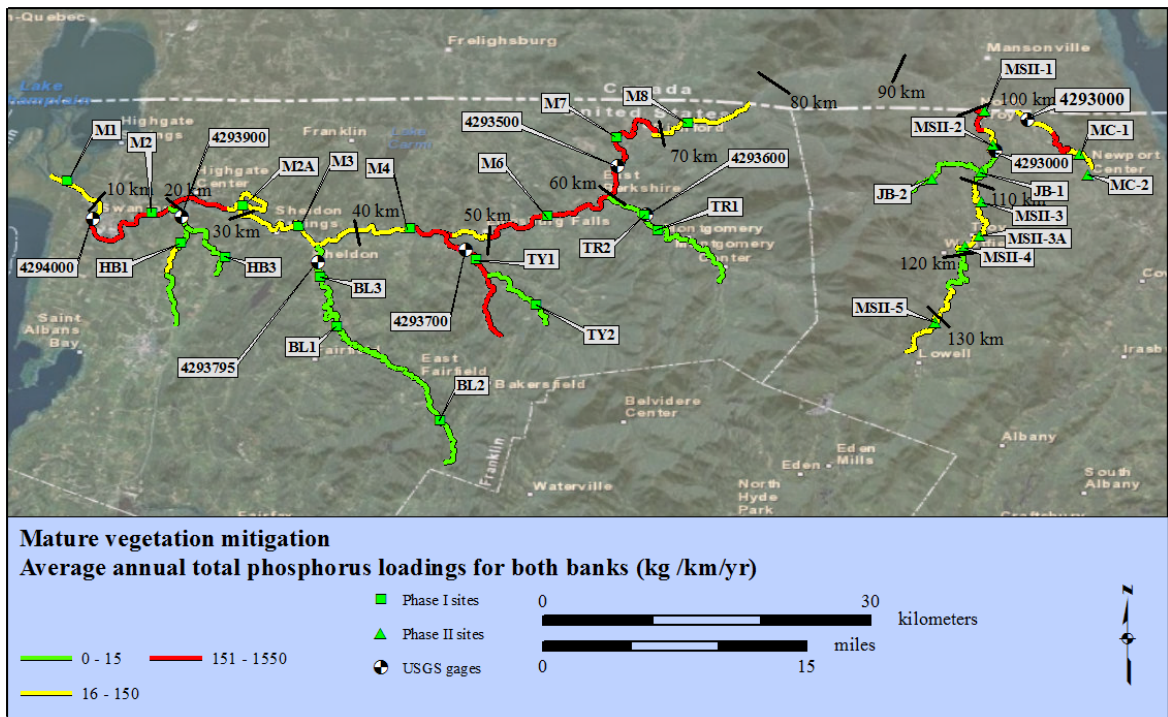
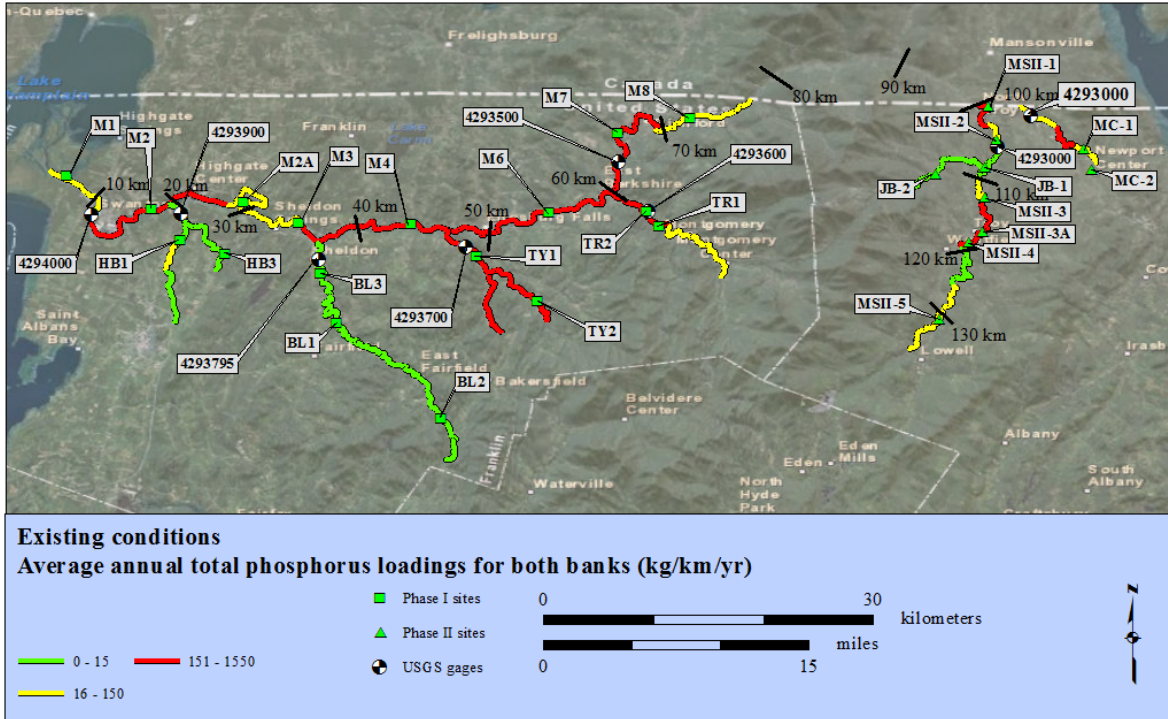
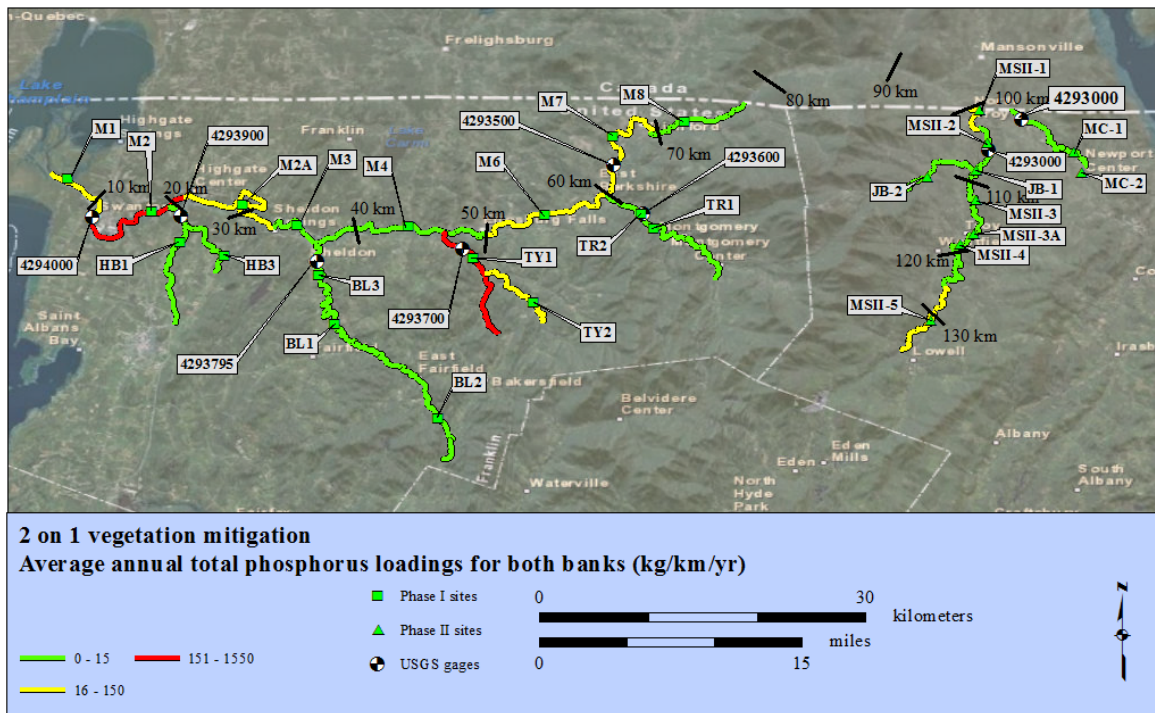
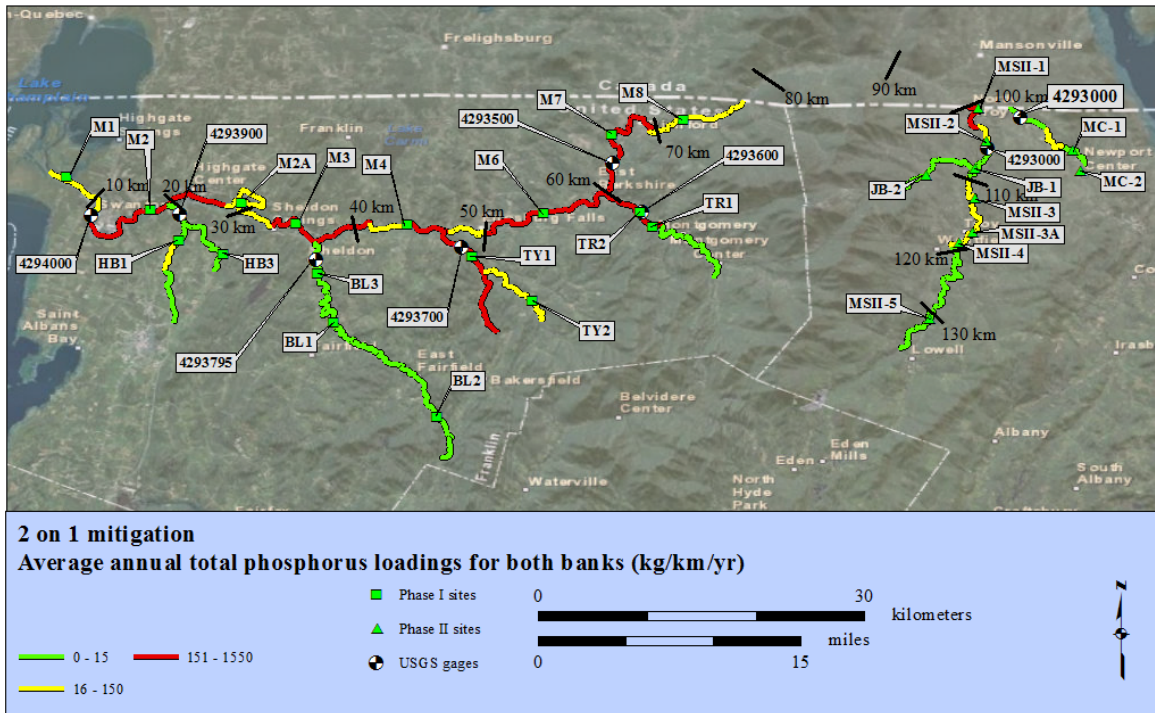


**Figure 24 – Maps of average annual total phosphorus loadings from bank erosion for: (a) current conditions scenario, (b) mature vegetation mitigation scenario, (c) mitigation in which the bank profiles are graded at a 2H:1V slope, and (d) mitigation in which the bank profiles are graded at a 2H:1V slope in combination with a vegetative treatment on bank face and bank top. (continued on next page)**



(continued from previous page) Figure 24 – Map of average annual total phosphorus loadings from bank erosion for: (a) current conditions scenario, (b) mature vegetation mitigation scenario, (c) mitigation in which the bank profiles are graded at a 2H:1V slope, and (d) mitigation in which the bank profiles are graded at a 2H:1V slope in combination with a vegetative treatment on bank face and bank top.

The BSTEM calculated loadings from the studied reaches under existing conditions contribute 35.7% of the estimated TSS load near the mouth of the Missisquoi River. Under the three mitigation scenarios, the contribution from streambank erosion along the studied reaches is reduced by 21% to 28.2% of estimated TSS load (mature vegetation), 12% to 31.3% of estimated TSS load (2H:1V bank grading scenario), and 85% to 5.5% of estimated TSS load (2H:1V bank grading + vegetation scenario).

The BSTEM computed phosphorus loadings from the studied reaches contribute a similar proportion to annual average TP load near the mouth of the Missisquoi River than the corresponding contributions to TSS load. The contribution to the TP load is 35.8% under existing conditions, 25.6% for the mature vegetation mitigation scenario, 30.9% for the 2H:1V bank grading scenario, and 5.8% for the 2H:1V bank grading scenario in combination with a vegetation treatment.

## **Discussion**

The section “Data Collection and Methods” listed the following assumptions made in the BSTEM modeling methodology:

1. Channel slope is constant during the modeling period. This assumes that channel morphology is static, that is channel grade and width adjustment as a response to runoff and sediment supply is not accounted for. Typically in a disturbed stream system channel slope (representing stream power) will reduce over time and therefore shear stress and possibly bank erosion.
2. Percent reach failing is constant during the modeling period and is the same for each scenario. For the mitigation scenarios, one could reasonably expect percent reach failing to be reduced. Therefore, calculated bank material loadings for the mitigation scenarios can be seen as an upper bound of expected loadings.
3. As BSTEM is a single site model, no sediment routing is performed. The fate of eroded material is therefore not known. Assumptions have to be made regarding the portion of the eroded material transported to the watershed outlet. Further, the model does not account for possible armoring of the bank caused by failed bank material blocks.
4. The bank profile and bank soil properties measured at a study site are assumed to be representative for both sides of the channel and constant over reach lengths exceeding 6 miles at times.

The below sections discuss how these assumptions could impact the modeling results.

### ***Stage of Channel Evolution***

The section “Channel Stability and Evolution” on page 3 introduced the conceptual channel evolution model of Simon and Hupp (1986). At each intensive study site the stage of channel evolution was determined as part of the Rapid Geomorphic Assessment survey. Figure 25 plots the observed stages of channel evolution along the Missisquoi channel network. At the intensive



### ***Percent Reach Failing***

The previous section showed that all the studied reaches were in either stage V or VI of the conceptual channel evolution model of Simon and Hupp (1986). This suggests that percent reach failing may slightly reduce (stage V) or remain fairly constant. The percent reach failing for the meandering reaches may change spatially as the focus of erosion shifts up or down the reach, but over the long-term (the period over which one meander bend is replaced by another) the percent reach failing is fairly constant. Therefore, it is a reasonable assumption that the percent reach failing should be representative for the entire 30-year simulation period.

### ***Transport of Failed Material and Calculated Loads at the Watershed Outlet***

Appendix C lists the grain size distributions from the bank- and bed-material samples collected in this study. Bed material along the main stem of the Missisquoi River was characterized between study sites MSII-2 and MSII-5. Unfortunately, flow depths were too large at sites M1 to MSII-1 to collect bed-material samples by hand. However, Lyttle (Undated) characterized bed-material at seven sites along the lower portion of the Missisquoi River. Lyttle's most downstream site is located just upstream of study site M1. Lyttle's most upstream site is located about midway between study sites M2 and M2A.

The median texture (expressed as %clay and silt (particle diameter < 63  $\mu\text{m}$ ), %sand (particle diameter between 63  $\mu\text{m}$  and 2 mm), and %gravel (particle diameter > 2 mm)) of the eroded bank material listed in Table C- is 45% clay and silt, 44% sand, and < 1% of gravel). The 25<sup>th</sup>- and 75<sup>th</sup>-percentiles of %silt and clay are 20 and 67%, respectively. The 25<sup>th</sup>- and 75<sup>th</sup>-percentiles of %sand are 23 and 69%, respectively. Hence, eroded bank material consists primarily of fines (clay and silts) and sands, which are about equally present.

The bed material along the upper reach of the Missisquoi River consists primarily of gravel, about 79%, with about 19% sand and 2% cobble or bed rock. From the reported bed-material texture by Lyttle (Undated) the following mean values for bed material are calculated: 3% clay and silt, 22% sand, 18% gravel, and 58% cobble, boulder or bedrock. Hence, also the lower portion of the Missisquoi River is comprised of bed materials dominated by gravels, cobbles, boulders, or bedrock.

The calculated contributions of bank-material loadings to suspended load at the USGS gage 04294000 (MISSISQUOI RIVER AT SWANTON, VT) only account for particles smaller than 125  $\mu\text{m}$  (page 40). The measured bed-material grain-size distribution shows that these sizes are primarily transported as suspended or wash load as they are not present in the bed material. The sand-sized bank-material loading is not discussed in this report. However, it could be assumed that these materials also move relatively quickly through the stream network. Though, temporary storage in point bars could be important. The contributions to suspended load were reported relative to the suspended load calculated by the FLUX program (see Section "Contribution of Bank Material to Suspended Sediment Load" on page 40). It should be noted that the FLUX-derived values also have an inherent uncertainty.

### Variability of Bank-Material Properties

Appendix D tabulates the measured resistance to erosion (critical shear stress and erodibility) and measured shear strength (cohesion and friction angle) of the bank soils tested at the study sites. Figure 26 plots the measured erosion rate ( $k_d$ ) versus critical shear stress ( $\tau_c$ ). In general, the measured resistance-to-erosion values exhibit the smallest variation for the upper reach of the Missisquoi River (between study sites MSII-1 to MSII-5). The lower reach of the Missisquoi (between study sites M1 and M8) shows a relatively small variation in critical shear stress and a larger variation in the erosion rate coefficient. The measured values in the tributaries exhibit the greatest amounts of variability. Also note that there are many small critical shear stress values (< 0.5 Pa) along the tributaries than along the main channel.

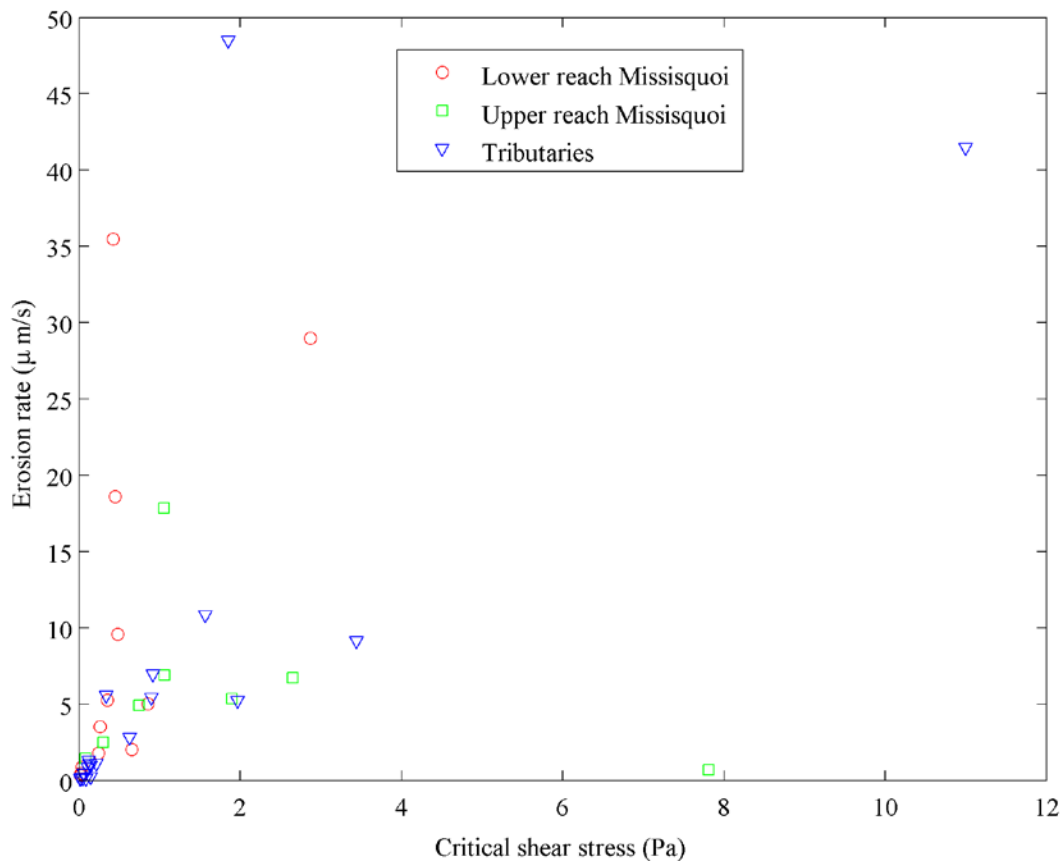


**Figure 26 – Plot of erosion rate ( $k_d$ ) versus critical shear stress ( $\tau_c$ ) measured with the submerged jet test device.**

Generally, the rate of simulated bank retreat by BSTEM is proportional to the used value of  $k_d$ , and could therefore vary reasonably by a factor of 2 or 3 given the values shown in Figure 26. In nature, bank retreat due to fluvial erosion is modulated by the retention of failed bank materials at the toe of the bank, commonly reducing bank retreat rates. As failed bank materials in the Missisquoi River have relatively large portions of sands, retention of failed bank material should therefore be controlled by herbaceous plant species growing on the bank. As retention of failed

material was not accounted for, it can be reasoned that the bank-material loadings calculated by BSTEM should be fairly conservative, that is tending towards the upper end of those probable.

### ***Mitigation Scenarios***

To extrapolate the at-a-site bank-material loadings calculated by BSTEM to the reach scale, the loadings are multiplied by the %Reach Failing. For the mitigation scenarios, the %Reach Failing was the same as for the Existing Conditions Scenario. As bank protection measures should reduce bank erosion, it is reasonable to assume that %Reach Failing would also reduce. Streambank material loadings for each 2-mile reach are linearly related to %Reach Failing, that is if %Reach Failing is twice as small, reach-scale bank-material loadings will be twice as small also. Hence, the predicted bank-material loadings for the mitigation scenarios can be seen as upper bounds.

On the other hand, over 50% of bank-material loadings consist of materials (medium to coarse sands, gravels, and cobbles) that will be moved as bed-material load. Reducing the loadings of these materials may lead to channel incision if there are no local bedrock controls. This may result in increased bank erosion through increased shear stresses exerted by the flow on the bank toe, temporarily increasing bank erosion rates.

### ***Closing***

Varied uncertainties exist in the BSTEM modeling results. However, given the above assumptions it can be reasoned that the reported values of eroded bank-material volumes, their contribution to suspended sediment load and phosphorus load at the mouth of the Missisquoi River could be viewed as an upper bound of expected values.

Finally, the effects of ice on streambank erosion are not accounted for. These effects are also varied, both increasing and reducing possible erosion (Prowse, 2001). Ice cover typically reduces shear stresses, thereby reducing erosion. However, ice breakup and the formation of ice jams and their release can increase streambank erosion significantly. The Ice Jam database hosted by the Cold Regions Research and Engineering Laboratory of the US Army Corps of Engineers (<https://rsgisias.crrel.usace.army.mil/icejam/>) reports that ice jams occur occasionally throughout the entire Missisquoi River basin but regularly near study site M6 (34 reported ice jams) and study site MSII-2 (12 reported ice jams). 2-mile reaches using these study sites could have additional erosion that is not accounted for. However, as predicted bank-material loading can be seen as an upper bound, the exclusion of ice scour effects should have limited influence on the reported loading values.

## CONCLUSIONS

Missisquoi Bay (Vermont and Québec) exhibits high in-lake phosphorus concentrations, which exceed the target levels endorsed by the governments of Vermont, Québec, and New York. Fine-grained sediments eroded from streambanks along the Missisquoi River and its tributaries could be a significant source of phosphorus. Observations along the main stem of the Missisquoi River located in the US and select Tributaries (Black Creek, Hungerford Brook, Jay Branch, Mud Creek, Trout River and Tyler Branch) have indicated that the river's streambanks could be a significant source of both suspended sediment and associated phosphorus. Indeed, significant portions of the study reach were estimated to have greater than 50% of their banks failing in analysis carried out as part of this report (Figure 9). The main objective of this study, therefore, was to determine rates and loadings of sediment from streambank erosion along main stem reaches of the Missisquoi River and the tributaries: Black Creek, Hungerford Brook, Jay Branch, Mud Creek, Trout River and Tyler Branch. Further, three mitigation scenarios were analyzed to determine the percent reduction in loadings that can be obtained by stabilizing streambanks (Figure 15): mitigation scenario 1) 25 year old mature trees on the bank top, mitigation scenario 2) banks graded to a 2H:1V slope, and mitigation scenario 3) banks graded to a 2H:1V slope in combination with 5-year old vegetative treatment of bank top and face.

Conceptual models of bank retreat and the delivery of bank sediments to the flow emphasize the importance of interactions between hydraulic forces acting at the bed and bank toe, and gravitational forces acting on in situ bank materials. As such, analyzing streambank stability is a matter of characterizing the gravitational forces acting on the bank and the geotechnical strength of the in situ bank material. Twenty-seven study sites were selected along the studied reach (Figure 1), to act as representative conditions for the entire reach. At each site data pertaining to geotechnical strength and hydraulic resistance were measured to use as input data to BSTEM. At-a-site sediment and phosphorus loadings calculated by BSTEM were then converted to annual loading rates before being extrapolated from site loadings to reach length loadings. To extrapolate to reaches of 2 mi in length, the bank length and percent of the banks failing in a given reach (determined from aerial RGAs) were multiplied by the at-a-site loading for the site located closest to that reach (Appendix A). In this way we were able to produce average annual sediment and phosphorus loadings emanating from the entire study reach.

BSTEM simulations were carried out using a 30-year flow record, which was constructed separately for each study site using the observed discharges at USGS gages 04293000 (MISSISQUOI RIVER NEAR NORTH TROY, VT) and 04293500 (MISSISQUOI RIVER NEAR EAST BERKSHIRE, VT) for the period 10/1/79 to 9/30/10. Predicted volumes of sediment eroded from the streambanks under Existing Conditions at each site ranged from 0.0559 to 1780 m<sup>3</sup> of sediment per 1 km reach per year (m<sup>3</sup>/km/yr) with a median value of 69.3 m<sup>3</sup>/km/yr and an interquartile range (IQR) of 367 m<sup>3</sup>/km/yr (Figure 16 or Table 6). Largest volumes of eroded sediment were predicted at study sites M2, M7, MSII-1, TR1, and TY1. BSTEM calculated reduced volumes of eroded bank soils for each mitigation scenario with the largest reduction for mitigation scenario 3. Mitigation scenarios 1 and 2 provided similar percent reductions in sediment loadings. The metrics of the eroded volume distribution for the three mitigation scenarios are:

- Scenario (1) median value is 27.7 m<sup>3</sup>/km/yr, IQR is 190 m<sup>3</sup>/km/yr, and maximum value is 2510 m<sup>3</sup>/km/yr;
- Scenario (2) median value is 34.8 m<sup>3</sup>/km/yr, IQR is 221 m<sup>3</sup>/km/yr, and maximum value is 2360 m<sup>3</sup>/km/yr; and
- Scenario (3) median value is 0.0 m<sup>3</sup>/m, IQR is 3.12 m<sup>3</sup>/km/yr, and maximum value is 740 m<sup>3</sup>/km/yr.

Typically, the sites with greatest sediment loadings under existing conditions (M2, M7, MSII-1, TR1, and TY1) were also the greatest contributors in case of the mitigation scenarios. Bank erosion volumes at sites M2 and MSII-1 were large due to the erodible bank soils. At site M7 channel slope increased significantly (almost tenfold) along the main stem of the Missisquoi compared to that downstream (sites M1 through M6), however the erodibility of the bank soils did not change much. A combination of steeper channel slopes and relatively erodible bank soils resulted in greater bank erosion rates at sites TR1 and TY1.

Contributions of sediment from streambank erosion along the US study reaches of the Missisquoi River were found to be about 36% (31,600 t/yr) of the total suspended-sediment load entering Missisquoi Bay. Mitigation lowered the contributions by: Scenario 1) 21% (25,000 t/yr), Scenario 2) 12% (27,700 t/yr), and Scenario 3) 85% (4,870 t/yr).

As phosphorus loadings are directly related to bank material loadings, they show a similar spatial distribution (compare Figure 23 with Figures 17 to 20). Maximum phosphorus loadings are found along the middle reach of the Missisquoi River and the lower reaches of Trout River and Tyler Branch with maximum loadings up to 1,540 kg/km/yr (Fig. 23 and Table 8). These loadings are much higher than are found elsewhere and result in rather large mean annual loading values (Table 8). Mitigation scenarios 1 and 2 do not significantly reduce total phosphorus loadings; mean annual load reductions are 29% and 14%, respectively. Grading the banks in combination with a vegetative treatment reduces the median phosphorus loadings by approximately 84%. The contribution to the TP load into Missisquoi Bay is 35.8% under existing conditions, 25.6% for mitigation scenario 1, 30.9% for mitigation scenario 2, and 5.8% for mitigation scenario 3.

It is important to note the following assumptions made in the BSTEM modeling methodology:

1. Channel slope was constant during the modeling period. This assumes that channel morphology is static, that is channel grade and width adjustment as a response to runoff and sediment supply is not accounted for over the 30-year simulation period. Typically in a disturbed stream system, channel slope (representing stream power) will reduce over time and therefore shear stress and possibly bank erosion may reduce also.
2. Percent reach failing was constant during the modeling period and was the same for each scenario. For the mitigation scenarios, one could reasonably expect percent reach failing to be reduced compared to that under existing conditions. Therefore, calculated bank material loadings for the mitigation scenarios should be seen as an upper bound on expected loadings.
3. As BSTEM is a single site model, no sediment routing is performed. The fate of eroded material is therefore not known. Assumptions have to be made regarding the portion of the eroded material transported to the watershed outlet. Further, the model does not

account for possible armoring (protection) of the bank caused by failed bank material blocks.

4. The bank profile and bank soil properties measured at a study site are assumed to be representative for both sides of the channel and constant over reach lengths exceeding 6 miles at times.

Improved bank-material loading estimates can be obtained using a channel evolution model such as CONCEPTS (Langendoen, 2000), which routs flow and sediment and calculates bank retreat along an entire channel instead of a single location. The above four issues are explicitly resolved in CONCEPTS.

## REFERENCES

- Abernethy, B., and Rutherford, I.D., 2001. The distribution and strength of riparian tree roots in relation to riverbank reinforcement. *Hydrological Processes*, 15(1), 63-79.
- Ariathurai, R., and Arulanandan, K., 1978. Erosion rates of cohesive soils. *Journal of the Hydraulics Division, ASCE*, 104(HY2), 279-283.
- Arulanandan, K., 1975. Fundamental aspects of erosion of cohesive soils. *Journal of the Hydraulics Division, ASCE*, 101(HY5), 635-639.
- Arulanandan, K., Gillogley, E., and Tully, R., 1980. Development of a quantitative method to predict critical shear stress and rate of erosion of natural undisturbed cohesive soils, Technical Report GL-80-5. U.S. Army Engineers Waterways Experiment Station: Vicksburg, MS.
- ASTM, 1995. Annual Book of ASTM Standards: Section 4, Construction, v. 04-09. American Society for Testing and Materials: West Conshohocken, PA.
- Bankhead, N., and Simon, A., 2009. Analysis of bank stability and potential load reduction along reaches of the Big Sioux River, South Dakota. U.S. Department of Agriculture, Agricultural Research Service, National Sedimentation Laboratory, Technical Report 64, Oxford, Mississippi.
- Blaisdell, F.W., Clayton, L.A., and Hebaus, G.G., 1981. Ultimate dimension of local scour, *Journal of the Hydraulics Division, Proceedings of the American Society of Civil Engineers*, 107(HY3), 327-337.
- Bohm, W., 1979. *Methods of Studying Root Systems*. Berlin: Springer-Verlag.
- Carson, M.A., and Kirkby, M.J., 1972. *Hillslope Form and Process*. Cambridge University Press: Cambridge, UK.
- Casagli, N., Curini, A., Gargini, A., Rinaldi, M. and Simon, A., 1997. Effects of pore pressure on the stability of streambanks: Preliminary results from the Sieve River, Italy, In: S.S.Y. Wang, E.J. Langendoen, and F.D. Shields Jr. (eds.), *Management of Landscapes Disturbed by Channel Incision*. University of Mississippi: University; pp.243-248.
- Chow, V.T., 1959. *Open Channel Hydraulics*. McGraw-Hill: New York, NY.
- Coppin, N.J., and Richards, I.G., 1990. *Use of Vegetation in Civil Engineering*. Butterworths: London, UK.
- Einstein, H.A., 1942. Formulas for the transportation of bed load. *Transactions of the ASCE*, 107, 561-597.
- Endo, T., and Tsuruta, T., 1969. On the effect of tree roots upon the shearing strength of soil. Annual report of the Hokkaido branch, Forest Place Experimental Station: Sapporo, Japan; pp.167-183.
- Ennos, A.R., 1990. The anchorage of leek seedlings: The effect of root length and soil strength. *Annals of Botany*, 65(4), 409-416.
- Fan, C.-C., and Su, C.-F., 2008. Role of roots in the shear strength of root-reinforced soils with high moisture content. *Ecological Engineering*, 33(2), 157-166.
- Fredlund, D.G., and Rahardjo, H., 1993. *Soil Mechanics of Unsaturated Soils*. John Wiley and Sons, Inc.: New York.
- Fredlund, D.G., Morgenstern, N.R., and Widger, R.A., 1978. The shear strength of unsaturated soils. *Canadian Geotechnical Journal*, 15, 313-321.
- Gray, D.H., and Leiser, A.T., 1982. *Biotechnical Slope Protection and Erosion Control*. Van Nostrand Reinhold Company: New York, NY.

- Gray, D.H., and Sotir, R.B., 1996. Biotechnical and Soil Bioengineering Slope Stabilization: A Practical Guide for Erosion Control. John Wiley & Sons, Inc.: New York, NY.
- Grissinger, E.H., 1982. Bank erosion of cohesive materials, In: R.D. Hey, J.C. Bathurst, and C.R. Thorne (eds.), Gravel-bed Rivers. John Wiley & Sons Ltd.: Chichester, UK; pp.273-287.
- Hanson, G.J., 1990, Surface erodibility of earthen channels at high stress, Part II - Developing an in situ testing device, Transactions of the American Society of Agricultural Engineers, 33(1), 132-137.
- Hanson, G.J., and Cook, K.R., 1997. Development of excess shear stress parameters for circular jet testing, American Society of Agricultural Engineers Paper No. 97-2227. American Society of Agricultural Engineers: St. Joseph.
- Howe, E., Howland, W., and Strouse, S., 2011. Modeling efforts and identification of critical source areas of phosphorus in the Vermont sector of the Missisquoi Bay basin. Technical Report No. 63, Lake Champlain Basin Program, Grand Isle, Vermont, 279 pp.
- Hupp, C.R. 1992. Riparian vegetation recovery patterns following stream channelization: A geomorphic perspective. Ecology, 73, 1209-1226.
- Kelly, W.E., and Gularte, R.C., 1981. Erosion resistance of cohesive soils. Journal of the Hydraulics Division, ASCE, 107, 1211-1223.
- Kuhnle, R.A., and Simon, A., 2000. Evaluation of Sediment Transport Data for Clean Sediment TMDLs, U.S. Department of Agriculture, Agricultural Research Service, National Sedimentation Laboratory Research Report 17, Oxford, Mississippi, 65 p.
- Langendoen, E.J., 2000. CONCEPTS - CONservational Channel Evolution and Pollutant Transport System, U.S. Department of Agriculture, Agricultural Research Service, National Sedimentation Laboratory, Research Report 16, Oxford, Mississippi, 160 p.
- Langendoen, E.J., 2010. Assessing post-dam removal sediment dynamics using the CONCEPTS computer model. In: Proceedings of the 2<sup>nd</sup> Joint Federal Interagency Conference, Las Vegas, NV, June 27-July 1, 2010, 12 p.
- Little, W.C., Thorne, C.R., and Murphy, J.B., 1982. Mass bank failure analysis of selected Yazoo Basin streams. Transactions of the American Society of Agricultural Engineers, 25, 1321-1328.
- Lohnes, R.A., and Handy, R.L., 1968. Slope angles in friable loess. Journal of Geology, 76(3), 247-258.
- Lutenegger, J.A., and Hallberg, B.R., 1981. Borehole shear test in geotechnical investigations. ASTM Special Publication 740, 566-578.
- Lyttle, M., Undated. Spawning habitat suitability for Walleye and lake Sturgeon in the Missisquoi River. Report prepared for the Lake Champlain Fishery Technical Committee. US Fish and Wildlife, Lake Champlain Fish and Wildlife Resources Office. Downloaded from [http://www.vtfishandwildlife.com/library/Reports\\_and\\_Documents/Fish\\_and\\_Wildlife/Spawning\\_Habitat\\_Suitability\\_for\\_Walleye\\_and\\_Lake\\_Sturgeon\\_in\\_the\\_Missisquoi\\_River.pdf](http://www.vtfishandwildlife.com/library/Reports_and_Documents/Fish_and_Wildlife/Spawning_Habitat_Suitability_for_Walleye_and_Lake_Sturgeon_in_the_Missisquoi_River.pdf) on 10/8/2012.
- Mehta, A.J., 1991. Review notes on cohesive sediment erosion. In: N.C. Kraus, K.J. Gingerich, and D.L. Kriebel, (eds.), Coastal sediment '91, Proceedings of Specialty Conference on Quantitative Approaches to Coastal Sediment Processes, ASCE; pp.40-53.
- Morgenstern, N.R., and Price, V.R., 1965. The analysis of the stability of general slip surfaces. Geotechnique, 15, 79-93.

- Parchure, T.M., and Mehta, A.J., 1985. Erosion of soft cohesive sediment deposits. *Journal of Hydraulic Engineering*, ASCE, 110(10), 1308-1326.
- Partheniades, E., 1965. Erosion and deposition of cohesive soils. *Journal of the Hydraulics Division*, ASCE, 91(HY1), 105-139.
- Pollen, N., 2007. Temporal and spatial variability in root reinforcement of streambanks: Accounting for soil shear strength and moisture. *Catena*, 69(3), 197-205.
- Pollen, N., and Simon, A., 2005. Estimating the mechanical effects of riparian vegetation on streambank stability using a fiber bundle model. *Water Resources Research*, 41, W07025, doi:10.1029/2004WR003801.
- Pollen, N., Simon, A., and Collison, A.J.C., 2004. Advances in assessing the mechanical and hydrologic effects of riparian vegetation on streambank stability. In: S. Bennett and A. Simon, (eds.), *Riparian Vegetation and Fluvial Geomorphology*, Water Science and Applications 8. AGU: Washington, DC; pp.125-139.
- Prowse, T., 2001. River-ice ecology. I: Hydrologic, geomorphic, and water-quality aspects. *Journal of Cold Regions Engineering*, 15(1), 1-16.
- Riestenberg, M., and Sovonick-Dunford, S.S., 1983. The role of woody vegetation in stabilizing slopes in the Cincinnati area. *Ohio Geological Society of America Bulletin*, 94(4), 506-518.
- Rinaldi, M., and Casagli, N., 1999. Stability of streambanks in partially saturated soils and effects of negative pore water pressures: the Sieve River (Italy), *Geomorphology*, 26(4), 253-277.
- Rinaldi, M., and Simon, A., 1998. Adjustments of the Arno River, Central Italy, *Geomorphology*, 22, 57-71.
- Schumm, S.A., Harvey, M.D., and Watson, C.C., 1984. *Incised Channels Morphology, Dynamics and Control*. Water Resources Publications: Littleton, CO.
- Simon, A., 1989. A model of channel response in disturbed alluvial channels. *Earth Surface Processes and Landforms*, 14(1), 11-26.
- Simon, A., 1994. Gradation processes and channel evolution in modified West Tennessee streams: Process, response and form. U.S. Geological Survey Professional Paper 1470. US Government Printing Office: Washington, DC.
- Simon, A., 1999. Channel and drainage-basin response of the Toutle River system in the aftermath of the 1980 eruption of Mount St. Helens, Washington. U.S. Geological Survey Open-File Report 96-633. US Government Printing Office: Washington, DC.
- Simon A., and Collison, A.J.C., 2001. Pore-water pressure effects on the detachment of cohesive streambeds: seepage forces and matric suction, *Earth Surface Processes and Landforms* 26(13), 1421-1442.
- Simon, A., and Collison, A.J.C., 2002. Quantifying the mechanical and hydrologic effects of riparian vegetation on stream-bank stability, *Earth Surface Processes and Landforms*, 27(5), 527-546.
- Simon, A., and Darby, S.E., 1997. Process-form interactions in unstable sand-bed river channels: A numerical modeling approach, *Geomorphology* 21(2), 85-106.
- Simon, A., and Hupp, C.R., 1986. Channel evolution in modified Tennessee channels. *Proceedings of the Fourth Interagency Sedimentation Conference*, March 1986, Las Vegas, Nevada, 2, 5-71 to 5-82.

- Simon, A., and Hupp, C.R., 1992. Geomorphic and vegetative recovery processes along modified stream channels of West Tennessee. U. S. Geological Survey Open-File Report 91-502. US Government Printing Office: Washington, DC.
- Simon, A., Wolfe, W.J., and Molinas, A., 1991. Mass wasting algorithms in an alluvial channel model, Proceedings of the Fifth Federal Interagency Sedimentation Conference, Las Vegas, Nevada, 2, 8-22 to 8-29.
- Simon, A., Curini, A., Darby, S.E., and Langendoen, E.J., 1999, Streambank mechanics and the role of bank and near-bank processes in incised channels, In: S. E. Darby and A. Simon (eds.), *Incised River Channels: Processes, Forms, Engineering and Management*. John Wiley & Sons Ltd.: Chichester, UK; pp.123-152.
- Simon, A., Kuhnle, R.A., and Dickerson, W., 2002. Reference sediment-transport rates for Level III ecoregions for use in developing clean-sediment TMDLs. In: Proceedings of the Water Resources Planning and Management Conference, EWRI-ASCE, May 19-22, 2002, Roanoke, 10 p. ASCE, Reston, VA.
- Stein, O.R., and Nett, D.D., 1997. Impinging jet calibration of excess shear sediment detachment parameters, *Transactions of the American Society of Agricultural Engineers* 40 (6), 1573-1580.
- Stein, O.R., Julien, P.Y., and Alonso, C.V., 1993. Mechanics of jet scour downstream of a headcut. *Journal of Hydraulic Research*, 31, 723-738.
- Temple, D.M., 1980. Tractive force design of vegetated channels. *Transactions of the American Society of Agricultural Engineers*, 23(4), 884-890.
- Temple, D.M., Robinson, K.M., Ahring, R.M., and Davis, A.G., 1987. *Stability Design of Grass-Lined Open Channels*. USDA ARS Agriculture Handbook Number 667. US Government Printing Office: Washington, DC.
- Thomas, R.E., and Pollen-Bankhead, N., 2010. Modeling root-reinforcement with a fiber-bundle model and Monte Carlo simulation. *Ecological Engineering*, 36(1), 47-61.
- Thorne, C.R., 1982, Processes and mechanisms of river bank erosion. In: R.D. Hey, J.C. Bathurst and C.R. Thorne, (eds.), *Gravel-Bed Rivers*. John Wiley & Sons Ltd.: Chichester, UK, pp. 227-271.
- Thorne, C.R., 1990. Effects of vegetation on riverbank erosion and stability, In: J.B. Thornes, (ed.), *Vegetation and Erosion*. John Wiley & Sons Ltd.: Chichester, UK; pp.125-144.
- Thorne, C.R., and Tovey, N.K., 1981. Stability of composite river banks. *Earth Surface Processes and Landforms*, 6, 469-484.
- Thorne, C.R., Murphey, J.B., and Little, W.C., 1981. Bank stability and bank material properties in the bluffline streams of Northwest Mississippi, *Stream Channel Stability*, Appendix D, Section 32 Program, Work Unit 7, U. S. Army Corps of Engineers, Vicksburg District: Vicksburg, Mississippi.
- van Genuchten, M. Th., 1980. A closed-form equation for predicting the hydraulic conductivity of unsaturated soils. *Soil Science Society of America Journal*, 44, 892-898.
- Waldron, L.J., 1977. The shear resistance of root-permeated homogeneous and stratified soil. *Soil Science Society of America Journal*, 41(5), 843-849.
- Waldron, L.J., and Dakessian, S., 1981. Soil reinforcement by roots: Calculation of increased soil shear resistance from root properties. *Soil Science*, 132(6), 427-435.
- Walker, W.W., 1996. *Simplified Procedures for Eutrophication Assessment and Prediction: User Manual*. Instruction Report W-96-2, Waterways Experiment Station, US Army Corps of Engineers: Washington, DC.

- Winterwerp, J.C., and van Kesteren, W.G.M., 2004. Introduction to the physics of cohesive sediment dynamics in the marine environment. Elsevier: Amsterdam.
- Wu, T.H., 1984. Effect of vegetation on slope stability, Transportation Research Record, 965, 37-46.
- Wu, T.H., McKinnell III, W.P., and Swanston, D.N., 1979. Strength of tree roots and landslides on Prince of Wales Island, Alaska. Canadian Geotechnical Journal, 16(1), 19-33.

## APPENDIX A. COMPARTMENTALIZATION OF MISSISQUOI RIVER AND ITS TRIBUTARIES FOR BANK LOADING CALCULATIONS

This appendix presents the 2-mile reaches used to calculate the loadings of sediment and phosphorus from streambank erosion.

### Two-mile reaches

The loadings of sediment and phosphorus caused by streambank erosion are calculated on a reach basis, where each reach has a length of 2 mi. Figure A-1 shows a map of the 2-mile reaches and the locations of the intensive study sites that were modeled using BSTEM. Table A-1 lists: (1) the study site used to calculate the loadings for each reach, and (2) the percent reach failing applied to the bank-material loading of the study site.

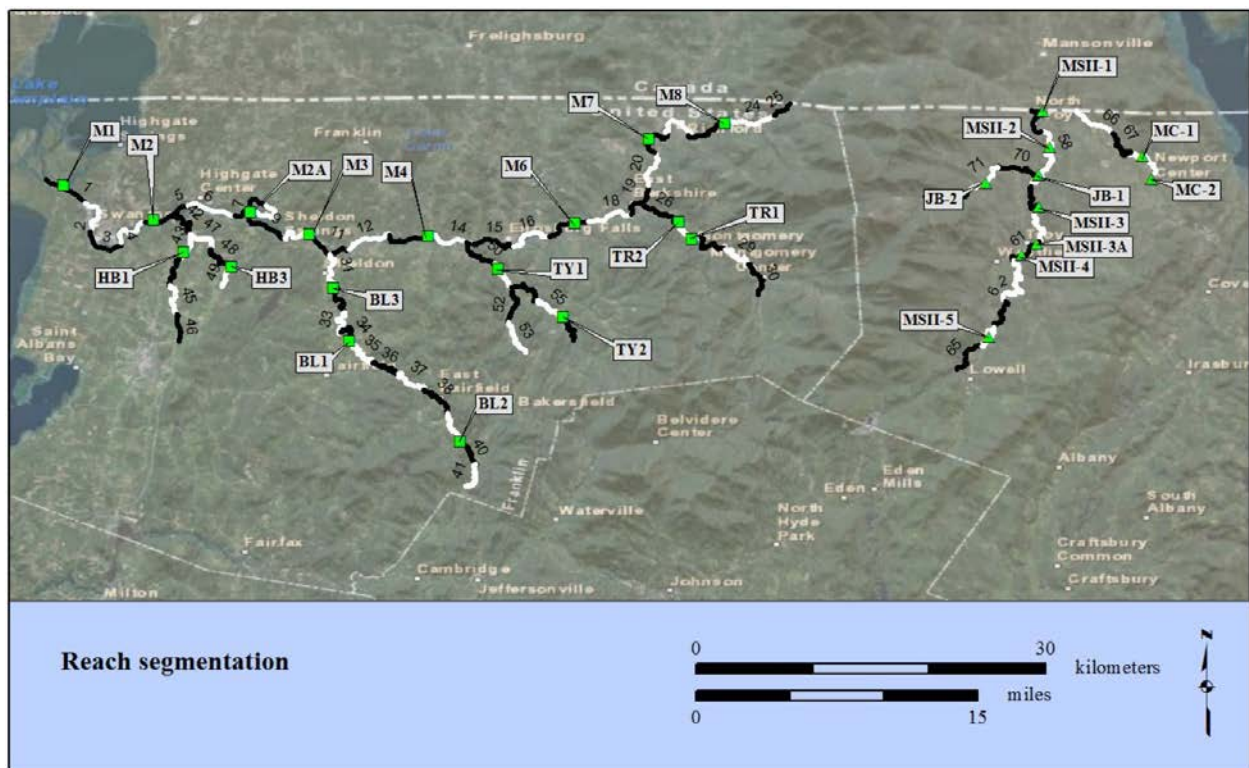


Figure A-1 – Map showing the locations of the 2-mile reaches and the intensive study sites.

**Table A-1 – List of the study site assigned to each 2-mile reach.**

Reach	Study Site Used	Percent Reach Failing	Reach	Study Site Used	Percent Reach Failing	Reach	Study Site Used	Percent Reach Failing
1	M1	25	25	M8	45	49	HB3	12.5
2	M1	20	26	TR1	20	50	TY1	24
3	M2	27.5	27	TR1 & TR2	36.5	51	TY1	18
4	M2	22.5	28	TR2	19	52	TY1	30.5
5	M2	22.5	29	TR2	26	53	TY1	17
6	M2	20	30	TR2	21	54	TY2	15
7	M2A	12.5	31	BL3	16.5	55	TY2	26
8	M2A	35	32	BL3	14	56	TY2	17.5
9	M2A	25	33	BL1	30.5	57	MSII-1	37.5
10	M3	17.5	34	BL1	22.5	58	MSII-2	70
11	M3	40	35	BL1	20.5	59	MSII-3	54
12	M3	30	36	BL1	44.5	60	MSII-3 & MSII-3A	80
13	M4	27.5	37	BL1	28.5	61	MSII-3A & MSII-4	70
14	M4	47.5	38	BL2	20	62	MSII-4	90
15	M4	20	39	BL2	22.5	63	MSII-5	27.5
16	M6	40	40	BL2	17.5	64	MSII-5	67.5
17	M6	44	41	BL2	10	65	MSII-5	85
18	M6	34	42	HB1	17.5	66	MC-1	10
19	M7	55.5	43	HB1	21	67	MC-1	80
20	M7	50.5	44	HB1	52	68	MC1 & MC2	85
21	M7	35.5	45	HB1	15	69	MSII-2	27
22	M7	28.5	46	HB1	20	70	JB-1	24
23	M8	33.5	47	HB3	18.5	71	JB-2	47.5
24	M8	28	48	HB3	20	72	JB-2	16

**APPENDIX B. CHANNEL STABILITY RANKING OF THE MISSISQUOI RIVER AND ITS TRIBUTARIES**

This appendix presents the results of the channel stability ranking using Rapid Geomorphic Assessments conducted at each intensive study site (see Section “Rapid Geomorphic Assessments: RGAs” on page 14).

**Table B-1 – Rapid Geomorphic Assessment conducted at the intensive study sites.**

Study site	Bed material	Bed or bank protection	Incision	Constriction	Streambank erosion		Streambank instability		Woody vegetative cover		Bank accretion		Stage of channel evolution	Channel stability index
					Left	Right	Left	Right	Left	Right	Left	Right		
<b>Missisquoi River</b>														
M1	3	1	1	0	0	0	1	0	1.5	0	2	0.5	1.5	11.5
M2	2.5	1	1	0	1	1	0.5	0.5	0	0.5	2	2	1.5	13.5
M3	3	1	1	0	0	0	0.5	0.5	2	1	2	1.5	1.5	14
M4	2.5	1	2	0	0	2	0.5	1.5	0.5	1.5	1	2	3	17.5
M6	2.5	1	1	0	2	0	2	0.5	2	1.5	2	1	3	18.5
M7	2	1	2	0	2	1	1.5	0.5	1.5	0.5	2	1	3	18
M8	1.5	0	2	0	1	0	1	0	1	0	1.5	0.5	1.5	10
MSII-1	3	1	2	0	0	2	0	2	0	1.5	0	2	3	16.5
MSII-2	2.5	1	2	0	2	0	2	0.5	2	1	2	0.5	3	18.5
MSII-3	3	1	2	0	0	2	0	1.5	0	1.5	0	2	3	16
MSII-3a	2.5	1	2	0	2	0	1.5	0	2	0	2	0	3	16
MSII-4	1.5	1	2	0	2	0	2	0	1.5	0	2	0.5	3	15.5
MSII-5	2	1	3	0	0	2	0	2	0	2	0	2	3	17
<b>Black Creek</b>														
BL1	3.5	1	3	0	0	0	0	1	0	0	0.5	0.5	1.5	11
BL2	3.5	1	1	0	0	0	0.5	0.5	0.5	0.5	2	2	1.5	13
BL3	3.5	1	1	0	0	0	0	0	1	0.5	2	2	1.5	12.5
<b>Hungerford Brook</b>														
HB1	3	1	3	0	2	0	1.5	0	2	0.5	2	0.5	3	18.5
HB2	2.5	1	4	0	0	0	0.5	0.5	0.5	0.5	2	1.5	1.5	14.5
<b>Trout River</b>														
TR1	1.5	1	3	0	2	0	1.5	0	2	0	2	0	3	16
TR2	2	1	3	0	2	0	1.5	0	2	0.5	2	0.5	3	17.5
<b>Tyler Branch</b>														
TY1	2	1	3	0	0	2	0	2	1	2	0	2	3	18
TY2	2	1	3	0	0	2	0.5	1.5	0.5	1	1	2	3	17.5
<b>Jay Branch</b>														
JB-1	1.5	1	3	0	0	1	0	1	1	1	0.5	1.5	1.5	13
JB-2	1	1	4	0	0	1	0	0.5	0	0	0.5	1.5	1.5	11
<b>Mud Creek</b>														
MC-1	1.5	1	3	1	2	0	1.5	0	2	1.5	2	0.5	3	19
MC-2	2	1	2	0	0	2	0	1.5	0.5	2	0.5	2	3	16.5

## APPENDIX C. BANK AND BED MATERIAL GRAIN SIZE DISTRIBUTIONS

Table C-1 lists the grain-size distributions of the dominant soil of the evaluated bank at each study site and that of the simulated eroded material. Table C-2 lists the grain-size distributions of the collected bed-material samples.

**Table C-1 – Grain size distribution of the dominant bank soil layer and that of the simulated eroded bank material for each study site.**

Study site	Dominant bank material			Eroded bank material		
	% clay and silt	% sand	% gravel and greater	% clay and silt	% sand	% gravel and greater
<b>Missisquoi River</b>						
M1	44.9	55.1	0	44.9	55.1	0.0
M2	46.5	53.5	0	18.7	81.3	0.0
M2A				13.9	69.4	13.9
M3	57.1	42.3	0.6	45.0	52.7	2.4
M4	96.3	3.7	0	43.6	36.7	19.7
M6	47.4	51.7	0.9	42.2	57.5	0.3
M7	45.7	54.3	0	23.0	71.4	5.6
M8	51.1	48.8	0.1	30.9	69.1	0.0
MSII-1	61.9	38.1	0	68.8	31.2	0.0
MSII-2	63.2	36.8	0	6.8	43.5	49.7
MSII-3	29.5	70.4	0.1	67.1	32.3	0.6
MSII-3a	83.0	17.0	0	67.5	32.5	0.0
MSII-4	88.8	11.2	0	0.0	14.3	85.7
MSII-5	78.4	21.5	0.1	52.8	47.2	0.0
<b>Black Creek</b>						
BL1	42.1	57.9	0	47.5	52.5	0.0
BL2	28.1	71.9	0	28.1	70.9	0.0
BL3	96.4	3.6	0	96.4	3.6	0.0
<b>Hungerford Brook</b>						
HB1	85.4	14.6	0	85.4	14.6	0.0
HB2	37.5	62.5	0	80.7	15.3	4.0
<b>Trout River</b>						
TR1	56.6	43.4	0	63.0	37.0	0.0
TR2	29.3	61.6	9.1	11.9	70.6	17.5
<b>Tyler Branch</b>						
TY1	65.9	33.9	0.2	13.3	86.7	0.0
TY2	30.9	67.3	1.8	31.5	66.9	1.6
<b>Jay Branch</b>						
JB-1	58.7	40.9	0.4	58.7	40.9	0.4
JB-2				0.0	15.0	85.0
<b>Mud Creek</b>						
MC-1	82.6	10	7.4	87.0	10.6	2.4
MC-2	77.2	22.8	0	79.6	20.4	0.0

**Table C-2 – Grain-size distribution of collected bed-material samples.**

Study site	% clay	% silt	% sand	% gravel	% cobble and greater
Missisquoi River					
MSII-2	< 0.2%	< 0.2%	18	77	5
MSII-3	< 0.1%	< 0.4%	18	82	0
MSII-3a	< 0.4%	< 0.3%	35	62	2
MSII-4	0	0	16	75	9
MSII-5	< 0.2%	< 0.8%	14	85	0
Mud Creek					
MC-1	0	0	12	51	37
MC-2	0	0	8	92	0

**APPENDIX D. BANK MATERIAL PROPERTIES**

Table D-1 summarizes the erodibility data collected with the submerged jet test device on the bank toe or bank face. Table D-2 summarizes the shear strength data collected with the Borehole Shear Test device.

**Table D-1 – Resistance to erosion of bank face and toe materials measured using a submerged jet-test device.**

Study site	Bank face			Bank toe		
	Test id	Critical shear stress (Pa)	Erodibility coefficient (cm <sup>3</sup> /N-s)	Test id	Critical shear stress (Pa)	Erodibility coefficient (cm <sup>3</sup> /N-s)
<b>Missisquoi River</b>						
M1	1	2.87	10.1	1	0.148	11.2
				2	0.026	18.2
M2	1	0.017	20.0			
	2	0.025	18.6			
	3	0.477	20.1			
M2A				1	3.78	1.28
M3	1	0.657	3.09			
	2	0.240	7.47			
M4	3	0.851	5.88			
	1	0.351	15.0			
M6	1	0.037	23.1	1	0.141	8.73
	2	0.258	13.6			
M7	1	0.446	41.7			
	2	0.423	83.9			
MSII-1	1	0.299	8.37	1	0.038	10.5
	2	2.65	2.54	2	0.324	1.81
MSII-2	1	1.90	2.82			
	2	0.747	6.60			
MSII-3	1	7.81	0.089	1	1.39	4.93
MSII-3a	1	1.06	6.51	1	0.016	7.20
				2	11.0	0.852
MSII-4	1	1.05	17.0			
	2	0.079	18.5			
MSII-5				1	0.602	2.74
				2	0.445	8.10
<b>Black Creek</b>						
BL1				1	0.064	14.5
				2	0.133	3.58
BL2	1	0.117	11.3			
	2	0.111	7.42			
BL3	1	3.44	2.66	1	3.00	2.05
	2	0.901	6.02	2	1.33	2.36
<b>Hungerford Brook</b>						
HB1	1	0.339	16.4	1	1.29	2.38
HB2	1	0.144	6.65			
HB3				1	0.999	2.74
				2	0.074	5.23
<b>Trout River</b>						
TR1	1	0.132	8.04			
	2	0.015	7.98			
TR2	1	0.058	8.13			
TR3	1	1.57	6.91			
	2	11.0	3.77			
<b>Tyler Branch</b>						
TY1	1	1.85	26.2			
	2	0.628	4.49			
TY2	1	0.022	7.16			
	2	0.049	3.42			
<b>Jay Branch</b>						
JB-1	1	0.918	7.60	1	0.185	1.48
	2	0.218	5.05	2	0.546	3.35
<b>Mud Creek</b>						
MC-1	1	1.97	2.65	1	0.317	0.829
				2	0.459	1.33
MC-2	1	0.087	1.23	1	0.694	1.76
	2	0.144	1.47			

**Table D-2 – Shear strength of bank materials measured using a borehole shear test device.**

Study site	Layer depth (m)	Layer description	Sample depth (m)	Friction angle (degrees)	Effective cohesion (kPa)	Dry unit weight (kN/m <sup>3</sup> )
Missisquoi River						
M1	0 - 0.9	Sand with silt	0.5	25.9	10.2	12.7
	0.9 - 1.2	Sand lens		30.3	0.4	
	> 1.2	Sand with silt	1.25	22.0	0.81	
M2	0 - 1.45	Sand with silt	0.97	37.3	0	12.5
	1.45 - 1.72	Sand	1.6	30.3	0.4	
	1.72 - 2.26	Silt/sand	1.9	36.1	3.35	10.9
			1.9	34.0	0.77	10.9
	> 2.26	Sand	2.3	30.3	0.4	
M2A	0 - 1.6	Sand		30.3	0.4	
	1.6 - 3	Sand with gravel		33.2	0.2	
	3 - 3.6	Fine Sand		30.3	0.4	
	3.6 - 6	Sand with silt	4	34.5	6.35	14.5
			4	24.8	0.00	14.5
	6 - 20	Blue gray silt and clay	16.8	23.5	4.40	15.3
		16.8	20.8	7.8	15.3	
M3	0 - 0.7	Sand with some narrow silt layers	0.63	21.0	5.53	12.6
			0.63	27.6	2.67	12.6
	0.7 - 1.6	Silt and sand	1.35	26.0	0.19	12.2
			1.5	40.7	1.55	12.2
	1.6 - 1.9	Coarse sand with small gravel	1.75	33.2	0.2	
> 1.9	Wet sand with silt		24.3	4.1		
M4	0 - 0.6	Brown sand with silt	0.5	31.6	2.04	10.1
			0.5	36.2	7.49	10.1
	0.6 - 1.57	Gray silt	1	32.7	1.57	9.9
			1	31.2	1.8	9.9
	1.57 - 1.67	Fine sand		30.3	0.4	
	1.67 - 2.57	Coarse sand, some fine gravel	1.99	33.2	0.2	
> 2.57	Gravel and sand	2.7				
M5	0 - 2.0	Sand with gravel				
	2.0 - 2.25	Brown clay	2.16	25.0	3.96	13.6
	2.25 - 3.57	Sand - saturated	2.6			13.2
			3.55			15.2
	3.57 - 24.39	Blue grey silty clay	4.58	11.3	3.89	14.0
		12.27	24.1	1.41	12.5	
M6	0 - 1.48	Sand with some silt	0.7	30.2	3.16	13.2
			0.7	36.9	4.79	13.2
	> 1.48	Silt with sand	1.7	37.23	2.47	12.1
M7	0 - 1.34	Sand (some silt)	0.63	33.6	4.3	14.3
			0.63	32.1	0.0	14.3
	1.34 - 1.82	Sand with silt	1.75	27.5	0.86	
	1.82 - 2.3	Coarse sand	1.83			12.7
> 2.3	Gravel and sand		33.2	0.2		
M8	0 - 0.45	Topsoil with gravel				
	0.45 - 1.0	Coarse sand	0.53	32.8	0.0	13.0
	1.0 - 1.3	Sand gravel with silt				
	> 1.3	Gravel and sand				
MSII-1	0 - 0.7	Brown silt (some sand)	0.5	26.3	1.75	13.5
			0.5	32.4	2.1	13.5
	0.7 - 1.96	Brown grey mottled sand with silt	0.96	26.6	1.23	12.2
			0.95	27.8	3.52	12.2
	1.96 - 2.7	Blue grey silt sand (more cohesive)	2.1	26.9	4.7	12.6
2.1			20.0	5.83	12.6	
MSII-2	0 - 1.3	Brown silt sand	0.5	31.9	2.43	12.4
			0.5	31.0	2.7	12.4
	1.3 - 2	Sand	1.4	22.9	0	12.8
MSII-3	0 - 1.6	Light brown-gray silty sand	0.65	9.4	1.44	12.5
			0.65	9.3	1.34	12.5
			0.65	22.9	10.59	12.5
			0.68	8.1	11.3	12.5
			0.74	32.9	11.62	12.5
			0.75	32.2	3.84	12.9
			0.75	32.2	3.84	12.9
	1.6 - 2.15	Silt sand	1.9	34.1	0.36	16.1
			1.93	28.5	2.18	
			2	28.7	4.57	
2.15 - 2.3	Sand					
MSII-3a	0 - 0.9	Brown silt sand	0.6	31.9	0	13.8
			0.6	32.5	0	13.8
	0.9 - 1.9	Brown grey silt, some gravel	1.35	38.5	6.1	12.7
		1.38	31.4	5.05	12.7	

Study site	Layer depth (m)	Layer description	Sample depth (m)	Friction angle (degrees)	Effective cohesion (kPa)	Dry unit weight (kN/m <sup>3</sup> )
MSII-4	0 - 1.2	Brown gray silt	0.75	35.3	0.05	14.8
			0.75	33.6	2.77	14.8
			0.75	21.9	7.41	14.8
	1.2 - 2.25	Gravel with sand				
MSII-5	0 - 1.4	Silt sand	0.75	34.2	1.76	10.5
			0.75	36.7	5.17	10.5
<b>Black Creek</b>						
BL1	0 - 0.4	Root permeated silt		26.6	4.3	
	0.4 - 1.2	Silty sand	0.55	23.5	2.93	14.0
			0.55	26.0	6.04	
	> 1.2	Sandy silt	1.7	35.7	3.72	14.8
BL2	0 - 0.9	Silt	0.67	33.7	0.76	13.6
	> 0.9	Tan sand some grey oxidation	1.13	28.0	5.02	14.4
		Brown sand (close to saturation)	1.3	37.8	1.29	14.4
BL3	0 - 0.5	Organic top soil	0.35	34.1	0	11.9
			0.35	40.2	0.69	11.9
	> 0.5	Silt-clay	0.6	0	11	11.2
			0.67	0	18	11.2
			0.67	0	20	11.2
<b>Hungerford Brook</b>						
HB1	0 - 0.4	Brown silt	0.3	32.5	2.88	11.6
	0.4 - 1.2	Gray mottled silt-clay	0.75	35.1	10.6	13.4
HB2	0 - 0.55	Silt (some sand)	0.5	26.6	2.78	
	0.55 - 1.02	Sandy clay	1.3	27.0	9.68	16.6
	1.02 - 1.3	Sand		30.3	0.4	
HB3	0 - 0.7	Clay and sand	0.4	26.9	16.6	15.7
	0.7 - 0.9	Mixed shale				
	0.9 - 1.35	Silt and sand some clay (more sand with depth)	1.15	31.8	0.28	13.3
<b>Trout River</b>						
TR1	0 - 1.2	Silt with wood intrusions	0.68	32.44	3.75	12.9
	1.2 - 2.8		1.65	34.47	3.35	9.0
TR2	0 - 0.75	Silt-sand-gravel	0.33	30.4	0.39	13.4
	0.75 - 1.75	Large gravel		36	0.0	
TR3	0 - 1.38	Silt and sand	0.8	34.3	0.0	12.8
	1.38 - 1.48	Sand				
	1.48 - 1.67	Silt and sand		34.3	1.0	
	1.67 - 2.1	Gravel and sand (gravel larger with depth)		33.2	0.2	
<b>Tyler Branch</b>						
TY1	0 - 0.4	Light brown silt; grass roots	0.25	34.5	3.13	12.6
			0.35	36.8	3.18	13.1
	0.4 - 0.5	Sand				
	0.5 - 1.5	Unconsolidated, poorly sorted, silt-sand-gravel	0.8	30.3	0.4	
TY2	0 - 0.72	Brown sand	0.46	38.6	3.01	12.0
	> 0.72	Light brown sand	0.85	34.9	0.66	11.9
<b>Jay Branch</b>						
JB-1	0 - 1.77	Silt sand	0.65	30.7	1.78	12.2
		NB: cobbles at 1.16m	0.65	31.2	2.45	12.2
JB-2	0 - 0.2	Sand				
	0.2 - 2.5	Boulder cobble				
<b>Mud Creek</b>						
MC-1	0 - 1.24	Light brown silt	0.8	27.6	8.05	12.1
	1.24 - 1.85	Blue gray silt clay	1.4	27.3	8.24	13.6
			1.4	31.7	7.21	13.6
MC-2	0 - 0.4	Brown silt	0.35	25.9	16.34	12.7
			0.35	31.3	11.03	12.7
	0.4 - 1.4	Blue gray silt/clay	0.7	32.7	6.57	13.4
			0.7	28.6	0.53	13.4
			0.7	27.2	2.36	13.4
	> 1.4	Gravel sand				